Available online at www.sciencedirect.com
SCIENCE DIRECT®
Coordination Chemistry Reviews 248 (2004) 757–815
COORDINATION CHEMISTRY REVIEWS
www.elsevier.com/locate/ccr

Review

Zero-field splitting in metal complexes

Roman Boča*

Department of Inorganic Chemistry, Slovak Technical University, SK-812 37 Bratislava, Slovakia

Received 27 June 2003; accepted 1 March 2004

Contents

1. Introduction 758
1.1. Motivation 758
1.2. The scope of review 759
1.3. Notations used 759

Abbreviations: [Cu_3BuBz·2EtOH], bis(μ-benzoato-*O*,*O*′)-bis(benzoato-*O*)-bis{μ-[2-di(*n*-butyl)amino)]-ethanolato-*O*,*N*}-bis(ethanol)tricopper(II); [Cu_3BuBz·H_2O], bis(μ-benzoato-*O*,*O*′)-bis(benzoato-*O*)-bis{μ-[2-di(*n*-butyl)amino)]-ethanolato-*O*,*N*}-aqua-tricopper(II); [Cu_3BuNaEs·2MeOH], bis(μ-(1-naphtylacetato)-*O*,*O*′)-bis(1-naphtylacetato-*O*)-bis{μ-[2-di(*n*-butyl)amino)]-ethanolato-*O*,*N*}-bis(methanol)tricopper(II); [Cu_3EtBz·2MeOH], bis(μ-benzoato-*O*,*O*′)-bis(benzoato-*O*)-bis[μ-(2-diethylamino)ethanolato-*O*,*N*]-bis(methanol)tricopper(II); [Cu_3EtBz·H_2O], bis(μ-benzoato-*O*,*O*′)-bis(benzoato-*O*)-bis[μ-(2-diethylamino)ethanolato-*O*,*N*]-aqua-tricopper(II); $\{L^{10}_{NNNO(O)}\}$, dinucleating carboxylato-bis(2-pyridylmethyl)amine based ligand; $\{L^{11}_{NO}\}$, 3-carboxy-5,6-dimethoxy-1-(methoxycarbonyl)benzo[*f*]quinolinato(1-); $\{L^{12}_{N3O3N2O4}\}$(mpdp)$_2$, 2(*N*,*N*-bis(2-methylpyridyl)aminomethyl)-6-(*N*-(2-hydroxyphenyl)-*N*-(2-pyridylmethyl)aminomethyl)-4-methylphenol (mpdp = *m*-phenylenedipropionate); $\{L^{13}_{NNOO}\}$, *N*,*N*′-(1,1-dimethylethylene)bis(salicylaldimine); $\{L^{14}_{NNOO}\}$, *N*,*N*′-(1,1-dimethylethylene)bis(3-methoxysalicylaldimine); $\{L^{15}_{NNNSSS}\}$, 1,4,7-tris(4-*tert*-butyl-2-mercaptobenzyl)-1,4,7-triazacyclononane; $\{L^{16}_{NNOOO(O)}\}$, *N*,*N*′-bis(3-methoxysalicylidene)-1,3-diamino-2,2′-dimethylpropane(2−); $\{L^{17}_{NNOOO(O)}\}$, *N*,*N*′-bis(3-methoxysalicylidene)-1,2-diamino-2-methylpropane(2−); $\{L^{18}_{ONNOR1R2}\}$, bis(3-R_1-salicyliden)tetraisothio(R_2)semicarbazide; $\{L^{19}_{NNN}\}$, 1,4,7-trimethyl-1,4,7-triazacyclononane; $\{L^{1}_{NNSS}\}$, 5-formylpyrazole-based thiolato Schiff base; $\{L^{20}_{NNNSSS}\}$, 1,4,7-tris(4-^{t}Bu-2-mercaptobenzyl)-1,4,7-triazacyclononane(3−); $\{L^{2}_{NNSS}\}$, 5-formylpyrazole-based thiolato Schiff base; $\{L^{3}_{SSOO}\}$, $Ph_2C(S)COO$; $\{L^{4}_{NNOO}\}$, HMPA–B = bis(2-hydroxy-2-methylpropanamido)benzene; $\{L^{5}_{NNNOO}\}$, *N*,*N*′-bis(3-*tert*-butyl-2-hydroxy-5-methylbenzyliden)-1,7-diamino-4-methyl-4-azaheptane; $\{L^{6}_{NNOO}\}$, $C(CN)_2NO$·MeOH chelating ligand; $\{L^{7}_{NNNN}\}$, Me_6[14]ane = 5,7,7,12,14,14-hexamethyl-1,4,8,11-tetraazacyclotetradecane; $\{L^{8}_{NNNN}\}$, bis-imidazolyl tetradentate Schiff base formed of condensation of imidazole-2-carbaldehyde and 1,3-diaminopropane; $\{L^{9}_{NNNNNN}\}$, bis(bipyridyl)-Me-pyrimidine; 1,3,7,10-CT, Me_6[14]-1,4,8,11-tetraene N_4; 1,7-CT, Me_6[14]-4,11-diene N_4; 3-Prbi, 3-propyl-biuret(2−); ac, acetato(1−); acac, acetylacetonato(1−); aepn, *N*-(2-aminoethyl)-1,3-propanediamine; alaw, 3-amino-lawsonat = 3-amino-2-hydroxy-1,4-naphtoquinone; bdt, 1,2-benzenedithiolato(1−); bhmp, 2,6-bis(bis(2-hydroxyethyl)aminomethyl)-4-methylphenolato(1−); BiIm, biimidazolate; bipy, 2,2′-bipyridyl; biq, 2,2′-biquinoline; bispictn, *N*,*N*′-bis(2-pyridylmethyl)-1,3-propanediamine; bomp, 2,6-bis(bis(2-methoxyethyl)aminomethyl)-4-methylphenolato(1−); bomp, 2,6-bis[bis(2-methoxyethyl)-aminimethyl]-4-methylphenolato(1−); bpym, 2,2′-bipyrimidine; bz, benzoato(1−); bzimpy, bis(benzimidazole)pyridine; cit, citrate; cor, 8,12-diethyl-2,3,7,13,17,18-hexamethylcorrolato(3−); Cp, cyclopentadienyl(1−); Cp*, pentamethylcyclopentadienyl(1−); cth, rac-5,5,7,12,12,14-hexamethyl-1,4,8,11 tetraazacyclotetradecane or rac-5,7,7,12,14,14-hexamethyl-1,4,8,11 tetraazacyclotetradecane; cyclam, 1,4,8,11-tetraazacyclotetradecane; daDP, 2,4-diacetyldeuteroporphyrin IX dimethyl ester; dbm, 1,3-diphenyl-1,3-propanedionato(1−); dedtc, diethyldithiocarbamato(1−); dien, diethylenetriamine; DMF, dimethylformamide; dmiz, dimethylimidazole; dmp, 2,9-dimethyl-1,10-phenanthroline; DP, deuteroporphyrin IX dimethyl ester; en, ethylenediamine, 1,2-diaminoethane; HAT, 1,4,5,8,9,12-hexaazatriphenylene; hfa, hexafluoroacetylacetonato(1−); iphos, imino-bis(methylphosphonic acid); iz, imidazole; L^{2-}, $dmSALPD^{2-}$ = *N*,*N*′-bis(salicylidene)-1,3-propanediaminato(2−); macro, 1,4,8,11-tetramethyl-1,4,8,11-tetraazacyclotetradecane; mal, malonate; Me_2pba, 2,2′-dimethyl-1,3-propylenebis(oxamato); Me_2-tpa, bis[(6-methyl-2-pyridyl)methyl](2-pyridylmethyl)amine; Me_3[12]N_3, 2,4,4-trimethyl-1,5,9-triazacyclododec-1-ene; Me_3-tpa, tris[(6-methyl-2-pyridyl)methyl]amine; Me_4[12]N_3, 2,4,4,9-tetramethyl-1,5,9-triazacyclododec-1-ene; mea, 2-aminoethanole; medpt, *N*,*N*-bis(3-aminopropyl)methylamine; mepn, 1,2-diamino-2-methylpropane; miz, 2-methylimidazole; mpy, 4-methylpyridine; nsalpro, 1,3-bis(5-NO_2-salicylideneamino)propan-2-ol; OEP, octeethylporphyrin; opba, *o*-phenylenebis(oxamato); ox, oxalato(2−); pba, 1,3-propylenebis(oxamato); pba, propane-1,3-diylbis(oxamato); pbaOH, 2-hydroxyl-1,3-propylenebis(oxamato); PC, phtalocyaninato(2−); pdca, 2,3-pyrazinedicarboxylato(1−); pip, piperidine; PP, protoporphyrin IX; ppn, bis(triphenylphosphonium)iminium(1+); PTC, phthalocyanine; py, pyridine; Pydtc, pyrrolidine-1-carbodithiolato(1−); pyO, pyridine-N-oxide; pz, pyrazole; sal, salicylato (1−); sal-2,4-tol, *N*,*N*′-bis(salicylidene)toluene-2,4-diamine; sal-2,6-tol, *N*,*N*′-bis(salicylidene)toluene-2,6-diamine; salen, N,N′-ethylenebis(salicylaldiminato)(2−); sal-*m*-phen, *N*,*N*′-bis(salicylidene)-*m*-phenylenediamine; sal-tabp(4−), Schiff base formed of 2,2′,6,6′-tetraaminobiphenyl with salicylaldehyde; SOD, native superoxide dismutase; tdt, 3,4-toluenedithiolato(1−); terpy, 2,2′:6′,2″-terpyridine; teta, triethylenetetramine; TMC, 1,4,8,11-tetramethyl-1,4,8,11-tetraazacyclotetradecane, tetramethylcyclam; TMPP, tris(2,4,6-trimethoxyphenyl)phosphine; tn, 1,3-diaminopropane; tpfc, 5,10,15-tris(pentafluorophenyl)corrolato(3−); TPP, tetraphenylporphyrinato(2−); TPP, tetraphenylporphyrinato(2−); tren, 2,2′,2″-triaminotriethylamine; trop, tropolonato(1−); TTP, tetratolylporphyrinato(2−)

* Tel.: +421-7-59325-610; fax: +421-7-52493-198.
E-mail address: roman.boca@stuba.sk (R. Boča).

doi:10.1016/j.ccr.2004.03.001

2. Spin-Hamiltonian for mononuclear complexes 759
2.1. Occurrence of the ZFS 759
2.2. Formal spin-Hamiltonian 760
2.3. Bilinear ZFS 761
2.4. Biquadratic ZFS 765
2.5. Modeling the magnetization 768
2.6. Modeling the magnetic susceptibility 771
2.7. Modeling the heat capacity 772
3. Binuclear and polynuclear complexes 774
3.1. Formal spin-Hamiltonian for polynuclear systems 774
3.2. Binuclear systems 775
3.3. Trinuclear systems 780
4. Experimental data on ZFS 784
4.1. Data analysis 784
4.2. Magnetic susceptibility 785
4.2.1. Ni(II) complexes 791
4.2.2. Mn(III) complexes 791
4.2.3. V(III) complexes 792
4.2.4. Cr(III) complexes 792
4.2.5. Fe(III) and Mn(II) complexes 793
4.2.6. Co(III) and Fe(II) complexes 793
4.2.7. Co(II) complexes 793
4.2.8. Dinuclear complexes 794
4.2.9. Trinuclear complexes 794
4.3. Magnetization studies 798
4.4. Electron paramagnetic resonance 800
4.5. Calorimetry 804
4.6. Far infrared spectroscopy 807
4.7. Inelastic neutron scattering 807
4.8. Nuclear magnetic relaxation dispersion 808
4.9. Magnetic circular dichroism 808
5. Conclusions 810
Acknowledgements 812
References 812

Abstract

Using the spin-Hamiltonian formalism the magnetic parameters are introduced through the components of the Λ-tensor involving only the matrix elements of the angular momentum operator. The energy levels for a variety of spins are generated and the modeling of the magnetization, the magnetic susceptibility and the heat capacity is done. The strategy in dealing with binuclear and polynuclear systems is explained. Experimental data on the zero-field splitting (ZFS) are reviewed; the extensive tabulations involve data from different sources: the magnetic susceptibility and magnetization measurements, the electron paramagnetic resonance (EPR), calorimetry, far-infrared spectroscopy, circular magnetic dichroism, and some other experimental methods. The limits of the spin-Hamiltonian formalism are shown.

Keywords: Magnetism; Zero-field splitting; Magnetic susceptibility; Magnetization; Transition metal complexes

1. Introduction

1.1. Motivation

In recent years, considerable attention was paid to molecular magnets and single-molecule magnets [1–10]. This effort is motivated by the idea of having denser information-recording media which would allow data storage several orders of magnitude greater than at present. To have the magnetic productivity (the magnetization) large enough, molecules possessing a large value of the molecular spin S are desirable. Then for temperature low enough the only populated state could be that of $M_S = -S$ (Fig. 1). However, with respect to retaining the recorded information there is a competitive magnetic tunneling effect which will degrade the information (the antiferromagnetic state is thermodynamically more stable). The energy barrier must be large enough to prevent such degradation of information and therefore the magnetic anisotropy need to be high.

The design of high-spin molecules possessing a tunable value of the zero-field splitting (ZFS) parameter D is far from a routine objective at present. The conditions that determine the sign and value of the D-parameter are, so far, unclear. Motivated by the above considerations we went back to simple mononuclear complexes where the magnetic anisotropy (the D-parameter) is easy to investigate. The investigation of the axial ZFS parameter is a long story. This subject is incorporated in monographs dealing with magnetism to a

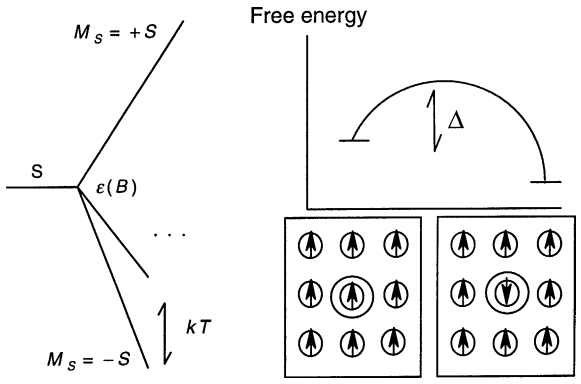

Fig. 1. Thermal population of only the $M_S = -S$ state (left); a scheme of the magnetic tunneling (right).

varying extent and complexity (from almost nothing to a very broad presentation) [11–34]. However, the main experimental source for ZFS is electron paramagnetic resonance (EPR) [35–43]. As will be seen later, owing to internal limitations the bracketing the ZFS parameters is limited to only small values by the EPR.

Both, the magnetochemical and EPR sources utilize extensively the operator equivalent approach in treating the ZFS along with the crystal field of lowered symmetry. Such an approach, however, is limited to the ground electron terms obeying the Hund rules. The ZFS parameters (D, E, a and F) are considered as parameters of the theory that are fixed by fitting the experimental data for each system under investigation. Until now, there has been no rational approach that could correlate the ZFS parameters to some other, more fundamental data (integrals). A tailoring and tuning of the ZFS parameters is a dream which is not yet fulfilled. What could help to reach this objective is an intensive theoretical analysis. This is the main target of the present work. However, a sufficient description of the situation requires much more effort and we will see later that there is a demand for combining the information from the electronic structure of atoms [44–49], the crystal/ligand field theory [50–58], fundaments of the angular momentum [59–62], and finally the irreducible tensor operator (ITO) approach [63–70] as a real working tool. Let us note that contemporary monographs utilize the ITO approach as a common standard [32,33,42,56].

1.2. The scope of review

Section 2 deals with the spin-Hamiltonian formalism for mononuclear systems. The magnetic parameters are introduced through the components of the Λ-tensor involving only the matrix elements of the angular momentum operator. The energy levels for a variety of spins are generated and the modeling of the magnetization, the magnetic susceptibility and the heat capacity is done.

The strategy in dealing with binuclear and polynuclear systems is explained in Section 3.

Experimental data on the ZFS are reviewed in Section 4. The extensive tabulations involve data from different sources: the magnetic susceptibility and magnetization measurements, the EPR, calorimetry, far-infrared spectroscopy, circular magnetic dichroism, and some other experimental methods. Notice, the majority of the experimental data are interpreted in terms of the spin-Hamiltonian formalism.

1.3. Notations used

1. The SI units are used consistently through the paper; $\chi_{\mathrm{mol}}[\mathrm{SI}] = 4\pi \times 10^{-6}\chi_{\mathrm{mol}}$ (cgs and emu).
2. The energy quantities E (like ε, J, D, E, a, F, etc.) are presented in the form of the corresponding wavenumber, i.e. E/hc and given in units of cm^{-1}.
3. The isotropic exchange constants are uniformly thought in the form $-J_{ij}(\vec{S}_i \cdot \vec{S}_j)$. The data from original sources differing from this definition have been rescaled to the above form.
4. The angular momentum operators bring the reduced Planck constant $\bar{h}$ when operating to a corresponding wavefunction (a ket).
5. The fundamental physical constants (c, ε_0, μ_0, N_{A}, $k = k_{\mathrm{B}}$, R, μ_{B}, e, h, $\bar{h}$) adopt their usual meaning. The reduced Curie constant $C_0 = N_{\mathrm{A}}\mu_0\mu_{\mathrm{B}}^2/k$ is met in the paper.

2. Spin-Hamiltonian for mononuclear complexes

2.1. Occurrence of the ZFS

The essence of ZFS lies in a weak interaction of the spins mediated by the spin–orbit coupling. ZFS appears as a small energy gap of a few cm^{-1} between the lowest energy levels. In magnetism, the ZFS becomes visible when the thermal population of energy levels is considerably unequal and thus it can be detected on temperature lowering so that kT is lower than the energy gap $2D$ (Fig. 2).

The ZFS case is met in transition metal complexes having spin $S \geq 1$ and with no first-order contribution to the angular momentum. The last statement means that

$$\langle 0|\vec{L}|0\rangle = a\langle 0|K\rangle = 0 \tag{2.1}$$

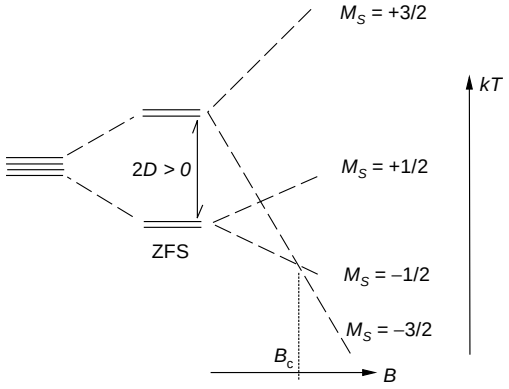

Fig. 2. Example of a ZFS system with $S = 3/2$.

Table 1
Examples of the ZFS systems

d^n	Tetrahedral				Octahedral			
	Configuration	Term	Type	Example	Configuration	Term	Type	Example
d^2	e^2	$^3A_2$	$S = 1$	Ti(II), V(III)				
d^3					t_{2g}^3	$^4A_{2g}$	$S = 3/2$	Cr(III)
d^5	$e^2t_2^3$	$^6A_1$	$S = 5/2$	Mn(II), Fe(III)	$t_{2g}^3e_g^2$	$^6A_{1g}$	$S = 5/2$	Mn(II), Fe(III)
d^7	$e^4t_2^3$	$^4A_2$	$S = 3/2$	Co(II)				
d^8					$t_{2g}^6e_g^2$	$^3A_{2g}$	$S = 1$	Ni(II)

holds true where $|0\rangle$ is the ground electronic state, in fact the A- or B-state for octahedral and tetrahedral complexes (Table 1).

2.2. Formal spin-Hamiltonian

The Hamiltonian which describes the interaction of the single magnetic center with the external magnetic field involves the spin Zeeman term, the orbital Zeeman term and the operator of the spin–orbit coupling, i.e.

$$\hat{H}' = \hbar^{-1}\mu_B g_e(\vec{S}\cdot\vec{B}) + \hbar^{-1}\mu_B(\vec{L}\cdot\vec{B}) + \hbar^{-2}\lambda(\vec{L}\cdot\vec{S}) \tag{2.2}$$

The above Hamiltonian acts as a perturbation operator so that perturbation theory yields the first- and the second-order corrections

$$\hat{H}^{(1)} = \langle 0|\hat{H}'|0\rangle \tag{2.3}$$

$$\hat{H}^{(2)} = -\sum_{K\neq 0}\frac{\langle 0|\hat{H}'|K\rangle\langle K|\hat{H}'|0\rangle}{E_K - E_0} \tag{2.4}$$

It is assumed that the state vectors are represented by orthonormal kets of spatial variables, viz. $|K\rangle = |\alpha, L, M_L\rangle$.

The first–order correction can be rewritten as follows:

$$\hat{H}^{(1)} = \hbar^{-1}\mu_B g_e(\vec{B}\cdot\vec{S})\langle 0|0\rangle + (\hbar^{-1}\mu_B\vec{B} + \hbar^{-2}\lambda\vec{S})\cdot\langle 0|\vec{L}|0\rangle \tag{2.5}$$

where the last term vanishes in the absence of the first-order angular momentum and thus

$$\hat{H}^{(1)} = \hbar^{-1}\mu_B g_e(\vec{B}\cdot\vec{S}) \tag{2.6}$$

The second–order correction contains the terms

$$\langle 0|\hat{H}'|K\rangle = \hbar^{-1}(\mu_B\vec{B} + \hbar^{-1}\lambda\vec{S})\cdot\langle 0|\vec{L}|K\rangle + \hbar^{-1}\mu_B g_e\vec{B}\cdot\vec{S}\,\langle 0|K\rangle \tag{2.7}$$

where the last contribution vanishes owing to the orthogonality of the state vectors. The complete second-order correction is

$$\hat{H}^{(2)} = -\hbar^{-2}\sum_{K\neq 0}\frac{[(\mu_B\vec{B} + \hbar^{-1}\lambda\vec{S})\cdot\langle 0|\vec{L}|K\rangle][(\mu_B\vec{B} + \hbar^{-1}\lambda\vec{S})\cdot\langle K|\vec{L}|0\rangle]}{E_K - E_0} \tag{2.8}$$

and after introducing the Λ-tensor

$$\Lambda_{ab} = -\hbar^{-2}\sum_{K\neq 0}\frac{\langle 0|\hat{L}_a|K\rangle\langle K|\hat{L}_b|0\rangle}{E_K - E_0} \quad (\text{energy}^{-1}) \tag{2.9}$$

it can be rewritten in the form

$$\hat{H}^{(2)} = (\mu_B\vec{B} + \hbar^{-1}\lambda\vec{S})\cdot\bar{\bar{\Lambda}}\cdot(\mu_B\vec{B} + \hbar^{-1}\lambda\vec{S}) \tag{2.10}$$

(One should be careful in the definition of the sign of the Λ-tensor since the opposite sign can be met in the literature.) The overall result of perturbation theory up to second order becomes

$$\begin{aligned}\hat{H}^S &= \hat{H}^{(1)} + \hat{H}^{(2)}\\ &= \sum_a\sum_b\{\mu_B^2\Lambda_{ab}B_aB_b + \hbar^{-1}\mu_B B_a(g_e\delta_{ab} + 2\lambda\Lambda_{ab})\hat{S}_b\\ &\quad + \hbar^{-2}\lambda^2\Lambda_{ab}\hat{S}_a\hat{S}_b\}\end{aligned} \tag{2.11}$$

or

$$\hat{H}^S = -\tfrac{1}{2}(\vec{B}\cdot\bar{\bar{\kappa}}\cdot\vec{B}) + \hbar^{-1}\mu_B(\vec{B}\cdot\bar{\bar{g}}\cdot\vec{S}) - \tfrac{1}{2}\hbar^{-2}(\vec{S}\cdot\bar{\bar{\Delta}}\cdot\vec{S}) \tag{2.12}$$

where we introduced the *κ-tensor* (reduced, temperature-independent paramagnetic susceptibility tensor) as

$$-\tfrac{1}{2}\kappa_{ab}^{\text{para}} = \mu_B^2\Lambda_{ab} \quad (\text{energy}\times\text{induction}^{-2}) \tag{2.13}$$

the *g*-tensor (magnetogyric ratio tensor) as

$$g_{ab} = g_e\delta_{ab} + 2\lambda\Lambda_{ab} \quad (\text{dimensionless}) \tag{2.14}$$

and the *D*-tensor (spin–spin interaction tensor) as

$$-\tfrac{1}{2}\Delta_{ab} = \lambda^2\Lambda_{ab} = D'_{ab} \quad (\text{energy}) \tag{2.15}$$

(The numerical prefactors, like $-1/2$ are the matter of the convention.)

The operator $\hat{H}^S$ is termed the *spin-Hamiltonian*: it acts only on the spin kets $|S, M_S\rangle$. It yields eigenvalues identical with those produced by the perturbation operator $\hat{H}'$ acting on the full set of variables $|\alpha, L, M_L, S, M_S\rangle$—see Table 2.

The temperature independent paramagnetic term is omitted hereafter (this can be included into the empirical

Table 2
Explanation of the magnetic Hamiltonian and the spin-Hamiltonian

Extended problem for spin–orbit kets		Truncated problem to spin kets	
$\langle L, M'_L, S, M'_S\|\hat{H}'\|L, M_L, S, M_S\rangle \xrightarrow{\text{diagonalization}} \varepsilon_i$		$\langle S, M'_S\|\hat{H}^S\|S, M_S\rangle \xrightarrow{\text{diagonalization}} \varepsilon_i$	
Hamiltonian matrix	Energy levels	Hamiltonian matrix	Energy levels
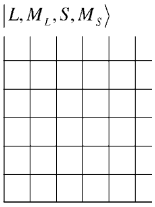	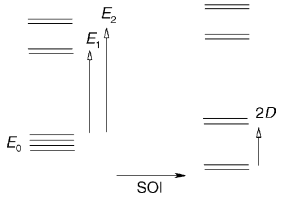	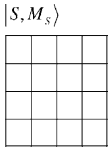	

correction of the experimental data, together with the diamagnetic term) so that we arrive at

$$\hat{H}^{\mathrm{S}} = \hbar^{-1}\mu_{\mathrm{B}}(\vec{B}\cdot\bar{\bar{g}}\cdot\vec{S}) + \hbar^{-2}(\vec{S}\cdot\bar{\bar{D}}'\cdot\vec{S}) \tag{2.16}$$

The ZFS Hamiltonian which includes the spin–spin interaction, in its bilinear form, is

$$\hat{H}^{\mathrm{s-s}} = \hbar^{-2}(\vec{S}\cdot\bar{\bar{D}}'\cdot\vec{S}) \tag{2.17}$$

and contains nine components of the D-tensor. Their experimental determination is an unrealistic task and thus some simplifications are desirable. Assuming a diagonal and traceless form of the D-tensor, the ZFS Hamiltonian can be rewritten to an equivalent form

$$\hat{H}^{\mathrm{s-s}} = \hbar^{-2}[D(\hat{S}_z^2 - \tfrac{1}{3}\hat{S}^2) + E(\hat{S}_x^2 + \hat{S}_y^2)] \tag{2.18}$$

where we introduce the axial ZFS parameter

$$D = \tfrac{1}{2}(-D'_{xx} - D'_{yy} + 2D'_{zz}) = \tfrac{3}{2}D_{zz} \tag{2.19}$$

and the rhombic ZFS parameter

$$E = \tfrac{1}{2}(D'_{xx} - D'_{yy}) \tag{2.20}$$

Normally, it is assumed that the ZFS parameters obey a relationship

$$|D| \geq 3E \geq 0 \tag{2.21}$$

One can interchange the Cartesian axes (which cannot influence the properties of the system) but the above relationship will still be fulfilled. The various conventions are compiled in Table 3.

2.3. Bilinear ZFS

As the ZFS Hamiltonian acts only on the spin kets $|S, M\rangle$, its matrix elements can easily be evaluated with the help of shift operators as follows:

$$\hat{S}_z|S, M\rangle = M\hbar|S, M\rangle \tag{2.22}$$

$$\hat{S}_+|S, M\rangle = \sqrt{(S-M)(S+M+1)}\hbar|S, M+1\rangle \tag{2.23}$$

$$\hat{S}_-|S, M\rangle = \sqrt{(S+M)(S-M+1)}\hbar|S, M-1\rangle \tag{2.24}$$

Then we get

$$\langle SM'|\hat{S}_x|SM\rangle = \tfrac{1}{2}\langle SM'|(\hat{S}_+ + \hat{S}_-)|SM\rangle \tag{2.25}$$

$$\langle SM'|\hat{S}_y|SM\rangle = -\tfrac{1}{2}\mathrm{i}\langle SM'|(\hat{S}_+ - \hat{S}_-)|SM\rangle \tag{2.26}$$

$$\langle SM'|\hat{S}_z|SM\rangle = M\hbar\delta_{M',M} \tag{2.27}$$

The spin–spin (zero-field) interaction matrices are compiled in Table 4.

Now the application of the spin Zeeman term

$$\hat{H}_a^{\mathrm{Z}} = \hbar^{-1}\mu_{\mathrm{B}}g_aB_a\hat{S}_a \tag{2.28}$$

will yield

(a) diagonal corrections for the z-direction;
(b) off-diagonal corrections for the x-direction (real, symmetric) and y-direction (complex, Hermitean).

Then the energy levels are obtained through the standard eigenvalue problem.

When we seek an analytical expression for the energy levels, the Taylor expansion could be applied

$$\varepsilon_i = \varepsilon_i^{(0)} + \varepsilon_i^{(1)}B + \varepsilon_i^{(2)}B^2 + O_3 \tag{2.29}$$

where the van Vleck coefficients $\varepsilon_i^{(n)}$ occur.

With neglect of the rhombic component ($E = 0$) the x- and y-directions become equivalent and the zero-field interaction matrix stays diagonal. The advantage of such a situation lies in the fact that the Zeeman term can be considered as a small perturbation (when D is large enough). This allows an application of the perturbation theory according to which the zero-field eigenvalues can be corrected by the second-order PT formula for non-degenerate states

$$\varepsilon_{M,x}^{(2)} = -\sum_{M'\neq M}\frac{(\hbar^{-1}\mu_{\mathrm{B}}g_xB_x\langle SM'|\hat{S}_x|SM\rangle)^2}{\varepsilon_{M'}^{(0)} - \varepsilon_M^{(0)}} \tag{2.30}$$

Just this formula, when applied to the perpendicular direction, yields the second-order van Vleck coefficients

Table 3
Interrelations among the spin-Hamiltonian parameters

Property	Formula
(a) *Negative* sign convention	
Angular momentum unquenching tensor	$\Lambda_{ab} = -\hbar^{-2}\sum_{K\neq 0}\langle 0\|\hat{L}_a\|K\rangle\langle K\|\hat{L}_b\|0\rangle/(E_K - E_0)$
Magnetogyric ratio-tensor	$g_{ab} = g_e\delta_{ab} + 2\lambda\Lambda_{ab}$
Spin–spin interaction tensor[a]	$-\frac{1}{2}D_{ab} = D'_{ab} = \lambda^2\Lambda_{ab}$
	$D = \frac{1}{2}(-D'_{xx} - D'_{yy} + 2D'_{zz}) = +\frac{1}{2}\lambda^2(-\Lambda_{xx} - \Lambda_{yy} + 2\Lambda_{zz})$
	$E = \frac{1}{2}(D'_{xx} - D'_{yy}) = \frac{1}{2}\lambda^2(\Lambda_{xx} - \Lambda_{yy}) > 0$
Temperature-independent paramagnetic susceptibility tensor	$-\frac{1}{2}\kappa^{\text{para}}_{ab} = \mu_B^2\Lambda_{ab}$
	$\chi^{\text{para}}_{ab} = N_A\mu_0\kappa^{\text{para}}_{ab} = -2N_A\mu_0\mu_B^2\Lambda_{ab}$
Temperature-independent paramagnetism	$\chi_{TIP} = -\frac{2}{3}N_A\mu_0\mu_B^2(\Lambda_{xx} + \Lambda_{yy} + \Lambda_{zz}) > 0$
(b) *Positive* sign convention	
Angular momentum unquenching tensor	$\Lambda_{ab} = +\hbar^{-2}\sum_{K\neq 0}\langle 0\|\hat{L}_a\|K\rangle\langle K\|\hat{L}_b\|0\rangle/(E_K - E_0)$
Magnetogyric ratio-tensor	$g_{ab} = g_e\delta_{ab} - 2\lambda\Lambda_{ab}$
Spin–spin interaction tensor[a]	$-\frac{1}{2}D_{ab} = D'_{ab} = -\lambda^2\Lambda_{ab}$
	$D = \frac{1}{2}(-D'_{xx} - D'_{yy} + 2D'_{zz}) = -\frac{1}{2}\lambda^2(-\Lambda_{xx} - \Lambda_{yy} + 2\Lambda_{zz})$
	$E = \frac{1}{2}(D'_{xx} - D'_{yy}) = -\frac{1}{2}\lambda^2(\Lambda_{xx} - \Lambda_{yy}) > 0$
Temperature-independent paramagnetic susceptibility tensor	$-\frac{1}{2}\kappa^{\text{para}}_{ab} = -\mu_B^2\Lambda_{ab}$
	$\chi^{\text{para}}_{ab} = N_A\mu_0\kappa^{\text{para}}_{ab} = +2N_A\mu_0\mu_B^2\Lambda_{ab}$
Temperature-independent paramagnetism	$\chi_{TIP} = +\frac{2}{3}N_A\mu_0\mu_B^2(\Lambda_{xx} + \Lambda_{yy} + \Lambda_{zz}) > 0$
(c) Interrelations	$g_z = g_e + 2D'_{zz}/\lambda = g_e + (4/3)D/\lambda$
	$g_x = g_e + 2D'_{xx}/\lambda$
	$g_y = g_e + 2D'_{yy}/\lambda$
	$g_x - g_y = 2(D'_{xx} - D'_{yy})/\lambda = 4E/\lambda$

[a] The traceless D-tensor is introduced $D_{ab} = D'_{ab} - \frac{1}{3}\delta_{ab}(D'_{xx} + D'_{yy} + D'_{zz})$; then $D_{xx} + D_{yy} + D_{zz} = 0$.

$$\begin{aligned}\varepsilon^{(2)}_{M,x} &= -\sum_{M'\neq M}\frac{(\hbar^{-1}\mu_B g_x\langle SM'|\frac{1}{2}(\hat{S}_+ + \hat{S}_-)|SM\rangle)^2}{\varepsilon^{(0)}_{M'} - \varepsilon^{(0)}_{M}}\\ &= -(\mu_B g_x)^2\left\{\frac{(S-M)(S+M+1)}{4D(1+2M)}\delta_{M',M+1}\right.\\ &\quad\left.+\frac{(S+M)(S-M+1)}{4D(1-2M)}\delta_{M',M-1}\right\}\\ &= (\mu_B g_x)^2\frac{M^2 + S(S+1)}{2(4M^2-1)D}\end{aligned} \tag{2.31}$$

For the Kramers doublet $|S, \pm\frac{1}{2}\rangle$, however, the zero-field energies are degenerate and thus the perturbation theory for degenerate states needs first to be applied. This yields the first-order PT correction (equal to the first-order van Vleck coefficient) in the form

$$\begin{aligned}\varepsilon^{(1)}_{M=\pm 1/2,x} &= \pm\left\langle SM'\left|\hbar^{-1}\mu_B g_x\frac{(\hat{S}_+ + \hat{S}_-)}{2}\right|SM\right\rangle\\ &= \pm\mu_B g_x\left(\frac{1}{2}\right)\left[\left(S+\frac{1}{2}\right)\left(S-\frac{1}{2}+1\right)\right]^{1/2}\\ &= \pm\mu_B g_x\frac{(S+1/2)}{2}\end{aligned} \tag{2.32}$$

and finally the second-order correction becomes

$$\begin{aligned}\varepsilon^{(2)}_{M=\pm 1/2,x} &= -(\mu_B g_x)^2\left\{\frac{(S\mp M)(S\pm M+1)}{4D(1\pm 2M)}\right\}\\ &= -(\mu_B g_x)^2\frac{(S-1/2)(S+3/2)}{8D}\end{aligned} \tag{2.33}$$

Having determined the van Vleck coefficients (Table 5) evaluation of the magnetic susceptibility components proceeds via the van Vleck formula

$$\bar{\chi}_{\text{mol}} = N_A\mu_0\frac{\sum_i[((\varepsilon^{(1)}_i)^2/kT) - 2\varepsilon^{(2)}_i]\exp(-\varepsilon^{(0)}_i/kT)}{\sum_i\exp(-\varepsilon^{(0)}_i/kT)} \tag{2.34}$$

The involvement of the rhombic components creates the difficulty that perturbation theory can no longer be applied. Thus, the energy levels must then be obtained by a numerical solution of the eigenvalue problem. Three values of the "working field" are needed to evaluate the van Vleck coefficients for each component (x-, y-, and z-) of the magnetic susceptibility. Alternative ways for the treatment of the ZFS systems are compiled in Table 6.

The energy levels for a set of ZFS systems are plotted in Fig. 3. One can see that

Table 4
Spin–spin interaction matrices (left) and Zeeman matrices (right) for a ZFS system

$S = 1$

$$\begin{pmatrix} (1/3)D & 0 & E \\ 0 & -(2/3)D & 0 \\ E & 0 & (1/3)D \end{pmatrix} \qquad \begin{pmatrix} G_z & (1/\sqrt{2})G_- & 0 \\ (1/\sqrt{2})G_+ & 0 & (1/\sqrt{2})G_- \\ 0 & (1/\sqrt{2})G_+ & -G_z \end{pmatrix}$$

$S = 3/2$

$$\begin{pmatrix} D & 0 & \sqrt{3}E & 0 \\ 0 & -D & 0 & \sqrt{3}E \\ \sqrt{3}E & 0 & -D & 0 \\ 0 & \sqrt{3}E & 0 & D \end{pmatrix} \qquad \begin{pmatrix} (3/2)G_z & (\sqrt{3}/2)G_- & 0 & 0 \\ (\sqrt{3}/2)G_+ & (1/2)G_z & G_- & 0 \\ 0 & G_+ & -(1/2)G_z & (\sqrt{3}/2)G_- \\ 0 & 0 & (\sqrt{3}/2)G_+ & -(3/2)G_z \end{pmatrix}$$

$S = 2$

$$\begin{pmatrix} 2D & 0 & \sqrt{6}E & 0 & 0 \\ 0 & -D & 0 & 3E & 0 \\ \sqrt{6}E & 0 & -2D & 0 & \sqrt{6}E \\ 0 & 3E & 0 & -D & 0 \\ 0 & 0 & \sqrt{6}E & 0 & 2D \end{pmatrix} \qquad \begin{pmatrix} 2G_z & G_- & 0 & 0 & 0 \\ G_+ & G_z & (\sqrt{6}/2)G_- & 0 & 0 \\ 0 & (\sqrt{6}/2)G_+ & 0 & (\sqrt{6}/2)G_- & 0 \\ 0 & 0 & (\sqrt{6}/2)G_+ & -G_z & G_- \\ 0 & 0 & 0 & G_+ & -2G_z \end{pmatrix}$$

Biquadratic ZFS correction, tetragonal axis

$$\begin{pmatrix} (1/10)a & 0 & 0 & 0 & (1/2)a \\ 0 & -(4/10)a & 0 & 0 & 0 \\ 0 & 0 & +(6/10)a & 0 & 0 \\ 0 & 0 & 0 & -(4/10)a & 0 \\ (1/2)a & 0 & 0 & 0 & (1/10)a \end{pmatrix}$$

$S = 5/2$

$$\begin{pmatrix} (10/3)D & 0 & \sqrt{10}E & 0 & 0 & 0 \\ 0 & -(2/3)D & 0 & \sqrt{18}E & 0 & 0 \\ \sqrt{10}E & 0 & -(8/3)D & 0 & \sqrt{18}E & 0 \\ 0 & \sqrt{18}E & 0 & -(8/3)D & 0 & \sqrt{10}E \\ 0 & 0 & \sqrt{18}E & 0 & -(2/3)D & 0 \\ 0 & 0 & 0 & \sqrt{10}E & 0 & (10/3)D \end{pmatrix} \qquad \frac{1}{2}\begin{pmatrix} 5G_z & \sqrt{5}G_- & 0 & 0 & 0 & 0 \\ \sqrt{5}G_+ & 3G_z & \sqrt{8}G_- & 0 & 0 & 0 \\ 0 & \sqrt{8}G_+ & G_z & 3G_- & 0 & 0 \\ 0 & 0 & 3G_+ & -G_z & \sqrt{8}G_- & 0 \\ 0 & 0 & 0 & \sqrt{8}G_+ & -3G_z & \sqrt{5}G_- \\ 0 & 0 & 0 & 0 & \sqrt{5}G_+ & -5G_z \end{pmatrix}$$

Biquadratic ZFS correction, tetragonal axis:

$$\begin{pmatrix} +(1/2)a' & 0 & 0 & 0 & (\sqrt{5}/2)a & 0 \\ 0 & -(3/2)a' & 0 & 0 & 0 & (\sqrt{5}/2)a \\ 0 & 0 & +a' & 0 & 0 & 0 \\ 0 & 0 & 0 & +a' & 0 & 0 \\ (\sqrt{5}/2)a & 0 & 0 & 0 & -(3/2)a' & 0 \\ 0 & (\sqrt{5}/2)a & 0 & 0 & 0 & +(1/2)a' \end{pmatrix}$$

Biquadratic ZFS correction, trigonal axis:

$$\begin{pmatrix} -(1/3)a & 0 & 0 & -(\sqrt{20}/3)a & 0 & 0 \\ 0 & a & 0 & 0 & 0 & 0 \\ 0 & 0 & -(2/3)a & 0 & 0 & (\sqrt{20}/3)a \\ -(\sqrt{20}/3)a & 0 & 0 & -(2/3)a & 0 & 0 \\ 0 & 0 & 0 & 0 & a & 0 \\ 0 & 0 & (\sqrt{20}/3)a & 0 & 0 & -(1/3)a \end{pmatrix}$$

$G_z = g_z\mu_B B l_z$; $G_\pm = G_x \pm iG_y = \mu_B B(g_x l_x \pm ig_y l_y)$, with l_x, l_y and l_z representing the direction cosines for the vector $\vec{B}$ relative to the symmetry axes; $a' = a + (2/3)F$.

Table 5
van Vleck coefficients for mononuclear ZFS systems

Spin	M	$B_M = \varepsilon_M^{(0)}$[a]	$C_{M,z} = \varepsilon_{M,z}^{(1)}/(\mu_B g_z)$	$C_{M,x} = \varepsilon_{M,x}^{(1)}/(\mu_B g_x)$	$D_{M,x} = \varepsilon_{M,x}^{(2)}/(\mu_B g_x)^2$
$S = 1$[b]	$+1$	D	$+1$	0	$+1/D$
	-1	D	-1	0	0
	0	0	0	0	$-1/D$
$S = 3/2$	$\pm 3/2$	$2D$	$\pm 3/2$	0	$+(3/8)/D$
	$\pm 1/2$	0	$\pm 1/2$	± 1	$-(3/8)/D$
$S = 2$	± 2	$4D$	± 2	0	$+(1/3)/D$
	± 1	D	± 1	0	$+(7/6)/D$
	0	0	0	0	$-3/D$
$S = 5/2$	$\pm 5/2$	$6D$	$\pm 5/2$	0	$+(5/16)/D$
	$\pm 3/2$	$2D$	$\pm 3/2$	0	$+(11/16)/D$
	$\pm 1/2$	0	$\pm 1/2$	$\pm 3/2$	$-1/D$
$S = 3$	± 3	$9D$	± 3	0	$+(3/10)/D$
	± 2	$4D$	± 2	0	$+(8/15)/D$
	± 1	D	± 1	0	$+(13/6)/D$
	0	0	0	0	$-6D$
$S = 7/2$	$\pm 7/2$	$12D$	$\pm 7/2$	0	$+(7/24)/D$
	$\pm 5/2$	$6D$	$\pm 5/2$	0	$+(11/24)/D$
	$\pm 3/2$	$2D$	$\pm 3/2$	0	$+(9/8)/D$
	$\pm 1/2$	0	$\pm 1/2$	± 2	$-(15/8)/D$

[a] Zero-field levels can be uniformly shifted.
[b] For $S = 1$, the secular equation has analytical solutions and the perturbation theory need not be applied. Then the square roots are expanded into a Taylor series in powers of B.

Table 6
Processing of the eigenvalue problem for a ZFS system

1. Analytical working out for the Hamiltonian $\hat{H}_a(D, g_a)$; $E = 0$
   (a) Perturbation theory, $D \gg g_\perp \mu_B B_\perp$, spin $S > 1$

$$\left.\begin{aligned} \varepsilon_{i,z} &= \varepsilon_i^{(0)} + \varepsilon_{i,z}^{(1)} B_z \\ \varepsilon_{i,x} &= \varepsilon_i^{(0)} + \varepsilon_{i,x}^{(1)} B_x + \varepsilon_{i,x}^{(2)} B_x^2 \end{aligned}\right\} \text{Table 5}$$

   (b) Variation method, $x \ll 1$, spin $S = 1$, 3/2, 5/2
   $\varepsilon_{i,z}$—straightforward (already diagonal)
   $\varepsilon_{i,x} \sim \sqrt{1+x} = 1 + x/2 - x^2/8 + O_3$ (Taylor expansion of the square root), where $x \sim \mu_B B/D \ll 1$ for a small field limit and $x \sim D/\mu_B B \ll 1$ for the strong field limit

   Mean susceptibility $\bar{\chi}_a$ (for linear magnetics)—by the van Vleck formula

2. Analytical development for the Hamiltonian $\hat{H}_a(D, E, g_a)$
   Restriction: spins $S = 1$, 3/2; directions $a = x, y, z$
   The secular equation (of the order of 3×3 or 4×4) has an analytical solution in the form of $\varepsilon_{i,a} = \alpha + \sqrt{\beta + \gamma}$ irrespective of the parameters and field magnitude
   Partition function $Z_a(B, T) = \sum_i \exp(-\varepsilon_{i,a}/kT)$
   Magnetization $M_a(B, T) = N_A kT(T_{1a}/Z_a)$
   Differential susceptibility $\tilde{\chi}_a(B, T) = N_A \mu_0 kT(T_{2a} Z_a - T_{1a}^2)/Z_a^2$ with the terms $T_{1a} \equiv \partial Z_a/\partial B_a$ and $T_{2a} \equiv \partial^2 Z_a/\partial B_a^2$

3. Numerical solution of the secular equation; S, B, and D—arbitrary
   (a) the Hamiltonian $\hat{H}_a(D, g_a)$ for $E = 0$ has two sets of eigenvalues: $\varepsilon_{i,z}$ and $\varepsilon_{i,x}$
   (b) the Hamiltonian $\hat{H}_a(D, E, g_a)$ has three sets of eigenvalues: $\varepsilon_{i,z}$, $\varepsilon_{i,x}$, and $\varepsilon_{i,y}$

   Mean susceptibility (for linear magnetics) is obtained through the sequence: three (more) sets of eigenvalues around a reference field $B_0 \rightarrow$ parabolic (polynomial) fit $\rightarrow$ van Vleck coefficients for each level $c_{i,a}^{(0)}$, $c_{i,a}^{(1)}$, and $c_{i,a}^{(2)} \rightarrow$ van Vleck formula
   Magnetization: one set of eigenvalues and eigenvectors at the field $B \rightarrow$ thermal average of the spin $\langle S_a \rangle_T \rightarrow M_a = N_A \langle \mu_a \rangle_T = -N_A g_a \langle S_a \rangle_T$; differential susceptibility through a numerical derivative of the magnetization $\tilde{\chi}_a = \mu_0(\partial M_a/\partial B_a)$
   Three (more) sets of eigenvalues near $B \rightarrow$ parabolic (polynomial) fit $\rightarrow$ derivatives for each level $\varepsilon_{i,a}^{(0)}$, $\varepsilon_{i,a}^{(1)}$, and $\varepsilon_{i,a}^{(2)} \rightarrow$ magnetization

$$M_a(B, T) = N_A kT(T_{1a}/Z_a) = N_A \frac{\sum_i (-\varepsilon_{i,a}^{(1)} - 2B\varepsilon_{i,a}^{(2)}) \exp(-\varepsilon_{i,a}^{(B)}/kT)}{\sum_i \exp(-\varepsilon_{i,a}^{(B)}/kT)}$$

   Susceptibility either by a numerical derivative or using first $\varepsilon_{i,a}^{(1)}$ and second $\varepsilon_{i,a}^{(2)}$ derivatives as $\tilde{\chi}_a(B, T) = N_A \mu_0 kT(T_{2a} Z_a - T_{1a}^2)/Z_a^2$

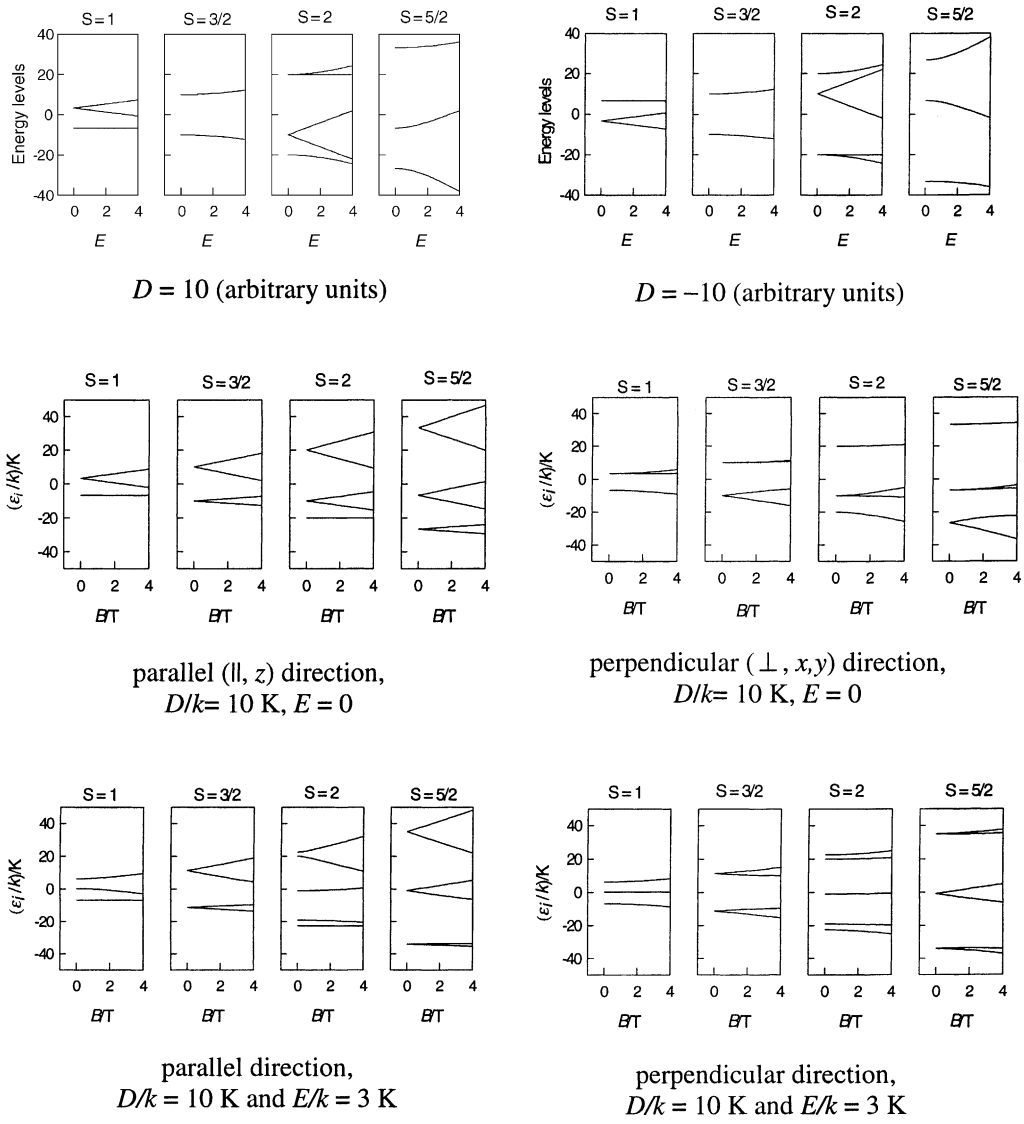

Fig. 3. Effect of the sign of the *D*-parameter and the rhombic ZFS component to the energy levels.

(a) the application of the magnetic field in the parallel direction results in a linear development of the magnetic energy levels;
(b) in the perpendicular direction the levels develop non-linearly;
(c) the reverse sign of the *D*-parameter inverts the level diagram;
(d) the *E*-parameter manifests itself in an additional splitting of energy levels.

2.4. Biquadratic ZFS

More complex spin–spin interaction can be treated with the help of the equivalent operators [36–41]. The concept of equivalent operators originates in the fact that the matrix elements of two different spherical tensor operators of rank *k* are reduced analogously according to the *Wigner–Eckart theorem*, i.e.

$$\langle jm|\hat{T}^k_q|jm'\rangle = (-1)^{j-m}\begin{pmatrix} j & k & j \\ -m & q & m' \end{pmatrix}\langle j||\boldsymbol{T}^k||j\rangle \tag{2.35}$$

and

$$\langle jm|\hat{O}^k_q|jm'\rangle = (-1)^{j-m}\begin{pmatrix} j & k & j \\ -m & q & m' \end{pmatrix}\langle j||\boldsymbol{O}^k||j\rangle \tag{2.36}$$

The 3*j*-symbol involved represents an integral over the angular momentum functions common for both matrix elements; the reduced matrix elements $\langle j||\boldsymbol{T}^k||j\rangle$ no longer depend upon the magnetic quantum numbers. Therefore the *replacement theorem* makes it possible to write

$$\langle jm|\hat{T}^k_q|jm'\rangle = \frac{\langle j||T^k||j\rangle}{\langle j||O^k||j\rangle}\langle jm|\hat{O}^k_q|jm'\rangle = \gamma(k,j)\langle jm|\hat{O}^k_q|jm'\rangle \tag{2.37}$$

Table 7
Equivalent operators $\hat{O}_k^n$, k—spherical tensor rank, n—component

$\hat{O}_0^0 = J(J+1)$
$\hat{O}_2^0 = 3\bar{h}^{-2}\hat{J}_z^2 - J(J+1)$
$\hat{O}_2^1 = \frac{1}{4}\bar{h}^{-2}[\hat{J}_z(\hat{J}_+ + \hat{J}_-) + (\hat{J}_+ + \hat{J}_-)\hat{J}_z]$
$\hat{O}_2^2 = \frac{1}{2}\bar{h}^{-2}(\hat{J}_+^2 + \hat{J}_-^2)$
$\hat{O}_4^0 = 35\bar{h}^{-4}\hat{J}_z^4 + [-30J(J+1)+25]\bar{h}^{-2}\hat{J}_z^2 - 6J(J+1) + 3J^2(J+1)^2$
$\hat{O}_4^1 = \frac{1}{4}\bar{h}^{-2}\{[7\bar{h}^{-2}\hat{J}_z^2 - 3J(J+1)-1]\hat{J}_z(\hat{J}_+ + \hat{J}_-) + (\hat{J}_+ + \hat{J}_-)\hat{J}_z[7\bar{h}^{-2}\hat{J}_z^2 - 3J(J+1)-1]\}$
$\hat{O}_4^2 = \frac{1}{4}\bar{h}^{-2}\{[7\bar{h}^{-2}\hat{J}_z^2 - J(J+1)-5](\hat{J}_+^2 + \hat{J}_-^2) + (\hat{J}_+^2 + \hat{J}_-^2)[7\bar{h}^{-2}\hat{J}_z^2 - J(J+1)-5]\}$
$\hat{O}_4^3 = \frac{1}{4}\bar{h}^{-4}[\hat{J}_z(\hat{J}_+^3 + \hat{J}_-^3) + (\hat{J}_+^3 + \hat{J}_-^3)\hat{J}_z]$
$\hat{O}_4^4 = \frac{1}{2}\bar{h}^{-4}(\hat{J}_+^4 + \hat{J}_-^4)$
$\hat{O}_6^0 = 231\bar{h}^{-6}\hat{J}_z^6 + [-315J(J+1)+735]\bar{h}^{-4}\hat{J}_z^4 + [105J^2(J+1)^2 - 525J(J+1)+294]\bar{h}^{-2}\hat{J}_z^2 - 5J^3(J+1)^3 + 40J^2(J+1)^2 - 60J(J+1)$
$\hat{O}_6^1 = \frac{1}{4}\bar{h}^{-2}\{[35\bar{h}^{-4}\hat{J}_z^4 - (30J(J+1)-15)\bar{h}^{-2}\hat{J}_z^2 + (5J^2(J+1)^2 - 10J(J+1)+12)]\hat{J}_z(\hat{J}_+ + \hat{J}_-) + (\hat{J}_+ + \hat{J}_-)\hat{J}_z[35\bar{h}^{-4}\hat{J}_z^4 - (30J(J+1)-15)\bar{h}^{-2}\hat{J}_z^2 + (5J^2(J+1)^2 - 10J(J+1)+12)]\}$
$\hat{O}_6^2 = \frac{1}{4}\bar{h}^{-2}\{[33\bar{h}^{-4}\hat{J}_z^4 - (18J(J+1)+123)\bar{h}^{-2}\hat{J}_z^2 + J^2(J+1)^2 + 10J(J+1)+102)](\hat{J}_+^2 + \hat{J}_-^2) + (\hat{J}_+^2 + \hat{J}_-^2)[33\bar{h}^{-4}\hat{J}_z^4 - (18J(J+1)+123)\bar{h}^{-2}\hat{J}_z^2 + J^2(J+1)^2 + 10J(J+1)+102)]\}$
$\hat{O}_6^3 = \frac{1}{4}\bar{h}^{-4}\{[11\bar{h}^{-2}\hat{J}_z^2 - 3J(J+1)-59]\hat{J}_z(\hat{J}_+^3 + \hat{J}_-^3) + (\hat{J}_+^3 + \hat{J}_-^3)\hat{J}_z[11\bar{h}^{-2}\hat{J}_z^2 - 3J(J+1)-59]\}$
$\hat{O}_6^4 = \frac{1}{4}\bar{h}^{-4}\{[11\bar{h}^{-2}\hat{J}_z^2 - J(J+1)-38](\hat{J}_+^4 + \hat{J}_-^4) + (\hat{J}_+^4 + \hat{J}_-^4)[11\bar{h}^{-2}\hat{J}_z^2 - J(J+1)-38]\}$
$\hat{O}_6^5 = \frac{1}{4}\bar{h}^{-6}[\hat{J}_z(\hat{J}_+^5 + \hat{J}_-^5) + (\hat{J}_+^5 + \hat{J}_-^5)\hat{J}_z]$
$\hat{O}_6^6 = \frac{1}{2}\bar{h}^{-6}(\hat{J}_+^6 + \hat{J}_-^6)$

The shift (raising and lowering) operators interrelate to their Cartesian analogues

$\frac{1}{2}(\hat{J}_+^2 + \hat{J}_-^2) = \hat{J}_x^2 - \hat{J}_y^2$
$\frac{1}{2}(\hat{J}_+^3 + \hat{J}_-^3) = \hat{J}_x^3 - \hat{J}_x\hat{J}_y^2 - \hat{J}_y\hat{J}_x\hat{J}_y - \hat{J}_y^2\hat{J}_x$
$\frac{1}{2}(\hat{J}_+^4 + \hat{J}_-^4) = \hat{J}_x^4 + \hat{J}_y^4 - \hat{J}_x^2\hat{J}_y^2 - \hat{J}_y^2\hat{J}_x^2 - \hat{J}_x\hat{J}_y^2\hat{J}_x - \hat{J}_y\hat{J}_x^2\hat{J}_y - \hat{J}_x\hat{J}_y\hat{J}_x\hat{J}_y - \hat{J}_y\hat{J}_x\hat{J}_y\hat{J}_x$

Now the matrix element of a tensor operator is proportional to that of an equivalent operator. The angular momentum operators serve in the role of equivalent operators: instead of the irreducible tensor components a proper combination of the angular momentum operators ($\hat{J}_z$, $\hat{J}_+$, $\hat{J}_-$) is applicable. However, the expansion coefficients (the potential constants) need to be redefined accounting for the proportionality factor $\gamma(k, j)$. A set of equivalent operators is compiled in Table 7.

It is quite practical to handle the equivalent operators since

1. they can be easily constructed by matrix multiplications with the help of computers;
2. no need of an explicit form of the kets.

Important note: it is conventional to write the equivalent operators in the form $\hat{O}_k^n$, k—spherical tensor rank, n—component. This notation is just opposite to the irreducible tensor approach (ITO) where the tensor rank is the superscript.

A more general form of the zero−field splitting operator is written as

$$\hat{H}^{\mathrm{zfs}} = \sum_{k=0}^{k}\sum_{n=0} B_k^n \hat{O}_k^n \tag{2.38}$$

where only even terms ($k = 0, 2, 4$ and 6) can contribute; $\hat{O}_k^n$ are the operator equivalents and B_k^n the interaction constants. The maximum power is determined by the value of the spin number since the restrictions are: $k \leq 2$ for $S = 1$ and 3/2, $k \leq 4$ for $S = 2$ and 5/2, $k \leq 6$ for $S = 3$ and 7/2. Now we can see that for $S \geq 2$, in addition to the second–order equivalent operators, the fourth–order equivalent operators can contribute. These, in fact, correspond to higher–order spin–spin interaction—a biquadratic spin–spin interaction, like

$$\hat{H}^{\mathrm{bq}} = b(\hat{S}\cdot\hat{S})^2 \tag{2.39}$$

The biquadratic ZFS involves the case of $S = 5/2$, e.g. the Fe(III) or Mn(II) complexes. The second relevant case of $S = 2$ is of lower applicability since the orbital contribution (e.g. in the high-spin Fe(II) complexes) dominates.

In the case of a perfect octahedral symmetry (the z-axis being coincident with the $\hat{C}_4$ rotational axis) the biquadratic term is

$$\begin{aligned}\hat{H}^{\mathrm{bq}} &= B_4^0\hat{O}_4^0 + B_4^4\hat{O}_4^4 = B_4(\hat{O}_4^0 + 5\hat{O}_4^4)\\ &= \tfrac{1}{6}a\{\bar{h}^{-4}(\hat{S}_x^4+\hat{S}_y^4+\hat{S}_z^4) - \tfrac{1}{5}S(S+1)(3S^2+3S-1)\}\end{aligned} \tag{2.40}$$

with the relationship among the Hamiltonian parameters as follows $a = 120B_4 = 120B_4^0 = 24B_4^4$. The corresponding matrix elements for $S = 5/2$ were included in Table 4 giving the zero–field eigenvalues: $\varepsilon_{1,2} = -2a$ and $\varepsilon_{3,4,5,6} = +a$. The separation of the quartet state from the ground doublet is $\Delta\varepsilon = 3a$. Such a result is correct from the viewpoint of the double group theory: the group $\mathbf{O}'$ can have only the doubly degenerate Γ_7 or quadruply degenerate Γ_8 irreducible

representations. The above result is well fulfilled either for perfect octahedral symmetry or perfect tetrahedral symmetry of the coordination polyhedron.

However one can pass from the fourfold axis coordinate system to a threefold one (the *z*-axis being coincident with the $\hat{C}_3$ rotational axis); the matrix elements are contained in Table 4 and they yield exactly the same eigenvalues as before.

The addition of the Zeeman term along either the fourfold or threefold axes leads to the eigenvalues listed in Table 8. The expansion of the square roots, restricted to the quadratic terms, yield approximate expressions for the energy levels. In this step it is assumed that the magnetic field is much lower than the cubic zero–field splitting parameter: $G_\parallel = \mu_B g_\parallel B \ll a$. Fig. 4 displays the information of how the energy levels are split under the influence of the magnetic field. As a consequence of the cubic symmetry the energy levels in the perpendicular direction should be the same as in the parallel direction and the *g*-values are isotropic.

In the case of the distorted cubic symmetry of the coordination polyhedron the zero–field splitting Hamiltonian adopts the form again contained in Table 8. (One must be careful of definitions of the Hamiltonian parameters when comparing different sources since other notations can also be met in literature.) The *F*-term enters only the diagonal matrix elements; the *a*-term enters the off-diagonal matrix elements situated by four positions outside the main diagonal (see Table 4).

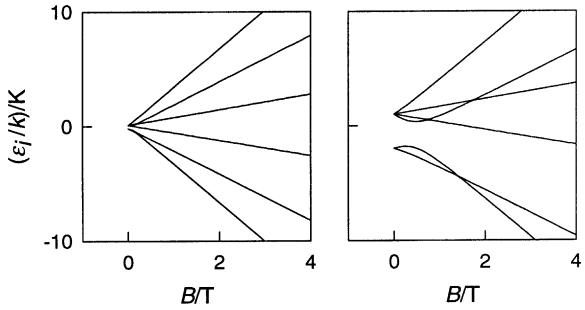

Fig. 4. Exact energy levels of an $S = 5/2$ system in the cubic symmetry: $a/k = 0.1$ K (left) and 1 K (right).

Table 8
Hamiltonian and energy levels for ZFS systems with $S = 5/2$

System	Exact energy levels ε_1 through ε_6	Approximate energy[a]
(a) Octahedral symmetry, $B = 0$	$\hat{H}^{bq}(\mathbf{O}_h, \hat{C}_4) = B_4^0\hat{O}_4^0 + B_4^4\hat{O}_4^4 = B_4(\hat{O}_4^0 + 5\hat{O}_4^4)$, $a = 120B_4 = 120B_4^0 = 24B_4^4$	
	$\hat{H}^{bq}(\mathbf{O}_h, \hat{C}_4) = \frac{1}{6}a\{\bar{h}^{-4}(\hat{S}_x^4 + \hat{S}_y^4 + \hat{S}_z^4) - \frac{1}{5}S(S+1)(3S^2+3S-1)\}$	
	$\hat{H}^{bq}(\mathbf{O}_h, \hat{C}_3) = -\frac{2}{3}B_4(\hat{O}_4^0 + 20\sqrt{2}\hat{O}_4^3)$, $a = -80B_4^0 = -1600\sqrt{2}B_4^3$	
	$\varepsilon_{1,2} = -2a$; $\varepsilon_{3,4,5,6} = a$	
(b) Magnetic field applied along the $\hat{C}_4$ axis	$\pm\frac{1}{2}G_\parallel + a$	$a \pm (1/2)G_\parallel$
	$\frac{1}{2}(\pm G_\parallel - a) + [(a \pm 2G_\parallel)^2 + \frac{5}{4}a^2]^{1/2}$	$a \pm (11/6)G_\parallel + (20/27)(G_\parallel^2/a)$
	$\frac{1}{2}(\pm G_\parallel - a) - [(a \pm 2G_\parallel)^2 + \frac{5}{4}a^2]^{1/2}$	$-2a \pm (5/6)G_\parallel - (20/27)(G_\parallel^2/a)$
(c) Magnetic field applied along the $\hat{C}_3$ axis	$\pm\frac{3}{2}G_\parallel + a$	$a \pm (3/2)G_\parallel$
	$\pm G_\parallel - \frac{1}{2}a + (1/6)[(a \pm 9G_\parallel)^2 + 80a^2]^{1/2}$	$a \pm (7/6)G_\parallel + (20/27)(G_\parallel^2/a)$
	$\pm G_\parallel - \frac{1}{2}a - (1/6)[(a \pm 9G_\parallel)^2 + 80a^2]^{1/2}$	$-2a \pm (5/6)G_\parallel - (20/27)(G_\parallel^2/a)$
(d) Tetragonal distortion, $\mathbf{D}_{4h}$, $B = 0$	$\hat{H}^{zfs(4)}(\mathbf{D}_{4h}, \hat{C}_4) = B_2^0\hat{O}_2^0 + (B_2^2\hat{O}_2^2) + B_4^0\hat{O}_4^0 + B_4(\hat{O}_4^0 + 5\hat{O}_4^4)$[b]	
	$\hat{H}^{zfs(4)} = D\{\bar{h}^{-2}\hat{S}_z^2 - \frac{1}{3}S(S+1)\} + E\bar{h}^{-2}(\hat{S}_x^2 - \hat{S}_y^2) + \frac{1}{6}a\{\bar{h}^{-4}(\hat{S}_\xi^4 + \hat{S}_\eta^4 + \hat{S}_\zeta^4) - \frac{1}{5}S(S+1)$	
	$(3S^2+3S-1)\} + \frac{1}{180}F\{35\bar{h}^{-4}\hat{S}_z^4 - 30S(S+1)\bar{h}^{-2}\hat{S}_z^2 + 25\bar{h}^{-2}\hat{S}_z^2 - 6S(S+1) + 3S^2(S+1)^2\}$	
	$a = 120B_4$, $D = 3B_2^0$, $E = B_2^2$, $F = 180B_4^0$	
	$a' - \frac{8}{3}D$	
	$-\frac{1}{2}a' + \frac{4}{3}D + [(a'+2D)^2 + \frac{5}{4}a^2]^{1/2}$	
	$-\frac{1}{2}a' + \frac{4}{3}D - [(a'+2D)^2 + \frac{5}{4}a^2]^{1/2}$	
	with $a' = a + \frac{2}{3}F$	
(e) Trigonal distortion, $\mathbf{D}_3$, $B = 0$	$\hat{H}^{zfs(4)}(\mathbf{D}_3, \hat{C}_3) = B_2^0\hat{O}_2^0 + (B_2^2\hat{O}_2^2) + B_4^0\hat{O}_4^0 - \frac{2}{3}B_4(\hat{O}_4^0 + \sqrt{800}\hat{O}_4^3)$[b]	
	$a = 120B_4$, $D = 3B_2^0$, $E = B_2^2$, $F = 180B_4^0$	
	$a'' - \frac{2}{3}D$	
	$-\frac{1}{2}a'' + \frac{1}{3}D + \frac{1}{6}[(a''+18D)^2 + 80a^2]^{1/2}$	
	$-\frac{1}{2}a'' + \frac{1}{3}D - \frac{1}{6}[(a''+18D)^2 + 80a^2]^{1/2}$	
	with $a'' = a - F$	

[a] After expansion of square root $\varepsilon = c_0 + c_1G + c_2G^2 + O_3$ for $G_\parallel = \mu_B g_\parallel B \ll a$.

[b] ξ, η and ζ—the fourfold axes for the cubic part of the crystal field. The *z*-axis is chosen along either the tetragonal axis (when *x*, *y* and *z* coincide with ξ, η and ζ) or the trigonal [1 1 1] axis of the crystal.

The g-values of the overall spin-Hamiltonian should retain axial symmetry: $g_z = g_\parallel$ and $g_x = g_y = g_\perp$. Having the energy levels determined and the van Vleck coefficient identified, one can proceed with the van Vleck formula for the mean magnetic susceptibility of a linear magnetic material. Alternatively, one can proceed with the solution of the eigenvalue problem for three input fields and a numerical determination of the van Vleck coefficients.

2.5. Modeling the magnetization

Having determined the magnetic energy levels, the partition function is defined

$$Z_a(B,T) = \sum_i \exp\left(\frac{-\varepsilon_{i,a}}{kT}\right) \tag{2.41}$$

from which the molar magnetization is calculated as

$$\begin{aligned} M_a(B,T) &= N_\mathrm{A}\frac{1}{Z_a}\frac{\partial Z_a}{\partial B_a} \\ &= N_\mathrm{A}\frac{1}{Z_a}\sum_i\left(-\frac{\partial\varepsilon_{i,a}}{\partial B_a}\right)\exp\left(\frac{-\varepsilon_{i,a}}{kT}\right) \end{aligned} \tag{2.42}$$

Since the exact eigenvalues for some ZFS systems are available (Table 9) they permit an exact modeling of the magnetization $M_a(B,T) = f(D,E,g_a)$ in the whole range of variables and parameters. The corresponding closed formulae are listed in Table 10.

In the case of $E = 0$, modeling of the magnetization in the parallel direction is an easy task since there exists a closed formula for the magnetic energy levels $\varepsilon_\parallel = f(D,B_z)$. In this case for positive D, wave-type behavior is observed (Fig. 5). This effect originates in a level crossing: with increasing field a magnetically more productive level becomes the ground state and this is going to be saturated unless an even more magnetically productive state is crossed (see Fig. 2 for the explanation). The resolution of the steps on the magnetization curve depends upon the balance between T, B and D. For fixed T and low D no resolution is observed. With increasing D the steps become readily visible at higher fields.

In the perpendicular direction, however, the situation is different. A complete modeling using a numerical approach is given by Fig. 6. The magnetization curves were generated at a fixed temperature as parametric functions of D. We can conclude that:

Table 9
Exact eigenvalues and magnetic functions for some ZFS systems[a]

Spin	Direction	Shifted eigenvalues ε_{ia}	
		For $E \neq 0$	For $E = 0$
$S = 1$	z	$\varepsilon_{1z} = D + (E^2 + G_z^2)^{1/2}$	$\varepsilon_{1z} = D + G_z$
		$\varepsilon_{2z} = 0$	$\varepsilon_{2z} = 0$
		$\varepsilon_{3z} = D - (E^2 + G_z^2)^{1/2}$	$\varepsilon_{3z} = D - G_z$
	x	$\varepsilon_{1x} = D + E$	$\varepsilon_{1x} = D$
		$\varepsilon_{2x} = \frac{1}{2}(D-E) - [\frac{1}{4}(D-E)^2 + G_x^2]^{1/2}$	$\varepsilon_{2x} = \frac{1}{2}[D - (D^2 + 4G_x^2)^{1/2}]$
		$\varepsilon_{3x} = \frac{1}{2}(D-E) + [\frac{1}{4}(D-E)^2 + G_x^2]^{1/2}$	$\varepsilon_{3x} = \frac{1}{2}[D + (D^2 + 4G_x^2)^{1/2}]$
	y	$\varepsilon_{1y} = \frac{1}{2}(D+E) + [\frac{1}{4}(D+E)^2 + G_y^2]^{1/2}$	
		$\varepsilon_{2y} = \frac{1}{2}(D+E) - [\frac{1}{4}(D+E)^2 + G_y^2]^{1/2}$	
		$\varepsilon_{3y} = D - E$	
$S = 3/2$[b]	z	$\varepsilon_{1z} = D + \frac{1}{2}G_z + [(D+G_z)^2 + 3E^2]^{1/2}$	$\varepsilon_{1z} = D + \frac{1}{2}G_z + \lvert D + G_z\rvert$
		$\varepsilon_{2z} = D - \frac{1}{2}G_z + [(D-G_z)^2 + 3E^2]^{1/2}$	$\varepsilon_{2z} = D - \frac{1}{2}G_z + \lvert D - G_z\rvert$
		$\varepsilon_{3z} = D + \frac{1}{2}G_z - [(D+G_z)^2 + 3E^2]^{1/2}$	$\varepsilon_{3z} = D + \frac{1}{2}G_z - \lvert D + G_z\rvert$
		$\varepsilon_{4z} = D - \frac{1}{2}G_z - [(D-G_z)^2 + 3E^2]^{1/2}$	$\varepsilon_{4z} = D - \frac{1}{2}G_z - \lvert D - G_z\rvert$
	x	$\varepsilon_{1x} = D + \frac{1}{2}G_x + [(D-\frac{1}{2}G_x)^2 + 3(E+\frac{1}{2}G_x)^2]^{1/2}$	$\varepsilon_{1x} = D + \frac{1}{2}G_x + (D^2 + G_x^2 - DG_x)^{1/2}$
		$\varepsilon_{2x} = D - \frac{1}{2}G_x + [(D+\frac{1}{2}G_x)^2 + 3(E-\frac{1}{2}G_x)^2]^{1/2}$	$\varepsilon_{2x} = D - \frac{1}{2}G_x + (D^2 + G_x^2 + DG_x)^{1/2}$
		$\varepsilon_{3x} = D + \frac{1}{2}G_x - [(D-\frac{1}{2}G_x)^2 + 3(E+\frac{1}{2}G_x)^2]^{1/2}$	$\varepsilon_{3x} = D + \frac{1}{2}G_x - (D^2 + G_x^2 - DG_x)^{1/2}$
		$\varepsilon_{4x} = D - \frac{1}{2}G_x - [(D+\frac{1}{2}G_x)^2 + 3(E-\frac{1}{2}G_x)^2]^{1/2}$	$\varepsilon_{4x} = D - \frac{1}{2}G_x - (D^2 + G_x^2 + DG_x)^{1/2}$
	y	$\varepsilon_{1y} = D + \frac{1}{2}G_y + [(D-\frac{1}{2}G_y)^2 + 3(E-\frac{1}{2}G_y)^2]^{1/2}$	
		$\varepsilon_{2y} = D - \frac{1}{2}G_y + [(D+\frac{1}{2}G_y)^2 + 3(E+\frac{1}{2}G_y)^2]^{1/2}$	
		$\varepsilon_{3y} = D + \frac{1}{2}G_y - [(D-\frac{1}{2}G_y)^2 + 3(E-\frac{1}{2}G_y)^2]^{1/2}$	
		$\varepsilon_{4y} = D - \frac{1}{2}G_y - [(D+\frac{1}{2}G_y)^2 + 3(E+\frac{1}{2}G_y)^2]^{1/2}$	

[a] Substitution: $G_a = g_a\mu_\mathrm{B}B_a$.
[b] The constant value of D can be omitted in the partition function (a shift of the energy origin).

Table 10
Exact magnetization formulae for some ZFS systems

For $S = 1$

$$M_z = \frac{1}{2}\frac{N_A\mu_B g_z}{Z_z}\left\langle \exp\left\{-\frac{D+\sqrt{E^2+G_z^2}}{kT}\right\}\left\{\frac{-2G_z}{\sqrt{E^2+G_z^2}}\right\} + \exp\left\{-\frac{D-\sqrt{E^2+G_z^2}}{kT}\right\}\left\{\frac{2G_z}{\sqrt{E^2+G_z^2}}\right\}\right\rangle$$

$$M_x = \frac{1}{2}\frac{N_A\mu_B g_x}{Z_x}\left\langle \exp\left\{-\frac{(D-E)/2-\sqrt{(D-E)^2/4+G_x^2}}{kT}\right\}\left\{\frac{2G_x}{\sqrt{(D-E)^2/4+G_x^2}}\right\}\right.$$
$$\left. +\exp\left\{-\frac{(D-E)/2+\sqrt{(D-E)^2/4+G_x^2}}{kT}\right\}\left\{\frac{-2G_x}{\sqrt{(D-E)^2/4+G_x^2}}\right\}\right\rangle$$

$$M_y = \frac{1}{2}\frac{N_A\mu_B g_y}{Z_y}\left\langle \exp\left\{-\frac{(D+E)/2+\sqrt{(D+E)^2/4+G_y^2}}{kT}\right\}\left\{\frac{-2G_y}{\sqrt{(D+E)^2/4+G_y^2}}\right\}\right.$$
$$\left. +\exp\left\{-\frac{(D+E)/2-\sqrt{(D+E)^2/4+G_y^2}}{kT}\right\}\left\{\frac{2G_y}{\sqrt{(D+E)^2/4+G_y^2}}\right\}\right\rangle$$

$$Z_z = \exp\left\{-\frac{D+\sqrt{E^2+G_z^2}}{kT}\right\} + 1 + \exp\left\{-\frac{D-\sqrt{E^2+G_z^2}}{kT}\right\}$$

$$Z_x = \exp\left\{-\frac{D+E}{kT}\right\} + \exp\left\{-\frac{(D-E)/2-\sqrt{(D-E)^2/4+G_x^2}}{kT}\right\} + \exp\left\{-\frac{(D-E)/2+\sqrt{(D-E)^2/4+G_x^2}}{kT}\right\}$$

$$Z_y = \exp\left\{-\frac{D-E}{kT}\right\} + \exp\left\{-\frac{(D+E)/2+\sqrt{(D+E)^2/4+G_y^2}}{kT}\right\} + \exp\left\{-\frac{(D+E)/2-\sqrt{(D+E)^2/4+G_y^2}}{kT}\right\}$$

For $S = 3/2$

$$M_z = -\frac{1}{2}\frac{N_A\mu_B g_z}{Z_z}\left\langle \exp\left\{-\frac{+G_z/2+\sqrt{(D+G_z)^2+3E^2}}{kT}\right\}\left\{+1+\frac{+2(D+G_z)}{\sqrt{(D+G_z)^2+3E^2}}\right\}\right.$$
$$+\exp\left\{-\frac{-G_z/2+\sqrt{(D-G_z)^2+3E^2}}{kT}\right\}\left\{-1+\frac{-2(D-G_z)}{\sqrt{(D-G_z)^2+3E^2}}\right\}$$
$$\left. +\exp\left\{-\frac{+G_z/2-\sqrt{(D+G_z)^2+3E^2}}{kT}\right\}\left\{+1-\frac{+2(D+G_z)}{\sqrt{(D+G_z)^2+3E^2}}\right\} + \exp\left\{-\frac{-G_z/2-\sqrt{(D-G_z)^2+3E^2}}{kT}\right\}\left\{-1-\frac{-2(D-G_z)}{\sqrt{(D-G_z)^2+3E^2}}\right\}\right\rangle$$

$$M_x = -\frac{1}{2}\frac{N_A\mu_B g_x}{Z_x}\left\langle \exp\left\{-\frac{+G_x/2+\sqrt{(D-G_x/2)^2+3(E+G_x/2)^2}}{kT}\right\}\left\{+1+\frac{-(D-G_x/2)+3(E+G_x/2)}{\sqrt{(D-G_x/2)^2+3(E+G_x/2)^2}}\right\}\right.$$
$$+\exp\left\{-\frac{-G_x/2+\sqrt{(D+G_x/2)^2+3(E-G_x/2)^2}}{kT}\right\}\left\{-1+\frac{+(D+G_x/2)-3(E-G_x/2)}{\sqrt{(D+G_x/2)^2+3(E-G_x/2)^2}}\right\}$$
$$+\exp\left\{-\frac{+G_x/2-\sqrt{(D-G_x/2)^2+3(E+G_x/2)^2}}{kT}\right\}\left\{+1-\frac{-(D-G_x/2)+3(E+G_x/2)}{\sqrt{(D-G_x/2)^2+3(E+G_x/2)^2}}\right\}$$
$$\left. +\exp\left\{-\frac{-G_x/2-\sqrt{(D+G_x/2)^2+3(E-G_x/2)^2}}{kT}\right\}\left\{-1-\frac{+(D+G_x/2)-3(E-G_x/2)}{\sqrt{(D+G_x/2)^2+3(E-G_x/2)^2}}\right\}\right\rangle$$

$$M_y = -\frac{1}{2}\frac{N_A\mu_B g_y}{Z_y}\left\langle \exp\left\{-\frac{+G_y/2+\sqrt{(D-G_y/2)^2+3(E-G_y/2)^2}}{kT}\right\}\left\{+1+\frac{-(D-G_y/2)-3(E-G_y/2)}{\sqrt{(D-G_y/2)^2+3(E-G_y/2)^2}}\right\}\right.$$
$$+\exp\left\{-\frac{-G_y/2+\sqrt{(D+G_y/2)^2+3(E+G_y/2)^2}}{kT}\right\}\left\{-1+\frac{+(D+G_y/2)+3(E+G_y/2)}{\sqrt{(D+G_y/2)^2+3(E+G_y/2)^2}}\right\}$$
$$+\exp\left\{-\frac{+G_y/2-\sqrt{(D-G_y/2)^2+3(E-G_y/2)^2}}{kT}\right\}\left\{+1-\frac{-(D-G_y/2)-3(E-G_y/2)}{\sqrt{(D-G_y/2)^2+3(E-G_y/2)^2}}\right\}$$
$$\left. +\exp\left\{-\frac{-G_y/2-\sqrt{(D+G_y/2)^2+3(E+G_y/2)^2}}{kT}\right\}\left\{-1-\frac{+(D+G_y/2)+3(E+G_y/2)}{\sqrt{(D+G_y/2)^2+3(E+G_y/2)^2}}\right\}\right\rangle$$

Table 10 (*Continued*)

$$Z_z = \exp\left\{-\frac{+G_z/2+\sqrt{(D+G_z)^2+3E^2}}{kT}\right\}+\exp\left\{-\frac{-G_z/2+\sqrt{(D-G_z)^2+3E^2}}{kT}\right\}$$
$$+\exp\left\{-\frac{+G_z/2-\sqrt{(D+G_z)^2+3E^2}}{kT}\right\}+\exp\left\{-\frac{-G_z/2-\sqrt{(D-G_z)^2+3E^2}}{kT}\right\}$$
$$Z_x = \exp\left\{-\frac{+G_x/2+\sqrt{(D-G_x/2)^2+3(E+G_x/2)^2}}{kT}\right\}+\exp\left\{-\frac{-G_x/2+\sqrt{(D+G_x/2)^2+3(E-G_x/2)^2}}{kT}\right\}$$
$$+\exp\left\{-\frac{+G_x/2-\sqrt{(D-G_x/2)^2+3(E+G_x/2)^2}}{kT}\right\}+\exp\left\{-\frac{-G_x/2-\sqrt{(D+G_x/2)^2+3(E-G_x/2)^2}}{kT}\right\}$$
$$Z_y = \exp\left\{-\frac{+G_y/2+\sqrt{(D-G_y/2)^2+3(E-G_y/2)^2}}{kT}\right\}+\exp\left\{-\frac{-G_y/2+\sqrt{(D+G_y/2)^2+3(E+G_y/2)^2}}{kT}\right\}$$
$$+\exp\left\{-\frac{+G_y/2-\sqrt{(D-G_y/2)^2+3(E-G_y/2)^2}}{kT}\right\}+\exp\left\{-\frac{-G_y/2-\sqrt{(D+G_y/2)^2+3(E+G_y/2)^2}}{kT}\right\}$$

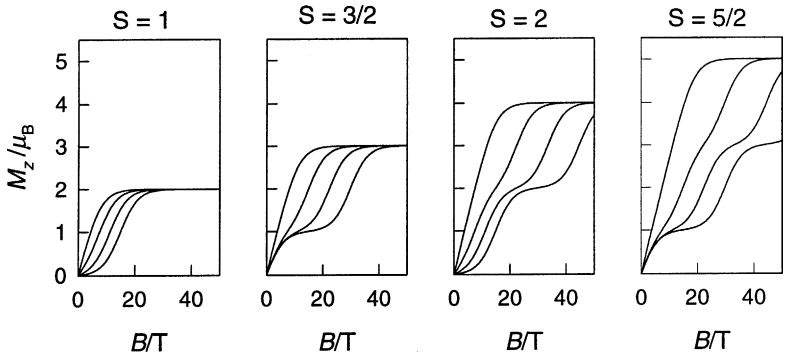

Fig. 5. Parallel magnetization per atom vs. magnetic field for zero-field splitting systems: $T = 4.2$ K; $D/k = 5$, 10, 15 and 20 K.

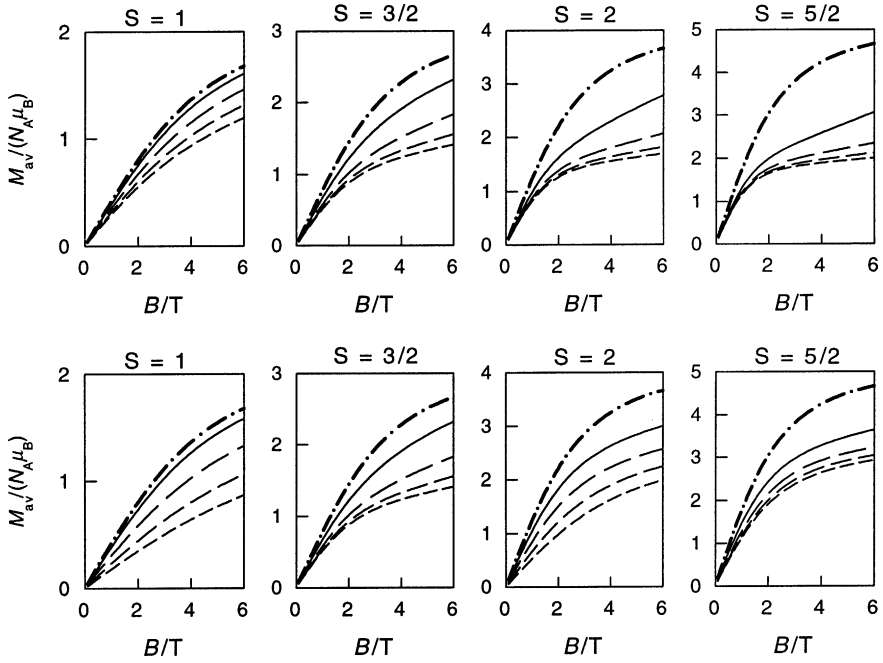

Fig. 6. Magnetization curves for various ZFS systems modeled as a powder average at $T = 4.2$ K; top panel: $D/k = -5$ K (solid), -10 K (long dashed), -15 K (medium dashed), -20 K (short dashed); bottom panel: $D/k = +5$ K (solid), 10 K (long dashed), 15 K (medium dashed), 20 K (short dashed). Brillouin function for a Curie paramagnet—dot-dashed.

(a) with increasing $|D|$ the magnetization curves clearly decline from the Brillouin function (that refers to a Curie paramagnet with no ZFS);
(b) the sign of the D-parameter is unambiguously determined if single crystal experiments are undertaken;
(c) the powder average is less able to distinguish the sign of the D-parameter as the behavior of the parallel and perpendicular components are opposite each to other;
(d) the lowering of the magnetization is more pronounced for negative D (except the $S = 1$ system).

The Brillouin-function behavior mentioned above means

$$M = (N_{\mathrm{A}} g_{\mathrm{eff}} \mu_{\mathrm{B}} S) \left\{ \frac{S+1/2}{S} \coth[\eta(S+1/2)] - \frac{1}{2S} \coth\left(\frac{\eta}{2}\right) \right\} \quad (2.43)$$

for the argument $\eta = g_{\mathrm{eff}} \mu_{\mathrm{B}} B_z / kT$.

2.6. Modeling the magnetic susceptibility

As discussed above, the magnetic susceptibility can be probed to several degrees of the complexity as classified below.

For low magnetic fields the van Vleck formula is applicable and perturbation theory yields the energy levels and susceptibility formulae presented in Table 11. In such a case, the closed formulae were derived for the individual components and these are listed in Table 12. One should be careful in the application of these formulae as they were derived on the basis of perturbation theory. The principal assumption that the ZFS is much larger than the spin Zeeman term should not be avoided: otherwise the perpendicular component of the susceptibility diverges for small D.

The modeling of the product functions for the individual ZFS systems is shown in Fig. 7. We observe that

1. the product functions (obeying the Curie law at higher temperature) drop as the temperature is lowered;
2. the magnetic anisotropy manifests itself not only in the different values of the susceptibility components but also in their different curvature;
3. when the temperature is not low enough it might be difficult (or even impossible) to determine the sign of the D-parameter from the powder data alone;
4. for $D > 0$ the parallel, χ_z, component decreases monotonously and the perpendicular, χ_x component passes through a maximum on lowering the temperature; for $D < 0$ the χ_x component drops to zero whereas the χ_z component reaches a plateau (variation method was applied in modeling in order to avoid singularities).

Modeling of non-linear magnetic behavior is shown in Fig. 8. It is seen that the parallel component of the susceptibility for $D > 0$ shows an oscillating behavior. This originates in the correct derivatives of the magnetization obtained via the formula

$$\tilde{\chi}_a(B,T) = N_{\mathrm{A}} \mu_0 kT \frac{T_{2a} Z_a - T_{1a}^2}{Z_a^2} \quad (2.44)$$

Table 11
Formulae for the zero-field splitting systems

Derivation
Hamiltonian: $\hat{H}_a = D\bar{h}^{-2}(S_z^2 - \hat{S}^2/3) + \mu_{\mathrm{B}}\bar{h}^{-1} g_a B_a \hat{S}_a$
Perturbation theory for eigenvalues (except $S = 1$, where the variation method is applied)
van Vleck equation (linear magnetics)

Restrictions
D—not too small, $D \gg g_x \mu_{\mathrm{B}} B$, otherwise χ_x diverges
B—not too high ($B < 1$ T)

Formula: $\bar{\chi}_a = \dfrac{C_0 g_a^2}{T} \dfrac{\mathrm{Num}_a}{\mathrm{Den}}$
Directions: $a = x, z$, denominator: $\mathrm{Den} = \sum_{M=-S}^{+S} \exp(-B_M \delta)$, argument $\delta = D/kT$

Parallel direction	Perpendicular direction
$\mathrm{Num}_z = \sum_{M=-S}^{+S} C_{M,z} \exp(-B_M \delta)$	$\mathrm{Num}_x = \sum_{M=-S}^{+S} (C_{M,x} - 2D_{M,x}/\delta) \exp(-B_M \delta)$
van Vleck coefficients	
$B_M = \varepsilon_M^{(0)} = D[M^2 - S(S+1)/3]$	$B_M = \varepsilon_M^{(0)} = D[M^2 - S(S+1)/3]$
$C_{M,z} = \varepsilon_{M,z}^{(1)}/(\mu_{\mathrm{B}} g_z)$	$C_{M,x} = \varepsilon_{M,x}^{(1)}/(\mu_{\mathrm{B}} g_x)$
$\varepsilon_{M,z}^{(1)} = \mu_{\mathrm{B}} g_z M$	$D_{M,x} = \varepsilon_{M,x}^{(2)}/(\mu_{\mathrm{B}} g_x)^2$
	$\varepsilon_{M,x}^{(1)} = 0$, except the Kramers doublet $\lvert S, \pm 1/2\rangle$
	$\varepsilon_{M,x}^{(2)} = (\mu_{\mathrm{B}} g_x)^2 \dfrac{M^2 + S(S+1)}{2(4M^2-1)D}$, except the Kramers doublet $\lvert S, \pm 1/2\rangle$
	For Kramers doublet $\lvert S, \pm 1/2\rangle$:
	$\varepsilon_{M=\pm 1/2,x}^{(1)} = \pm \mu_{\mathrm{B}} g_x (S+1/2)/2$
	$\varepsilon_{M=\pm 1/2,x}^{(2)} = -(\mu_{\mathrm{B}} g_x)^2 \left[(S-1/2)(S+3/2)\right]/8D$

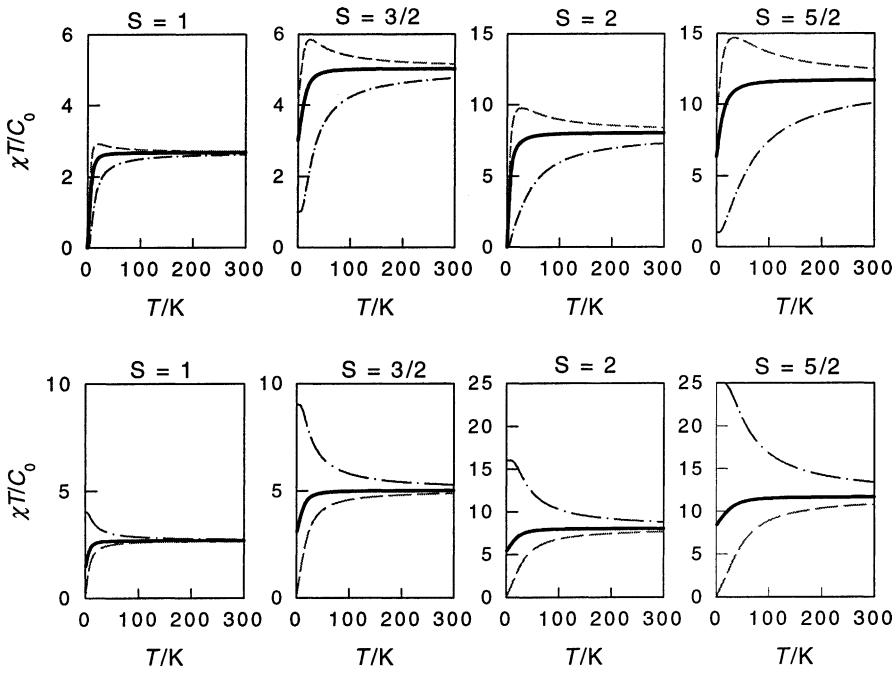

Fig. 7. Product functions for the ZFS systems ($E = 0$); top panel: $D/k = 20$ K; dot-dashed—$\chi_{\parallel}$; short dashed—$\chi_{\perp}$; solid—χ_{av}; bottom panel: $D/k = -20$ K; dot-dashed—$\chi_{\parallel}$; short dashed—$\chi_{\perp}$; solid—χ_{av}.

with the terms

$$T_{1a} \equiv \frac{\partial Z_a}{\partial B_a} = \frac{1}{kT}\sum_i \left(-\frac{\partial \varepsilon_{i,a}}{\partial B_a}\right) \exp\left(\frac{-\varepsilon_{i,a}}{kT}\right) \tag{2.45}$$

$$T_{2a} \equiv \frac{\partial^2 Z_a}{\partial B_a^2} = \frac{1}{kT}\sum_i \left[\frac{1}{kT}\left(\frac{\partial \varepsilon_{i,a}}{\partial B_a}\right)^2 - \left(\frac{\partial^2 \varepsilon_{i,a}}{\partial B_a^2}\right)\right] \times \exp\left(\frac{-\varepsilon_{i,a}}{kT}\right) \tag{2.46}$$

It was assumed so far that the powder average could be performed by a simple formula

$$\chi_{\mathrm{av}} = \tfrac{1}{3}(\chi_x + \chi_y + \chi_z) \tag{2.47}$$

For a more precise average of the powder molar susceptibility a numerical integration over the polar angles is possible

$$\chi_{\mathrm{av}} = \frac{1}{4\pi}\int_0^{\pi}\int_0^{2\pi} \chi(\vartheta,\varphi)\sin\vartheta\,\mathrm{d}\vartheta\,\mathrm{d}\varphi = -\frac{1}{4\pi}\int_{-1}^{+1}\left[\int_0^{2\pi}\chi(\vartheta,\varphi)\,\mathrm{d}\varphi\right]\mathrm{d}(\cos\vartheta) \tag{2.48}$$

The (spin) Zeeman term entering the total magnetic Hamiltonian is expressed as

$$\hat{H}'(\vartheta_k,\varphi_l) = \mu_{\mathrm{B}} B_m \hbar^{-1}(g_x \sin\vartheta_k\cos\varphi_l \hat{S}_x + g_y \sin\vartheta_k \sin\varphi_l \hat{S}_y + g_z \cos\vartheta_k \hat{S}_z) \tag{2.49}$$

and this generates the angular dependent susceptibility. In practice a sphere is cut into several discrete grid points, say 25 values for ϑ_k and 25 values for φ_l, at which the susceptibility is evaluated. Then the integral is substituted for the finite sum formula

$$\chi_{\mathrm{av}} = \frac{\sum_k \sum_l \chi(\vartheta_k,\varphi_l)\Delta_k(\cos\vartheta)\Delta_l(\varphi)}{\sum_k \sum_l \Delta_k(\cos\vartheta)\Delta_l(\varphi)} \tag{2.50}$$

When $E = 0$ the powder average runs only over the angle ϑ

$$\chi_{\mathrm{av}} = \frac{\sum_k \chi(\vartheta_k)\Delta_k(\cos\vartheta)}{\sum_k \Delta_k(\cos\vartheta)} \tag{2.51}$$

whereas the average over the angle φ results in the factor 2π.

2.7. Modeling the heat capacity

Temperature dependence of the magnetic susceptibility and field(temperature) dependence of the magnetization reflect the Boltzmann population of the lowest energy levels in the system under study. However, there is the third thermodynamic function reflecting the separation of the lowest energy levels—the heat capacity. Thus, from calorimetric data one can subtract the D-values as well [16,22].

In classical thermodynamics (the volume work is $\mathrm{d}w = -p\,\mathrm{d}V$ (J)) we are left with two kinds of heat capacities, namely

$$C_V = \left(\frac{\partial U(S,V)}{\partial T}\right)_V = N_{\mathrm{A}}\frac{\partial}{\partial T}\left[kT^2\left(\frac{\partial \ln Z}{\partial T}\right)_V\right]_V \tag{2.52}$$

$$C_p = \left(\frac{\partial E(S,p)}{\partial T}\right)_p = N_{\mathrm{A}}\frac{\partial}{\partial T}\left[kT^2\left(\frac{\partial \ln Z}{\partial T}\right)_V + kT\left(\frac{\partial \ln Z}{\partial \ln V}\right)_T\right]_p \tag{2.53}$$

Table 12
Formulae for the susceptibility components of an axial ZFS system ($D \neq 0$, $E = 0$)[a,b]

$S = 1$
$\chi_\parallel = (C_0 g_\parallel^2/T)(2d)/Z_0$
$\chi_\perp = (C_0 g_\perp^2/T)(2/\delta)(1-d)/Z_0$
$Z_0 = 1 + 2d$

$S = 2$
$\chi_\parallel = (C_0 g_\parallel^2/T)2(d + 4d^4)/Z_0$
$\chi_\perp = (C_0 g_\perp^2/T)(2/\delta)[3 - (7/3)d - (2/3)d^4]/Z_0$
$Z_0 = 1 + 2d + 2d^4$

$S = 3$
$\chi_\parallel = (C_0 g_\parallel^2/T)2(d + 4d^4 + 9d^9)/Z_0$
$\chi_\perp = (C_0 g_\perp^2/T)(2/\delta)[6 - (26/6)d - (16/15)d^4 - (6/10)d^9]/Z_0$
$Z_0 = 1 + 2d + 2d^4 + 2d^9$

$S = 3/2$
$\chi_\parallel = (C_0 g_\parallel^2/T)(1/4)(1 + 9d^2)/Z_0$
$\chi_\perp = (C_0 g_\perp^2/T)[1 + (3/4\delta)(1 - d^2)]/Z_0$
$Z_0 = 1 + d^2$

$S = 5/2$
$\chi_\parallel = (C_0 g_\parallel^2/T)(1/4)(1 + 9d^2 + 25d^6)/Z_0$
$\chi_\perp = (C_0 g_\perp^2/T)[9/4 + (2/\delta) - (11/8\delta)d^2 - (5/8\delta)d^6]/Z_0$
$Z_0 = 1 + d^2 + d^6$

$S = 7/2$
$\chi_\parallel = (C_0 g_\parallel^2/T)(1/4)(1 + 9d^2 + 25d^6 + 49d^{12})/Z_0$
$\chi_\perp = (C_0 g_\perp^2/T)[4 + (15/4\delta) - (9/4\delta)d^2 - (11/12\delta)d^6 - (7/12\delta)d^{12}]/Z_0$
$Z_0 = 1 + d^2 + d^6 + d^{12}$

[a] Argument $\delta = D/kT$; $d = \exp(-D/kT)$; $C_0 = N_A \mu_0 \mu_B^2/k$.
[b] Restriction: $D \gg g_\perp \mu_B B_\perp$; D—not too small, B—not too high, T—not too low.

In magnetism (the magnetic work is $\mathrm{d}w = \mu_0 H\,\mathrm{d}M$ ($\mathrm{J\,m^{-3}}$)) again two functions can be distinguished

$$C_M = \left(\frac{\partial U(S,M)}{\partial T}\right)_M = N_A \frac{\partial}{\partial T}\left[kT^2\left(\frac{\partial \ln Z}{\partial T}\right)_M\right]_M \tag{2.54}$$

$$C_H = \left(\frac{\partial E(S,H)}{\partial T}\right)_H = N_A \frac{\partial}{\partial T}\left[kT^2\left(\frac{\partial \ln Z}{\partial T}\right)_M + kT\left(\frac{\partial \ln Z}{\partial \ln M}\right)_T\right]_H \tag{2.55}$$

(The symbol E is used for enthalpy instead of H which is used for the magnetic field strength; units: μ_0 ($\mathrm{J\,A^{-2}\,m^{-1}}$), H ($\mathrm{A\,m^{-1}}$), M ($\mathrm{A\,m^{-1}}$), B ($\mathrm{J\,A^{-1}\,m^{-2}}$); the expression $\mathrm{d}w = \mu_0 H\,\mathrm{d}M$ has the dimension of ($\mathrm{J\,m^{-3}}$)—the volume energy.)

In systems with discrete, well separated energy levels, the contribution to the heat capacity is termed the *Schottky anomaly*. Let us consider a two-level system with energies $\varepsilon_0 = 0$ and $\varepsilon_1 > 0$ with associated degeneracies g_0 and g_1, respectively. The partition function is

$$Z = g_0 + g_1 \exp\left(\frac{-\varepsilon_1}{kT}\right) \tag{2.56}$$

and then the molar internal energy adopts the form of

$$U = N_A kT^2\left(\frac{\partial \ln Z}{\partial T}\right) = N_A \frac{g_1 \varepsilon_1}{Z} \exp\left(\frac{-\varepsilon_1}{kT}\right) \tag{2.57}$$

Consequently the contribution to the molar heat capacity is

$$C_V^{Sh} = \left(\frac{\partial U}{\partial T}\right)_V = R\left(\frac{\varepsilon_1}{kT}\right)^2 \frac{g_0}{g_1} \frac{\exp(\varepsilon_1/kT)}{[1 + (g_0/g_1)\exp(\varepsilon_1/kT)]^2} \tag{2.58}$$

Such a function is plotted in Fig. 9 (left) for several values of the degeneracy ratio.

The function increases for low temperatures according to

$$C_V^{Sh} \approx R\left(\frac{\varepsilon_1}{kT}\right)^2 \frac{g_1}{g_0} \exp\left(\frac{-\varepsilon_1}{kT}\right) \quad \text{for } T \ll \frac{\varepsilon_1}{k} \tag{2.59}$$

then passes through a maximum at $T \approx 0.42\varepsilon_1/k$ and then escapes at high temperature according to

$$C_V^{Sh} \approx R\frac{g_0 g_1}{(g_0 + g_1)^2}\left(\frac{\varepsilon_1}{kT}\right)^2 \quad \text{for } T \gg \frac{\varepsilon_1}{k} \tag{2.60}$$

For a multi-level system one can utilize a result that the heat capacity, in fact, is a thermal fluctuation of the total energy. Hence,

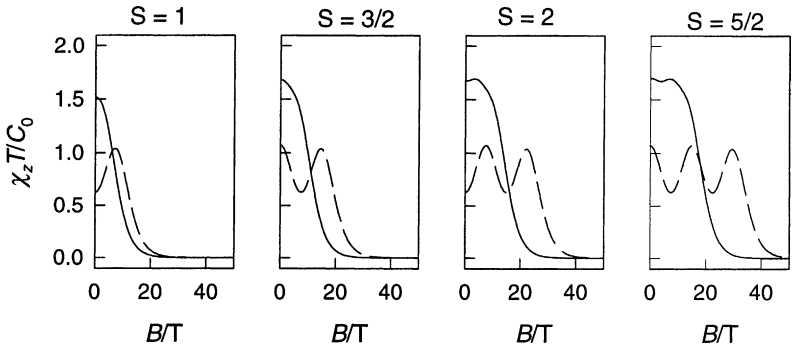

Fig. 8. Parallel differential susceptibility function for zero-field splitting systems: $T = 4.2\,\mathrm{K}$; $D/k = 5$ (solid) and 10 K (dashed).

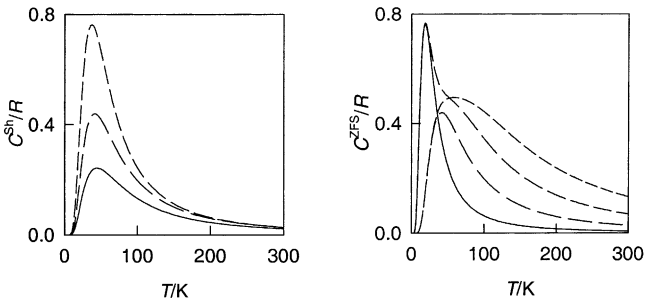

Fig. 9. Left—the Schottky heat capacity of a two-level system for several values of the degeneracy ratio, $r_g = g_1/g_0 = 0.5$ (solid), 1 and 2; $\varepsilon_1/k = 100\,\mathrm{K}$; right—contribution to the heat capacity of zero-field splitting systems for $D/k = 50\,\mathrm{K}$; individual curves correspond to $S = 1$ (solid), 3/2 (long-dashed), 2 (medium-dashed) and 5/2 (short-dashed).

$$C_V^{\mathrm{Sh}} = R\frac{1}{(kT)^2}(\langle\varepsilon^2\rangle - \langle\varepsilon\rangle^2) \tag{2.61}$$

with the thermal averages

$$\langle\varepsilon\rangle = \frac{1}{Z}\sum_i g_i\varepsilon_i \exp\left(\frac{-\varepsilon_i}{kT}\right) \tag{2.62}$$

$$\langle\varepsilon^2\rangle = \frac{1}{Z}\sum_i g_i\varepsilon_i^2 \exp\left(\frac{-\varepsilon_i}{kT}\right) \tag{2.63}$$

and the partition function

$$Z = \sum_i g_i \exp\left(\frac{-\varepsilon_i}{kT}\right) \tag{2.64}$$

The Schottky anomalies may originate in the presence of lattice defects, existence of the ZFS of electronic levels or splitting of nuclear spin levels (due to the electron-nuclear hyperfine coupling and quadrupole interaction, respectively).

The energy levels for a system with the spin $S = 1$ are split into a singlet ($M_S = 0$) and a doublet ($M_S = \pm 1$) separated by an amount D. Then the electronic partition function is

$$Z = 1 + 2\exp\left(\frac{-D}{kT}\right) \tag{2.65}$$

The particular result of interest is

$$\left(\frac{\ln Z}{\partial T}\right)_V = \frac{1}{Z}\left(\frac{\partial Z}{\partial T}\right) = \frac{1}{Z}\left(2\frac{D}{kT^2}\exp\left(\frac{-D}{kT}\right)\right) \tag{2.66}$$

and then the heat capacity results in the form

$$C_V^{\mathrm{ZFS}} = N_A k\left(\frac{D}{kT}\right)^2 \frac{2\exp(-D/kT)}{Z^2} \tag{2.67}$$

This function is displayed in Fig. 9 (right) and it can be seen that it passes through a single maximum.

The formulae for the other cases with $S = 3/2$, 2 and 5/2 can easily be derived by an analogous procedure taking into account the relevant partition function (Table 13). For a vanishing ZFS and for the $S = 1/2$ system the contribution to the heat capacity vanishes at zero field.

Table 13
Heat capacity for the zero-field-splitting systems[a]

S	Z	C_V^{ZFS}/R (dimensionless)
1	$1 + 2d$	$(D/kT)^2(2d)/Z^2$
3/2	$2 + 2d^2$	$(D/kT)^2 2[4d^2Z - 2(2d^2)^2]/Z^2$
2	$1 + 2d + 2d^4$	$(D/kT)^2 2[(d + 16d^4)Z - 2(d + 4d^4)^2]/Z^2$
5/2	$2 + 2d^2 + 2d^6$	$(D/kT)^2 2[(4d^2 + 36d^6)Z - 2(2d^2 + 6d^6)^2]/Z^2$

[a] Substitution $d = \exp(-D/kT)$.

3. Binuclear and polynuclear complexes

3.1. Formal spin-Hamiltonian for polynuclear systems

The Hamiltonian which describes the interaction of a set of magnetic centers with the external magnetic field involves the spin Zeeman term, the orbital Zeeman term, the operator of the local spin–orbit coupling, and the operator of the direct spin–spin interaction

$$\hat{H}' = \hbar^{-1}\mu_{\mathrm{B}} g_{\mathrm{e}}(\vec{B}\cdot\sum_A \vec{S}_A) + \hbar^{-1}\mu_{\mathrm{B}}(\vec{B}\cdot\sum_A \vec{L}_A) + \hbar^{-2}\sum_A \lambda_A(\vec{L}_A\cdot\vec{S}_A) + \hbar^{-2}\sum_A\sum_{B<A}(\vec{S}_A\cdot\bar{\bar{D}}_{AB}^{(1)}\cdot\vec{S}_B) \tag{3.1}$$

This Hamiltonian is regarded as a perturbation that yields the first-order and the second-order corrections to the zero-field and zero-interaction energy. The relevant kets could correspond to the uncoupled basis $|K\rangle = |\alpha, L_A, M_{LA}, L_B, M_{LB}, \ldots\rangle$, where α includes other degrees of freedom (e.g. spin). Alternatively, one can write the spin part explicitly, i.e. $|K\rangle = |L_A, M_{LA}, L_B, M_{LB}, \ldots\rangle|S_A, M_{SA}, S_B, M_{SB}, \ldots\rangle$. The ground state is denoted simply as $|0\rangle$.

The first−order correction can be rewritten as follows:

$$\hat{H}^{(1)} = \langle 0|\hat{H}'|0\rangle = \hbar^{-2}\sum_A\sum_{B<A}(\vec{S}_A\cdot\bar{\bar{D}}_{AB}^{(1)}\cdot\vec{S}_B)\langle 0|0\rangle + \hbar^{-1}\mu_{\mathrm{B}} g_{\mathrm{e}}\left(\vec{B}\cdot\sum_A\vec{S}_A\right)\langle 0|0\rangle + \hbar^{-1}\mu_{\mathrm{B}}\vec{B}\cdot\sum_A\cancel{\langle 0|\vec{L}_A|0\rangle} + \hbar^{-2}\sum_A\lambda_A\vec{S}_A\cdot\cancel{\langle 0|\vec{L}_A|0\rangle} \tag{3.2}$$

where the last two terms vanish assuming the absence of first-order angular momentum. The second-order correction contains the matrix elements

$$\langle 0|\hat{H}'|K\rangle = \hbar^{-2}\sum_A\sum_{B<A}(\vec{S}_A\cdot\bar{\bar{D}}_{AB}^{(1)}\cdot\vec{S}_B)\cancel{\langle 0|K\rangle} + \hbar^{-1}\mu_{\mathrm{B}} g_{\mathrm{e}} \times\left(\vec{B}\cdot\sum_A\vec{S}_A\right)\cancel{\langle 0|K\rangle} + \hbar^{-1}\mu_{\mathrm{B}}\vec{B}\cdot\sum_A\langle 0|\vec{L}_A|K\rangle + \hbar^{-2}\sum_A\lambda_A\vec{S}_A\cdot\langle 0|\vec{L}_A|K\rangle \tag{3.3}$$

and the orthogonality of the state vectors shows that the first two terms do not contribute. Then the second-order correction is

$$\hat{H}^{(2)} = -\sum_{K\neq 0}\frac{\langle 0|\hat{H}'|K\rangle\langle K|\hat{H}'|0\rangle}{E_K - E_0} = -\overline{h}^{-2}\sum_{K\neq 0}\frac{1}{E_K - E_0} \left[\mu_B\vec{B}\cdot\sum_A\langle 0|\vec{L}_A|K\rangle + \overline{h}^{-1}\sum_A\lambda_A\vec{S}_A\cdot\langle 0|\vec{L}_A|K\rangle\right] \left[\mu_B\vec{B}\cdot\sum_A\langle K|\vec{L}_A|0\rangle + \overline{h}^{-1}\sum_A\lambda_A\vec{S}_A\cdot\langle K|\vec{L}_A|0\rangle\right] \tag{3.4}$$

which can be rearranged as follows:

$$\hat{H}^{(2)} = -\overline{h}^{-2}\sum_A\sum_B(\mu_B\vec{B} + \overline{h}^{-1}\lambda_A\vec{S}_A) \cdot\sum_{K\neq 0}\frac{\langle 0|\vec{L}_A|K\rangle\langle K|\vec{L}_B|0\rangle}{E_K - E_0}\cdot(\mu_B\vec{B} + \overline{h}^{-1}\lambda_B\vec{S}_B) \tag{3.5}$$

By introducing the Λ-tensors (with the given sign convention)

$$\bar{\bar{\Lambda}}_{AB} \equiv -\overline{h}^{-2}\sum_{K\neq 0}\frac{\langle 0|\vec{L}_A|K\rangle\langle K|\vec{L}_B|0\rangle}{E_K - E_0} \tag{3.6}$$

we get the expression

$$\begin{aligned}\hat{H}^{(2)} &= \sum_A\sum_B(\mu_B\vec{B} + \overline{h}^{-1}\lambda_A\vec{S}_A)\cdot\bar{\bar{\Lambda}}_{AB}\cdot(\mu_B\vec{B} + \overline{h}^{-1}\lambda_B\vec{S}_B)\\ &= \vec{B}\cdot\left(\sum_A\sum_B\mu_B^2\bar{\bar{\Lambda}}_{AB}\right)\cdot\vec{B}\\ &\quad + \overline{h}^{-1}\mu_B\vec{B}\cdot\left(\sum_A\sum_B\bar{\bar{\Lambda}}_{AB}\lambda_B\right)\cdot\vec{S}_B\\ &\quad + \overline{h}^{-1}\mu_B\vec{B}\cdot\left(\sum_A\sum_B\bar{\bar{\Lambda}}_{AB}\lambda_A\right)\cdot\vec{S}_A\\ &\quad + \overline{h}^{-2}\sum_A\sum_B\vec{S}_A\cdot(\lambda_A\lambda_B\bar{\bar{\Lambda}}_{AB})\cdot\vec{S}_B\end{aligned} \tag{3.7}$$

The final spin-Hamiltonian for a polynuclear system becomes

$$\begin{aligned}\hat{H}^{S} &= \hat{H}^{(1)} + \hat{H}^{(2)}\\ &= -(1/2)(\vec{B}\cdot\bar{\bar{\kappa}}\cdot\vec{B}) + \overline{h}^{-1}\mu_B(\vec{B}\cdot\sum_A\bar{\bar{g}}_A\cdot\vec{S}_A)\\ &\quad -(1/2)\overline{h}^{-2}\sum_A\sum_B(\vec{S}_A\cdot\bar{\bar{\Delta}}_{AB}\cdot\vec{S}_B)\end{aligned} \tag{3.8}$$

where the magnetic parameters (tensors) result:

(a) the *κ-tensor* (reduced, temperature-independent paramagnetic susceptibility tensor)

$$-\frac{1}{2}\bar{\bar{\kappa}} = \left(\sum_A\sum_B\mu_B^2\bar{\bar{\Lambda}}_{AB}\right), \quad (\text{energy}\times\text{induction}^{-2}) \tag{3.9}$$

(b) the *g*-tensors (magnetogyric ratio tensors) as

$$\bar{\bar{g}}_A = g_e\bar{\bar{1}} + 2\sum_B\bar{\bar{\Lambda}}_{AB}\lambda_B, \quad (\text{dimensionless}) \tag{3.10}$$

(c) the *D*-tensors (spin–spin interaction tensors) as

$$-\frac{1}{2}\bar{\bar{D}}_{AB}^{(2)} = \lambda_A\lambda_B\bar{\bar{\Lambda}}_{AB}, \quad (\text{energy}) \tag{3.11}$$

$$\overline{\overline{\Delta_{AB}}} = \left[\frac{1-\delta_{A,B}}{2}\right]\bar{\bar{D}}_{AB}^{(1)} + \bar{\bar{D}}_{AB}^{(2)}, \quad (\text{energy}) \tag{3.12}$$

The spin–spin interaction consists of two terms: the first-order contribution $\bar{\bar{D}}_{AB}^{(1)}$ involves the direct spin–spin operators (that are thought to be small), and the second-order contribution $\bar{\bar{D}}_{AB}^{(2)}$, which covers the dominating $\bar{\bar{\Lambda}}_{AB}$ tensor due to spin–orbit coupling.

3.2. Binuclear systems

The spin-Hamiltonian that describes the spin–spin (exchange) interaction in a dinuclear system is

$$\hat{H}_{AB} = -\tfrac{1}{2}\overline{h}^{-2}\vec{S}_A\cdot\bar{\bar{\Delta}}_{AB}\cdot\vec{S}_B = \overline{h}^{-2}\vec{S}_A\cdot\bar{\bar{D}}'_{AB}\cdot\vec{S}_B \tag{3.13}$$

The Cartesian spin−spin interaction tensor $\bar{\bar{D}}'_{AB}$ (that absorbs the conventional numerical prefactor $-1/2$) can be decomposed into its irreducible components and the spin-Hamiltonian rewritten as follows

$$\begin{aligned}\hat{H}_{AB} &= \overline{h}^{-2}[J'_{AB}(\vec{S}_A\cdot\vec{S}_B) + \vec{d}_{AB}\cdot(\vec{S}_A\times\vec{S}_B)\\ &\quad + \vec{S}_A\cdot\bar{\bar{D}}_{AB}\cdot\vec{S}_B]\end{aligned} \tag{3.14}$$

Here:

1. the first term represents an *isotropic exchange* with a scalar (an exchange coupling constant)

$$J'_{AB} = \tfrac{1}{3}(D'_{AB,xx} + D'_{AB,yy} + D'_{AB,zz}) \tag{3.15}$$

2. the second term—an *antisymmetric exchange* with three parameters forming an antisymmetric vector $\vec{d}_{AB} = (d_{AB,yz}, d_{AB,zx}, d_{AB,xy})$, i.e.

$$d_{AB,ab} = \tfrac{1}{2}(D'_{AB,ab} - D'_{AB,ba}) = -d_{AB,ba} \tag{3.16}$$

3. the last term—the *asymmetric exchange* with five parameters forming a traceless symmetric tensor

$$D_{AB,ab} = \tfrac{1}{2}(D'_{AB,ab} + D'_{AB,ba}) - J'_{AB} = D_{AB,ba} \tag{3.17}$$

The isotropic exchange is met in several sign conventions and numerical prefactors in front of the scalar product of the spin operators, e.g.

$$\hat{H}_{AB}^{\mathrm{iso}} = J'\hbar^{-2}(\vec{S}_A \cdot \vec{S}_B) = -J\hbar^{-2}(\vec{S}_A \cdot \vec{S}_B) = -2J''\hbar^{-2}(\vec{S}_A \cdot \vec{S}_B) \quad (3.18)$$

Hereafter $\hat{H}_{AB}^{\mathrm{iso}} = -J\hbar^{-2}(\vec{S}_A \cdot \vec{S}_B)$ is applied.

The antisymmetric exchange is usually neglected and the only added contribution is the asymmetric exchange term

$$\hat{H}_{AB}^{\mathrm{asym}} = \hbar^{-2}(\vec{S}_A \cdot \bar{\bar{D}}_{AB} \cdot \vec{S}_B) \quad (3.19)$$

Then the complete spin-Hamiltonian appropriate for the ZFS problem in binuclear complexes also contains the local asymmetry terms

$$\hat{H}_A^{\mathrm{asym}} + \hat{H}_B^{\mathrm{asym}} = \hbar^{-2}(\vec{S}_A \cdot \bar{\bar{D}}_A \cdot \vec{S}_A + \vec{S}_B \cdot \bar{\bar{D}}_B \cdot \vec{S}_B) \quad (3.20)$$

and on adding the spin Zeeman terms it adopts the form of

$$\begin{aligned}\hat{H}_{AB}^{\mathrm{spin}} &= \hat{H}_{AB}^{\mathrm{iso}} + \hat{H}_{AB}^{\mathrm{asym}} + \hat{H}_A^{\mathrm{asym}} + \hat{H}_B^{\mathrm{asym}} + \hat{H}_A^Z + \hat{H}_B^Z \\ &= -J_{AB}\hbar^{-2}(\vec{S}_A \cdot \vec{S}_B) + \hbar^{-2}(\vec{S}_A \cdot \bar{\bar{D}}_{AB} \cdot \vec{S}_B \\ &\quad + \vec{S}_A \cdot \bar{\bar{D}}_A \cdot \vec{S}_A + \vec{S}_B \cdot \bar{\bar{D}}_B \cdot \vec{S}_B) \\ &\quad + \mu_{\mathrm{B}}\hbar^{-1}\vec{B} \cdot \bar{\bar{g}}_A \cdot \vec{S}_A + \mu_{\mathrm{B}}\hbar^{-1}\vec{B} \cdot \bar{\bar{g}}_B \cdot \vec{S}_B \end{aligned} \quad (3.21)$$

There are two alternative routes that can be followed:

1. In the strong-exchange limit it is assumed that the isotropic exchange is much larger than the asymmetric exchange, i.e. $|J_{AB}| \gg |D_{AB}|, |D_A|, |D_B|$. Consequently the isotropic exchange dominates the energy levels which are grouped into well-separated blocks. Then the effect of the asymmetric exchange + local anisotropy refers to a small perturbation, whose off-diagonal contributions could be neglected.
2. In the weak-exchange limit the isotropic exchange, asymmetric exchange, and the local anisotropy effects interfere strongly and no simplification is permitted. The coupling (as a kind of the unitary transformation) brings no longer an advantage and can be regarded as redundant. Then better to work in the basis set of uncoupled spin functions.

In the strong exchange limit the two local-Zeeman terms can be combined into a single term

$$\hat{H}^Z = \mu_{\mathrm{B}}\hbar^{-1}\vec{B} \cdot (\bar{\bar{g}}_A \cdot \vec{S}_A + \bar{\bar{g}}_B \cdot \vec{S}_B) \rightarrow \mu_{\mathrm{B}}\hbar^{-1}\vec{B} \cdot \bar{\bar{g}}_S \cdot \vec{S} \quad (3.22)$$

In other words, we seek for the expression of the molecular-state g-factor in terms of the local g-factors

$$\bar{\bar{g}}_S = c_A\bar{\bar{g}}_A + c_B\bar{\bar{g}}_B \quad (3.23)$$

Analogously, the three D-terms can be combined into a single molecular-state term

$$\begin{aligned}\hat{H}_S^{\mathrm{asym}} &= \hbar^{-2}(\vec{S}_A \cdot \bar{\bar{D}}_{AB} \cdot \vec{S}_B + \vec{S}_A \cdot \bar{\bar{D}}_A \cdot \vec{S}_A + \vec{S}_B \cdot \bar{\bar{D}}_B \cdot \vec{S}_B) \\ &= \hbar^{-2}(\vec{S} \cdot \bar{\bar{D}}_S \cdot \vec{S}) \end{aligned} \quad (3.24)$$

with

$$\bar{\bar{D}}_S = C_A\bar{\bar{D}}_A + C_B\bar{\bar{D}}_B + C_{AB}\bar{\bar{D}}_{AB} \quad (3.25)$$

The combination coefficients ($c_A, c_B, C_A, C_B, C_{AB}$) depend only upon the spin numbers (S_A, S_B, S). They fulfill the relationships

$$c_A + c_B = 1 \quad (3.26)$$

$$C_A + C_B + 2C_{AB} = 1 \quad (3.27)$$

Their values can be generated with explicit formulae presented elsewhere [33,42] and Table 14 offers their compilation.

All the D-tensors involved are symmetric and traceless, each having five independent components. If we assume a diagonal form of the D-tensors, the scalar products are expanded as follows:

$$\vec{S}_A \cdot \bar{\bar{D}} \cdot \vec{S}_B = D_{xx}\hat{S}_{Ax}\hat{S}_{Bx} + D_{yy}\hat{S}_{Ay}\hat{S}_{By} + D_{zz}\hat{S}_{Az}\hat{S}_{Bz} \quad (3.28)$$

A diagonal and traceless D-tensor obeys

$$D_{xx} + D_{yy} + D_{zz} = 0 \quad (3.29)$$

and one can proceed with the expression

$$\begin{aligned}&D_{xx}\hat{S}_{Ax}\hat{S}_{Bx} + D_{yy}\hat{S}_{Ay}\hat{S}_{By} + D_{zz}\hat{S}_{Az}\hat{S}_{Bz} \\ &\quad = \tfrac{1}{3}D(3\hat{S}_{Az}\hat{S}_{Bz} - \vec{S}_A \cdot \vec{S}_B) + E(\hat{S}_{Ax}\hat{S}_{Bx} - \hat{S}_{Ay}\hat{S}_{By}) \end{aligned} \quad (3.30)$$

where the *axial zero-field splitting parameter*

$$D = \tfrac{3}{2}D_{zz} \quad (3.31)$$

and the *rhombic zero-field splitting parameter*

$$E = \tfrac{1}{2}(D_{xx} - D_{yy}) \quad (3.32)$$

have been introduced.

The matrix elements of the D-tensors are then evaluated according to

$$\begin{aligned}&\langle S'M'|\vec{S}_A \cdot \bar{\bar{D}} \cdot \vec{S}_B|SM\rangle \\ &\quad = \tfrac{1}{3}D\langle S'M'|3\hat{S}_{Az}\hat{S}_{Bz} - \vec{S}_A \cdot \vec{S}_B|SM\rangle \\ &\qquad + E\langle S'M'|\hat{S}_{Ax}\hat{S}_{Bx} - \hat{S}_{Ay}\hat{S}_{By}|SM\rangle \end{aligned} \quad (3.33)$$

Table 14
The g-tensor coefficients, c_A, the second-order coefficients, d_S, and the D-tensor coefficients, C_A, C_B, and C_{AB}, in the dinuclear systems[a]

S_A	S_B	S	c_A	d_S	C_A	C_B	C_{AB}
1/2	1/2	0	1/2	+3/4	0	0	0
		1	1/2	−1/4	0	0	1/2
1/2	1	1/2	−1/3	+4/9	0	0	0
		3/2	+1/3	−2/9	0	+1/3	+1/3
1/2	3/2	1	−1/4	+5/16	0	+3/2	−1/4
		2	+1/4	−3/16	0	+1/2	+1/4
1/2	2	3/2	−1/5	+6/25	0	+7/5	−1/5
		5/2	+1/5	−4/25	0	+3/5	+1/5
1/2	5/2	2	−1/6	+7/36	0	+4/3	−1/6
		3	+1/6	−5/36	0	+2/3	+1/6
1/2	3	5/2	−1/7	+8/49	0	+9/7	−1/7
		7/2	+1/7	−6/49	0	+5/7	+1/7
1/2	7/2	3	−1/8	+9/64	0	+5/4	−1/8
		4	+1/8	−7/64	0	+3/4	+1/8
1	1	0	+1/2	+2	0	0	0
		1	+1/2	−1/4	−1/2	−1/2	+1
		2	+1/2	−1/4	+1/6	+1/6	+1/3
1	3/2	1/2	−2/3	+10/9	0	0	0
		3/2	+4/15	−44/225	−4/15	+1/5	+8/15
		5/2	+2/5	−6/25	+1/10	+3/10	+3/10
1	2	1	−1/2	+3/4	+1/10	+21/10	−3/5
		2	+1/6	−5/36	−1/6	+1/2	+1/3
		3	+1/3	−2/9	+1/15	+2/5	+4/15
1	5/2	3/2	−2/5	+14/25	+1/15	+28/15	−7/15
		5/2	+4/35	−124/1225	−4/35	+23/35	+8/35
		7/2	+2/7	−10/49	+1/21	+10/21	+5/21
1	3	2	−1/3	+9/4	+1/21	+12/7	−8/21
		3	+1/12	−11/144	−1/12	+3/4	+1/6
		4	+1/4	−3/16	+1/28	+15/28	+3/14
1	7/2	5/2	−2/7	+18/49	+1/28	+45/28	−9/28
		7/2	+4/63	−236/3969	−4/63	+17/21	+8/63
		9/2	+2/9	−14/81	+1/36	+7/12	+7/36
3/2	3/2	0	1/2	+6	0	0	0
		1	1/2	−1/4	−6/5	−6/5	+17/10
		2	1/2	−1/4	0	0	+1/2
		3	1/2	−1/4	+1/5	+1/5	+3/10
3/2	2	1/2	−1	+2	0	0	0
		3/2	+1/5	−4/25	−3/5	0	+4/5
		5/2	+13/35	−286/1225	−3/70	+3/14	+29/70
		7/2	+3/7	−12/49	+1/7	+2/7	+2/7
3/2	5/2	1	−3/4	+21/16	+3/10	+14/5	−21/20
		2	+1/12	−11/144	−5/14	+10/21	+37/84
		3	+7/24	−119/576	−1/20	+11/30	+41/120
		4	+3/8	−15/64	+3/28	+5/14	+15/56
3/2	3	3/2	−3/5	+24/25	+1/5	+12/5	−4/5
		5/2	+1/35	−34/1225	−33/140	+99/140	+37/140
		7/2	+5/21	−80/441	−1/21	+10/21	+2/7
		9/2	+1/3	−2/9	+1/12	+5/12	+1/4
3/2	7/2	2	−1/2	+3/4	+1/7	+15/7	−9/14
		3	0	0	−1/6	+5/6	+1/6
		4	+1/5	−4/25	−3/70	+39/70	+17/70
		5	+3/10	−21/100	+1/15	+7/15	+7/30
2	2	0	1/2	+15/4	0	0	0
		1	1/2	−1/4	−21/10	−21/10	+13/5
		2	1/2	−1/4	−3/14	−3/14	+5/7
		3	1/2	−1/4	+1/10	+1/10	+2/5
		4	1/2	−1/4	+3/14	+3/14	+2/7
2	5/2	1/2	−4/3	+28/9	0	0	0
		3/2	+2/15	−26/225	−1/10	−4/15	+17/15
		5/2	+12/35	−276/1225	−3/14	+1/10	+39/70
		7/2	+26/63	−962/3969	+1/21	+2/9	+23/63
		9/2	+4/9	−20/81	+1/6	+5/18	+5/18
2	3	1	−1	+2	+3/5	+18/5	−8/5

Table 14 (*Continued*)

S_A	S_B	S	c_A	d_S	C_A	C_B	C_{AB}
		2	0	0	−4/7	+3/7	+4/7
		3	+1/4	−3/16	−11/60	+19/60	+13/30
		4	+7/20	−91/400	+3/140	+9/28	+23/70
		5	+2/5	−6/25	+2/15	+1/3	+4/15
2	7/2	3/2	−4/5	+36/25	+2/5	+3	−6/5
		5/2	−2/35	+74/1225	−51/140	+3/4	+43/140
		7/2	+4/21	−68/441	−16/105	+7/15	+12/35
		9/2	+10/33	−230/1089	+1/132	+53/132	+13/44
		11/2	+4/11	−28/121	+6/55	+21/55	+14/55
5/2	5/2	0	1/2	+35/4	0	0	0
		1	1/2	−1/4	−16/5	−16/5	+37/10
		2	1/2	−1/4	−10/21	−10/21	+41/42
		3	1/2	−1/4	−1/45	−1/45	+47/90
		4	1/2	−1/4	+1/7	+1/7	+5/14
		5	1/2	−1/4	+2/9	+2/9	+5/18
5/2	3	1/2	−5/3	+40/9	0	0	0
		3/2	+1/15	−14/225	−22/15	−3/5	+23/15
		5/2	+11/35	−264/1225	−29/70	−3/70	+51/70
		7/2	+25/63	−950/3969	−4/63	+1/7	+29/63
		9/2	+43/99	−2408/9801	+19/198	+5/22	+67/198
		11/2	+5/11	−30/121	+2/11	+3/11	+3/11
5/2	7/2	1	−5/4	+45/16	+1	+9/2	−9/4
		2	−1/12	+13/144	−17/21	+5/14	+61/84
		3	+5/24	−95/576	−1/3	+1/4	+13/24
		4	+13/40	−351/1600	−29/385	+423/1540	1233/3080
		5	+23/60	−851/3600	+1/15	+3/10	+19/60
		6	+5/12	−35/144	+5/33	+7/22	+35/132
3	3	0	1/2	+12	0	0	0
		1	1/2	−1/4	−9/2	−9/2	+5
		2	1/2	−1/4	−11/4	−11/4	+9/7
		3	1/2	−1/4	−1/6	−1/6	+2/3
		4	1/2	−1/4	+9/154	+9/154	+34/77
		5	1/2	−1/4	+1/6	+1/6	+1/3
		6	1/2	−1/4	+5/22	+5/22	+3/11
3	7/2	1/2	−2	+6	0	0	0
		3/2	0	0	−2	−1	+2
		5/2	+2/7	−10/49	−9/14	−3/14	+13/14
		7/2	+8/21	−104/441	−4/21	+1/21	+4/7
		9/2	+14/33	−266/1089	+1/66	+1/6	+9/22
		11/2	+64/143	−5056/20449	+18/143	+3/13	+46/143
		13/2	+6/13	−42/169	+5/26	+7/26	+7/26
7/2	7/2	0	1/2	+63/4	0	0	0
		1	1/2	−1/4	−6	−6	+13/2
		2	1/2	−1/4	−8/7	−8/7	+23/14
		3	1/2	−1/4	−1/3	−1/3	+5/6
		4	1/2	−1/4	−3/77	−3/77	+83/154
		5	1/2	−1/4	+4/39	+4/39	+31/78
		6	1/2	−1/4	+2/11	+2/11	+7/22
		7	1/2	−1/4	+3/13	+3/13	+7/26

[a] The mean magnetic susceptibility, in terms of the van Vleck formula is

$$\bar{\chi}_{\mathrm{mol}} = \frac{C_0}{3T} \frac{\sum_{S=|S_A-S_B|}^{S_A+S_B} [g_S^2 S(S+1) + 2d_S/x](2S+1)\exp(-b_S x)}{\sum_{S=|S_A-S_B|}^{S_A+S_B} (2S+1)\exp(-b_S x)}$$

with $b_S = S(S+1)/2$ and $x = J/kT$.

The D-tensor, in fact, represents the irreducible second-rank tensor since it is true that:

$$\vec{S}_A \cdot \bar{\bar{D}} \cdot \vec{S}_B = \sum_{q=-2}^{+2} (-1)^q D_{2,-q}\, \hat{T}_{2,q}(\vec{S}_A \otimes \vec{S}_B)$$

$$= D_{2,+2}\, \hat{T}_{2,-2}(\vec{S}_A \otimes \vec{S}_B) - D_{2,+1}\, \hat{T}_{2,-1}(\vec{S}_A \otimes \vec{S}_B) + D_{2,0}\, \hat{T}_{2,0}(\vec{S}_A \otimes \vec{S}_B) - D_{2,-1}\, \hat{T}_{2,+1}(\vec{S}_A \otimes \vec{S}_B) + D_{2,-2}\, \hat{T}_{2,+2}(\vec{S}_A \otimes \vec{S}_B) \quad (3.34)$$

where $\hat{T}_{2,q}(\vec{S}_A \otimes \vec{S}_B)$ refers to the q-component of the second-rank tensor composed of the spin operators. The Cartesian and spherical components of the D-tensor are interrelated through the formulae [33,42]

$$D_{2,2} = \tfrac{1}{2}[(D_{xx} - D_{yy}) + \mathrm{i}(D_{xy} + D_{yx})] \rightarrow \tfrac{1}{2}(D_{xx} - D_{yy}) = E \quad (3.35)$$

$$D_{2,1} = -\tfrac{1}{2}[(D_{xz} + D_{zx}) + \mathrm{i}(D_{yz} + D_{zy})] \rightarrow 0 \quad (3.36)$$

$$D_{2,0} = \frac{1}{\sqrt{6}}(2D_{zz} - D_{xx} - D_{yy}) = \frac{1}{\sqrt{6}}[3D_{zz} - (D_{xx} + D_{yy} + D_{zz})] \rightarrow \frac{3}{\sqrt{6}} D_{zz} = \frac{2}{\sqrt{6}} D \quad (3.37)$$

$$D_{2,-1} = \tfrac{1}{2}[(D_{xz} + D_{zx}) - \mathrm{i}(D_{yz} + D_{zy})] \rightarrow 0 \quad (3.38)$$

$$D_{2,-2} = \tfrac{1}{2}[(D_{xx} - D_{yy}) - \mathrm{i}(D_{xy} + D_{yx})] \rightarrow \tfrac{1}{2}(D_{xx} - D_{yy}) = E \quad (3.39)$$

where the simplifications (denoted as $\rightarrow$) are obtained for the traceless diagonal D-tensor.

Table 15
van Vleck coefficients for the asymmetric exchange in homospin binuclear systems

Level	M	$\varepsilon_i^{(0)}$ [b]	$\varepsilon_{i,z}^{(1)}/(\mu_B g_z)$	$\varepsilon_{i,x}^{(2)}/(\mu_B^2 g_x^2)$
$S_A = S_B = 1/2$				
$S = 0$	0	0	0	0
$S = 1$	−1	$-J + (1/3)D_1$	−1	0
	0	$-J - (2/3)D_1$	0	$-1/D_1$
	+1	$-J + (1/3)D_1$	+1	$+1/D_1$
$S_A = S_B = 1$, as above plus new group				
$S = 2$ [a]	±2	$-3J + 2D_2$	±2	$+(1/3)/D_2$
	±1	$-3J - D_2$	±1	$+(7/6)/D_2$
	0	$-3J - 2D_2$	0	$-3/D_2$
$S_A = S_B = 3/2$, as above plus new group				
$S = 3$ [a]	±3	$-6J + 5D_3$	±3	$+(3/10)/D_3$
	±2	$-6J$	±2	$+(8/15)/D_3$
	±1	$-6J - 3D_3$	±1	$+(13/6)/D_3$
	0	$-6J - 4D_3$	0	$-6D_3$
$S_A = S_B = 2$, as above plus new group				
$S = 4$ [a]	±4	$-10J + (28/3)D_4$	±4	$+(2/7)/D_4$
	±3	$-10J + (7/3)D_4$	±3	$+(29/70)/D_4$
	±2	$-10J - (8/3)D_4$	±2	$+(4/5)/D_4$
	±1	$-10J - (17/3)D_4$	±1	$+(7/2)/D_4$
	0	$-10J - (20/3)D_4$	0	$-10/D_4$
$S_A = S_B = 5/2$, as above plus new group				
$S = 5$ [a]	±5	$-15J + 15D_5$	±5	$+(5/18)/D_5$
	±4	$-15J + 6D_5$	±4	$+(23/63)/D_5$
	±3	$-15J - D_5$	±3	$+(39/70)/D_5$
	±2	$-15J - 6D_5$	±2	$+(17/15)/D_5$
	±1	$-15J - 9D_5$	±1	$+(31/6)/D_5$
	0	$-15J - 10D_5$	0	$-15/D_5$

[a] Perturbation formula is used to get the approximate eigenvalues.
[b] The energy levels can be arbitrarily shifted.

In order to obtain the van Vleck coefficients the procedure outlined in Section 2.3 is applicable and the results are compiled in Table 15. Table 16 lists a few closed formulae based upon the van Vleck coefficients. The final energy levels are sketched in Fig. 10. The modeling of the product functions is shown in Figs. 11 and 12. Notice, all these presentations refer to the strong-exchange limit.

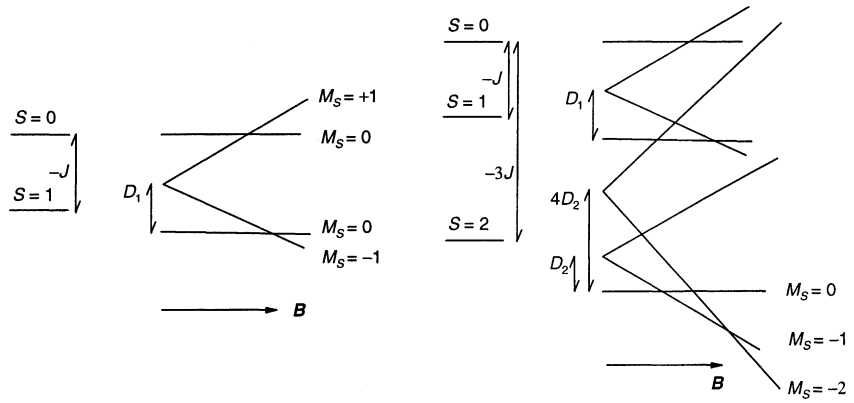

Fig. 10. Magnetic energy levels in the parallel direction for ferromagnetically coupled systems ($J > 0$) and positive zero-field splitting parameters D_1 and D_2. Left—$S_A = S_B = 1/2$, right—$S_A = S_B = 1$.

Table 16
Formulae for the magnetic susceptibility in homospin-binuclear complexes with asymmetric exchange in the strong-exchange limit

For $S_A = S_B = 1/2$: $A = \exp(J/kT)$, $B = \exp[(1/3)D_1/kT]$

$$\chi_z = \frac{C_0 g_z^2}{(TZ_0)} 2(A^1 B^{-1})$$
$$\chi_x = \frac{C_0 g_x^2}{Z_0(D_1/k)} 2A^1(-B^{-1} + B^2)$$
$$Z_0 = 1 + 2A^1(B^{-1} + B^2)$$

For $S_A = S_B = 1$: $A = \exp(J/kT)$, $B = \exp[(1/3)D_1/kT]$, $C = \exp(D_2/kT)$

$$\chi_z = \frac{C_0 g_z^2}{(TZ_0)} 2(A^1 B^{-1} + 4A^3 C^{-2} + A^3 C^1)$$
$$\chi_x = \frac{C_0 g_x^2}{Z_0(D_1/k)} 2A^1(-B^{-1} + B^2) + \frac{C_0 g_x^2}{Z_0(D_2/k)} A^3 \left[-\left(\frac{4}{3}\right) C^{-2} - \left(\frac{14}{3}\right) C^1 + 6C^2 \right]$$
$$Z_0 = 1 + 2A^1(B^{-1} + B^2) + 2A^3(C^{-2} + C^1 + C^2)$$

For other spins $S_A = S_B$

$$\chi_z = \frac{C_0 g_z^2}{TZ_0} \sum_{S=0}^{S_A+S_B} \sum_{M=-S}^{+S} M^2 \exp\left(\frac{-\varepsilon_{S,M}^{(0)}}{kT}\right)$$
$$\chi_x = \frac{C_0 g_x^2}{TZ_0} \sum_{S=0}^{S_A+S_B} \sum_{M=-S}^{+S} \frac{M^2 + S(S+1)}{2(4M^2-1)D_S} \exp\left(\frac{-\varepsilon_{S,M}^{(0)}}{kT}\right)$$
$$Z_0 = \sum_{S=0}^{S_A+S_B} \sum_{M=-S}^{+S} \exp\left(\frac{-\varepsilon_{S,M}^{(0)}}{kT}\right)$$
$$\varepsilon_{S,M}^{(0)} = -\tfrac{1}{2}JS(S+1) + D_S[M^2 - \tfrac{1}{3}S(S+1)]$$

3.3. Trinuclear systems

For trinuclear systems, in the strong-exchange limit, the molecular–state g-tensor and D-tensor are defined as

$$\bar{\bar{g}}_S = c_1\bar{\bar{g}}_1 + c_2\bar{\bar{g}}_2 + c_3\bar{\bar{g}}_3 \tag{3.40}$$

$$\bar{\bar{D}}_S = C_1\bar{\bar{D}}_1 + C_2\bar{\bar{D}}_2 + C_3\bar{\bar{D}}_3 + C_{12}\bar{\bar{D}}_{12} + C_{13}\bar{\bar{D}}_{13} + C_{23}\bar{\bar{D}}_{23} \tag{3.41}$$

where the combination coefficients depend upon the spin numbers $(S_1, S_2, S_3, S_{12}, S)$, including the intermediate

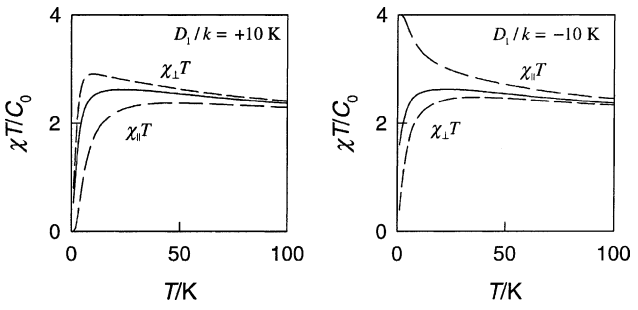

Fig. 11. Temperature dependence of the product function for a ferromagnetically coupled dimer with $S_A = S_B = 1/2$, $J/k = +100$ K, $g_\parallel = g_\perp = 2.0$; $\chi_\parallel T$—long dashed, $\chi_\perp T$—short dashed, $\chi_{av}T$—solid.

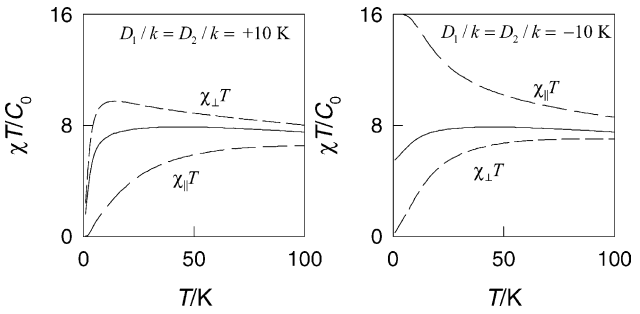

Fig. 12. Temperature dependence of the product function for a ferromagnetically coupled dimer with $S_A = S_B = 1$, $J/k = +100$ K, $g_\parallel = g_\perp = 2.0$; $\chi_\parallel T$—long dashed, $\chi_\perp T$—short dashed, $\chi_{av}T$—solid.

states, and fulfill the relationships

$$c_1 + c_2 + c_3 = 1 \tag{3.42}$$

$$C_1 + C_2 + C_3 + 2C_{12} + 2C_{13} + 2C_{23} = 1 \tag{3.43}$$

The evaluation of the matrix elements of the spin-Hamiltonian

$$H_{ij} = \langle S_1 S_2 S'_{12} S_3 S' M' | \hat{H}^S | S_1 S_2 S_{12} S_3 S M \rangle \tag{3.44}$$

is a complex task and the best way is to use irreducible tensor algebra. The final interaction matrix takes a band structure where each band is accompanied by some sub-bands [33,42].

In the case of $S' = S$ and $S'_{12} = S_{12}$ the combination coefficients for the triple can be obtained through recurrence relationships yielding

$$\begin{aligned}\bar{\bar{D}}_S = {} & C_1(S_{12}S_3S)C_1(S_1S_2S_{12})\bar{\bar{D}}_1 \\ & + C_1(S_{12}S_3S)C_2(S_1S_2S_{12})\bar{\bar{D}}_2 \\ & + C_1(S_{12}S_3S)C_{12}(S_1S_2S_{12})\bar{\bar{D}}_{12} + C_2(S_{12}S_3S)\bar{\bar{D}}_3 \\ & + C_{12}(S_{12}S_3S)c_1(S_1S_2S_{12})\bar{\bar{D}}_{13} \\ & + C_{12}(S_{12}S_3S)c_2(S_1S_2S_{12})\bar{\bar{D}}_{23}\end{aligned} \tag{3.45}$$

which implies that the triad-combination coefficients can be composed of the pair-combination coefficients as shown

Table 17
Recurrence formulae for evaluating the combination coefficients of g- and D-tensors for a trinuclear cluster[a]

(a) Combination coefficients of the g-tensors
$c_1(S_1S_2S_{12}S_3S) = c_1(S_{12}S_3S)c_1(S_1S_2S_{12})$
$c_2(S_1S_2S_{12}S_3S) = c_1(S_{12}S_3S)c_2(S_1S_2S_{12})$
$c_3(S_1S_2S_{12}S_3S) = c_2(S_{12}S_3S)$

(b) Combination coefficients of the local D-tensors
$C_1(S_1S_2S_{12}S_3S) = C_1(S_{12}S_3S)C_1(S_1S_2S_{12})$
$C_2(S_1S_2S_{12}S_3S) = C_1(S_{12}S_3S)C_2(S_1S_2S_{12})$
$C_3(S_1S_2S_{12}S_3S) = C_2(S_{12}S_3S)$

(c) Combination coefficients of the pair-interaction D-tensors
$C_{12}(S_1S_2S_{12}S_3S) = C_1(S_{12}S_3S)C_{12}(S_1S_2S_{12})$
$C_{13}(S_1S_2S_{12}S_3S) = C_{12}(S_{12}S_3S)c_1(S_1S_2S_{12})$
$C_{23}(S_1S_2S_{12}S_3S) = C_{12}(S_{12}S_3S)c_2(S_1S_2S_{12})$

[a] Combination coefficients for the dinuclear systems are collected in Table 14.

Table 18
Recurrence formulae for evaluating the combination coefficients of molecular-state g- and D-tensors for a general tetrad [42][a]

(a) Combination coefficients of the g-tensors
$c_1(S_1S_2S_{12}S_3S_4S_{34}S) = c_1(S_{12}S_{34}S)c_1(S_1S_2S_{12})$
$c_2(S_1S_2S_{12}S_3S_4S_{34}S) = c_1(S_{12}S_{34}S)c_2(S_1S_2S_{12})$
$c_3(S_1S_2S_{12}S_3S_4S_{34}S) = c_2(S_{12}S_{34}S)c_1(S_3S_4S_{34})$
$c_4(S_1S_2S_{12}S_3S_4S_{34}S) = c_2(S_{12}S_{34}S)c_2(S_3S_4S_{34})$

(b) Combination coefficients of the local D-tensors
$C_1(S_1S_2S_{12}S_3S_4S_{34}S) = C_1(S_{12}S_{34}S)C_1(S_1S_2S_{12})$
$C_2(S_1S_2S_{12}S_3S_4S_{34}S) = C_1(S_{12}S_{34}S)C_2(S_1S_2S_{12})$
$C_3(S_1S_2S_{12}S_3S_4S_{34}S) = C_2(S_{12}S_{34}S)C_1(S_3S_4S_{34})$
$C_4(S_1S_2S_{12}S_3S_4S_{34}S) = C_2(S_{12}S_{34}S)C_2(S_3S_4S_{34})$

(c) Combination coefficients of the pair-interaction D-tensors
$C_{12}(S_1S_2S_{12}S_3S_4S_{34}S) = C_1(S_{12}S_{34}S)C_{12}(S_1S_2S_{12})$
$C_{34}(S_1S_2S_{12}S_3S_4S_{34}S) = C_2(S_{12}S_{34}S)C_{12}(S_3S_4S_{34})$
$C_{13}(S_1S_2S_{12}S_3S_4S_{34}S) = C_{12}(S_{12}S_{34}S)c_1(S_1S_2S_{12})c_1(S_3S_4S_{34})$
$C_{14}(S_1S_2S_{12}S_3S_4S_{34}S) = C_{12}(S_{12}S_{34}S)c_1(S_1S_2S_{12})c_2(S_3S_4S_{34})$
$C_{23}(S_1S_2S_{12}S_3S_4S_{34}S) = C_{12}(S_{12}S_{34}S)c_2(S_1S_2S_{12})c_1(S_3S_4S_{34})$
$C_{24}(S_1S_2S_{12}S_3S_4S_{34}S) = C_{12}(S_{12}S_{34}S)c_2(S_1S_2S_{12})c_2(S_3S_4S_{34})$

[a] Combination coefficients for the dinuclear systems are collected in Table 14.

in Table 17. Analogous relationships exist for tetranuclear clusters as shown by Table 18.

The simplest trinuclear systems is a triangle formed of spins $S_1 = S_2 = S_3 = 1/2$. The structure of the asymmetric exchange matrix is [33]

$$\mathbf{H}^{\mathrm{asym}} = \left(\begin{array}{cccc|cc|cc} a_0 & 0 & a_2 & 0 & 0 & d_2 & 0 & e_2 \\ 0 & a_0 & 0 & a_2 & d_0 & 0 & e_0 & 0 \\ a_2 & 0 & a_0 & 0 & 0 & d_0 & 0 & e_0 \\ 0 & a_2 & 0 & a_0 & d_2 & 0 & e_2 & 0 \\ \hline 0 & d_0 & 0 & d_2 & a_0 & 0 & b_0 & 0 \\ d_2 & 0 & d_0 & 0 & 0 & a_0 & 0 & b_0 \\ \hline 0 & e_0 & 0 & e_2 & b_0 & 0 & a_0 & 0 \\ e_2 & 0 & e_0 & 0 & 0 & b_0 & 0 & a_0 \end{array}\right) \text{ for } \left[\begin{array}{lll} S_{12}=1 & S=3/2 & M=-3/2 \\ & & M=-1/2 \\ & & M=+1/2 \\ & & M=+3/2 \\ \hline S_{12}=1 & S=1/2 & M=-1/2 \\ & & M=+1/2 \\ \hline S_{12}=0 & S=1/2 & M=-1/2 \\ & & M=+1/2 \end{array}\right] \tag{3.46}$$

where "a" through "e" mean individual types of the reduced matrix elements and the subscript the degree of the corresponding 3j-symbol occurring in the Wigner–Eckart theorem. In the limit of the strong exchange coupling (J-large) the matrix elements of the d- and e-type are neglected. The molecular-state D-tensors are composed with the help of Tables 17 and 14. Since the local D-tensors for $S_i = 1/2$ all vanish, the only contribution arises from the pair-interaction D-tensors with

$$D_{3/2} = \tfrac{3}{2}D_{3/2,zz} = \tfrac{3}{2}\cdot\tfrac{1}{2}D_{AB.zz} \tag{3.47}$$

$$E_{3/2} = \tfrac{1}{2}(D_{3/2,xx} - D_{3/2,yy}) = \tfrac{1}{2}\cdot\tfrac{1}{2}(D_{AB.xx} - D_{AB,yy}) \tag{3.48}$$

After the evaluation of the matrix elements one gets the contribution of the asymmetric exchange in the form presented in Table 19.

Also the Zeeman matrix adopts a complex structure

$$\mathbf{H}^{Z} = \left(\begin{array}{cccc|cc|cc} a_0 & a_+^* & 0 & 0 & c_+^* & 0 & d_+^* & 0 \\ a_+ & a_0 & a_+^* & 0 & c_0 & c_+^* & d_0 & d_+^* \\ 0 & a_+ & a_0 & a_+^* & c_-^* & c_0 & d_-^* & d_0 \\ 0 & 0 & a_+ & a_0 & 0 & c_-^* & 0 & d_-^* \\ \hline c_+ & c_0 & c_- & 0 & a_0 & a_+^* & b_0 & b_+^* \\ 0 & c_+ & c_0 & c_- & a_+ & a_0 & b_-^* & b_0 \\ \hline d_+ & d_0 & d_- & 0 & b_0 & b_-^* & a_0 & a_+^* \\ 0 & d_+ & d_0 & d_- & b_+ & b_0 & a_+ & a_0 \end{array}\right) \tag{3.49}$$

and it requires the evaluation of the molecular−state g−tensors with the help of Tables 17 and 14 where we assumed identical local g-tensors $\bar{\bar{g}}_A$ (which does not necessarily be fulfilled). The remaining g−tensors ($\bar{\bar{g}}'(\mathrm{c;\,d}) = \bar{\bar{g}}_1 - \bar{\bar{g}}_2$ and $\bar{\bar{g}}''(\mathrm{c}) = \bar{\bar{g}}_2 - \bar{\bar{g}}_3$) vanish as well in this particular case since they are introduced through the difference of the local ones.

The eigenvalues can be easily obtained by assuming no rhombic anisotropy (i.e., $E_{3/2} = 0$) and no general triangle (i.e., $B_{1/2} = 0$, which is equivalent to $J_{13} = J_{23}$):

(1) In the z-direction
   (a) the block for $S = 3/2$ is already diagonal and it yields eigenvalues indicating a ZFS similar to the case of mononuclear complexes;
   (b) the two sub-blocks for $S = 1/2$ are also diagonal; they become degenerate for $A_{1/2} = A'_{1/2}$ (an equilateral triangle).
(2) In the x-direction
   (a) the sub-block for $S = 3/2$ reduces to the standard treatment for the ZFS. There are two degenerate levels ($H_{ii}^{(0)} = A_{3/2} - D_{3/2}$) coupled by an off-diagonal element ($H_{ij} = \mu_{\mathrm{B}}Bg_{A,x}$) so that the first-order perturbation theory is applied first and after solving the corresponding secular determinant the first-order energies are obtained: $\varepsilon_i^{(1)} = \pm\mu_{\mathrm{B}}Bg_{A,x}$. Then the second-order perturbation theory is used for all four energy levels.
   (b) the two sub-blocks for $S = 1/2$ are solved separately yielding only the first-order van Vleck coefficients (Table 20).

Having determined the van Vleck coefficients, one can then apply the van Vleck formula for the parallel and the perpendicular components of the magnetic susceptibility, hence

Table 19
Matrix elements of the spin-Hamiltonian for the $S_1 = S_2 = S_3 = 1/2$ triad[a]

Isotropic exchange

$$A_{3/2} = -\tfrac{1}{4}J_{12} - \tfrac{1}{4}(J_{13} + J_{23}) \rightarrow -\tfrac{1}{4}J - \tfrac{1}{2}J'$$
$$A_{1/2} = -\tfrac{1}{4}J_{12} + \tfrac{1}{2}(J_{13} + J_{23}) \rightarrow -\tfrac{1}{4}J + J'$$
$$A'_{1/2} = +\tfrac{3}{4}J_{12} \rightarrow \tfrac{3}{4}J$$
$$B_{1/2} = -\tfrac{1}{4}\sqrt{3}(J_{23} - J_{13}) \rightarrow 0$$

$$\mathbf{H}^{\mathrm{iso}} = \begin{pmatrix} A_{3/2} & 0 & 0 & 0 & & & & \\ . & A_{3/2} & 0 & 0 & & & & \\ . & . & A_{3/2} & 0 & & & & \\ . & . & . & A_{3/2} & & & & \\ \hline & & & & A_{1/2} & 0 & B_{1/2} & 0 \\ & & & & . & A_{1/2} & 0 & B_{1/2} \\ \hline & & & & . & . & A'_{1/2} & 0 \\ & & & & . & . & . & A'_{1/2} \end{pmatrix}$$

Asymmetric exchange

$$\bar{\bar{D}}(\mathrm{a}_{3/2}) \equiv \bar{\bar{D}}_{S=3/2} = \tfrac{1}{6}\bar{\bar{D}}_{12} + \tfrac{1}{6}\bar{\bar{D}}_{13} + \tfrac{1}{6}\bar{\bar{D}}_{23} = \tfrac{1}{2}\bar{\bar{D}}_{AB}$$
$$\bar{\bar{D}}(\mathrm{a}_{1/2}) \equiv \bar{\bar{D}}_{S=1/2,S'_{12}=1,S_{12}=1} = 0$$
$$\bar{\bar{D}}(\mathrm{a}'_{1/2}) \equiv \bar{\bar{D}}_{S=1/2,S'_{12}=0,S_{12}=0} = 0$$
$$\bar{\bar{D}}(\mathrm{b}_{1/2}) \equiv \bar{\bar{D}}_{S=1/2,S'_{12}=0,S_{12}=1} = 0$$

$$\mathbf{H}^{\mathrm{asym}} = \begin{pmatrix} +D_{3/2} & 0 & \sqrt{3}E_{3/2} & 0 & & & & \\ . & -D_{3/2} & 0 & \sqrt{3}E_{3/2} & & & & \\ . & . & -D_{3/2} & 0 & & & & \\ . & . & . & +D_{3/2} & & & & \\ \hline & & & & 0 & 0 & 0 & 0 \\ & & & & . & 0 & 0 & 0 \\ \hline & & & & . & . & 0 & 0 \\ & & & & . & . & . & 0 \end{pmatrix}$$

Zeeman *z*-term:

$$\bar{\bar{g}}(\mathrm{a}_{3/2}) \equiv \bar{\bar{g}}_{S=3/2} = \tfrac{1}{3}(\bar{\bar{g}}_1 + \bar{\bar{g}}_2 + \bar{\bar{g}}_3) \rightarrow \bar{\bar{g}}_A$$
$$\bar{\bar{g}}(\mathrm{a}_{1/2}) \equiv \bar{\bar{g}}_{S=1/2,S'_{12}=S_{12}=1} = \tfrac{1}{3}(2\bar{\bar{g}}_1 + 2\bar{\bar{g}}_2 - \bar{\bar{g}}_3) \rightarrow \bar{\bar{g}}_A$$

$$\mathbf{H}^{Z}_{z} = \mu_{\mathrm{B}}B_z g_{A,z} \begin{pmatrix} +3/2 & 0 & 0 & 0 & & & & \\ . & +1/2 & 0 & 0 & & & & \\ . & . & -1/2 & 0 & & & & \\ . & . & . & -3/2 & & & & \\ \hline . & . & . & . & +1/2 & 0 & 0 & 0 \\ . & . & . & . & . & -1/2 & 0 & 0 \\ \hline . & . & . & . & . & . & +1/2 & 0 \\ . & . & . & . & . & . & . & -1/2 \end{pmatrix}$$

Zeeman *x*-term

$$\bar{\bar{g}}(\mathrm{a}'_{1/2}) \equiv \bar{\bar{g}}_{S=1/2,S'_{12}=S_{12}=0} = 0 \cdot \bar{\bar{g}}_1 + 0 \cdot \bar{\bar{g}}_2 + 1 \cdot \bar{\bar{g}}_3 \rightarrow \bar{\bar{g}}_A$$
$$\bar{\bar{g}}(\mathrm{b}_{1/2}) \equiv \bar{\bar{g}}_{S=1/2,S'_{12}=0,S_{12}=1} = \tfrac{1}{3}(-\sqrt{3} \cdot \bar{\bar{g}}_1 + \sqrt{3} \cdot \bar{\bar{g}}_2 + 0 \cdot \bar{\bar{g}}_3) \rightarrow 0$$

$$\mathbf{H}^{Z}_{x} = \mu_{\mathrm{B}}B_x g_{A,x} \begin{pmatrix} 0 & +\sqrt{3}/2 & 0 & 0 & & & & \\ . & 0 & +1 & 0 & & & & \\ . & . & 0 & +\sqrt{3}/2 & & & & \\ . & . & . & 0 & & & & \\ \hline . & . & . & . & 0 & +1/2 & 0 & 0 \\ . & . & . & . & . & 0 & 0 & 0 \\ \hline . & . & . & . & . & . & 0 & +1/2 \\ . & . & . & . & . & . & . & 0 \end{pmatrix}$$

Zeeman *y*-term (complex-Hermitean)

$$\bar{\bar{g}}'(\mathrm{c;\,d}) = \bar{\bar{g}}_1 - \bar{\bar{g}}_2 \rightarrow 0$$
$$\bar{\bar{g}}''(\mathrm{c}) = \bar{\bar{g}}_2 - \bar{\bar{g}}_3 \rightarrow 0$$

$$\mathbf{H}^{Z}_{y} = \mu_{\mathrm{B}}B_y g_{A,y}\mathrm{i} \begin{pmatrix} 0 & +\sqrt{3}/2 & 0 & 0 & & & & \\ . & 0 & +1 & 0 & & & & \\ . & . & 0 & +\sqrt{3}/2 & & & & \\ . & . & . & 0 & & & & \\ \hline . & . & . & . & 0 & +1/2 & 0 & 0 \\ . & . & . & . & . & 0 & 0 & 0 \\ \hline . & . & . & . & . & . & 0 & +1/2 \\ . & . & . & . & . & . & . & 0 \end{pmatrix}$$

[a] Only the upper triangle of the symmetric matrices is shown (→ means a passage from a general to the isosceles triangle).

Table 20
van Vleck coefficients for the isosceles triangle ($J_{12} = J$ and $J_{13} = J_{23} = J'$) with $S_1 = S_2 = S_3 = 1/2$

i	$\varepsilon_i^{(0)}$	$\varepsilon_{i,z}^{(1)}/(\mu_B g_{A,z})$	$\varepsilon_{i,x}^{(1)}/(\mu_B g_{A,x})$	$\varepsilon_{i,x}^{(2)}/(\mu_B g_{A,x})^2$
1	$A_{3/2} + D_{3/2}$	+(3/2)	–	+(3/8)/$D_{3/2}$
2	$A_{3/2} - D_{3/2}$	+(1/2)	+1	−(3/8)/$D_{3/2}$
3	$A_{3/2} - D_{3/2}$	−(1/2)	−1	−(3/8)/$D_{3/2}$
4	$A_{3/2} + D_{3/2}$	−(3/2)	–	+(3/8)/$D_{3/2}$
5	$A_{1/2}$	+(1/2)	+(1/2)	–
6	$A'_{1/2}$	+(1/2)	+(1/2)	–
7	$A_{1/2}$	−(1/2)	−(1/2)	–
8	$A'_{1/2}$	−(1/2)	−(1/2)	–

$$\chi_z = \frac{N_A \mu_0 \mu_B^2}{k} \frac{g_{A,z}^2}{T} \frac{2}{Z_0} \frac{1}{4} \left\{ 9 \exp\left[\frac{-A_{3/2} - D_{3/2}}{kT}\right] + \exp\left[\frac{-A_{3/2} + D_{3/2}}{kT}\right] + \exp\left[\frac{-A_{1/2}}{kT}\right] + \exp\left[\frac{-A'_{1/2}}{kT}\right] \right\} \tag{3.50}$$

$$\chi_x = \frac{N_A \mu_0 \mu_B^2}{k} \frac{g_{A,x}^2}{T} \frac{2}{Z_0} \frac{1}{4} \left\{ -\left(\frac{3}{x}\right) \exp\left[\frac{-A_{3/2} - D_{3/2}}{kT}\right] + \left[4 + \left(\frac{3}{x}\right)\right] \exp\left[\frac{-A_{3/2} + D_{3/2}}{kT}\right] + \exp\left[\frac{-A_{1/2}}{kT}\right] + \exp\left[\frac{-A'_{1/2}}{kT}\right] \right\} \tag{3.51}$$

where

$$Z_0 = 2 \left\{ \exp\left[\frac{-A_{3/2} - D_{3/2}}{kT}\right] + \exp\left[\frac{-A_{3/2} + D_{3/2}}{kT}\right] + \exp\left[\frac{-A_{1/2}}{kT}\right] + \exp\left[\frac{-A'_{1/2}}{kT}\right] \right\} \tag{3.52}$$

$$x = \frac{D_{3/2}}{kT} \tag{3.53}$$

The corresponding plots are shown in Fig. 13 for the opposite sign of the D-parameter. It is worth noting that the averaged product function (or the effective magnetic moment) is absolutely insensitive to the sign of the D-parameter. This effect originates in the values of the second-order van Vleck coefficients in this particular case (an analogous situation has been met for the mononuclear $S = 3/2$ system). The net effect of the axial asymmetry parameter is also seen from Fig. 13 where, for comparison, the case of the pure ferromagnetic isotropic exchange is also included. The upturn of the product function and/or effective magnetic moment on the lowering of temperature is due to the depopulation of the magnetically productive $|3/2, \pm 3/2\rangle$ state.

The effect of the axial asymmetry is less pronounced for the case of the antiferromagnetic exchange coupling as seen from Fig. 14. For such a situation it is risky to determine the D-values from the susceptibility data alone.

The most important messages of this theoretical section are summarized as follows:

1. For binuclear and polynuclear magnetoactive systems the exchange interaction of the local spins should be considered. This consists of the isotropic part (the J_{AB} constants) and the asymmetric part (the D_{AB} constants). The D_{AB} constants refer to the pair-wise axial ZFS parameters.
2. There are some other interactions which are usually neglected: the pair-wise rhombic ZFS parameters (E_{AB}) the antisymmetric exchange and the biquadratic exchange. In some cases also the double exchange occurs [33].
3. Each magnetic centre contributes to the spin-Hamiltonian by its local axial ZFS parameter (D_A) and the local magnetogyric tensor $\bar{\bar{g}}_A$ taken in the diagonal form (g_{Ax}, g_{Ay}, g_{Az}). The local rhombic ZFS parameter (E_A) is usually neglected.
4. Spin-Hamiltonian formalism for polynuclear systems says that the $\bar{\bar{g}}_A$-components are shifted from the spin-only value of g_e by the local $\bar{\bar{\Lambda}}_{AA}$ and all pair-wise $\bar{\bar{\Lambda}}_{AB}$ components of the angular momentum unquenching tensor—see Eq. (3.10). At the same time these Λ-tensor

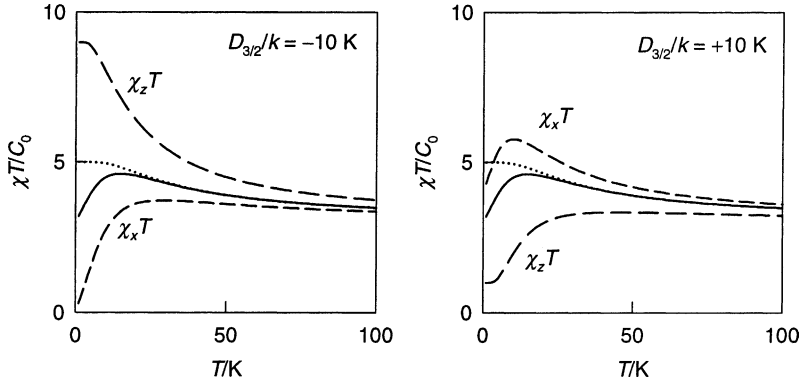

Fig. 13. Temperature variation of the product functions for an isosceles triangle with $S_1 = S_2 = S_3 = 1/2$ including asymmetric exchange: $g_A = 2.0$, $J/k = 50$ K, $J'/k = 25$ K, solid—$\chi_{av}T$; dotted—pure isotropic exchange ($D = 0$).

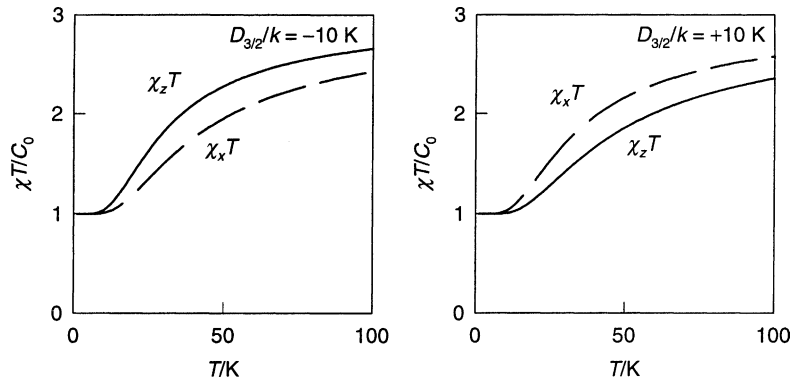

Fig. 14. Temperature variation of the product functions for an isosceles triangle with $S_1 = S_2 = S_3 = 1/2$ including asymmetric exchange: $g_A = 2.0$, $J/k = 50$ K, $J'/k = -25$ K.

components enter the local and pair-wise components of the D-tensor—Eq. (3.11). This means that the (g_{Az}, g_{Ax}, g_{Bz}, g_{Bx}) set is constrained with (D_A, D_B, D_{AB}) set through Λ_{AAz}, Λ_{ABz}, Λ_{BBz}, Λ_{AAx}, Λ_{ABx}, Λ_{BBx}. In the other words, with non-zero D_A, the pair g_{Az} and g_{Ax} should be split. Such a constraint is, as a rule, overlooked.

5. The strong exchange limit (when $|J_{AB}| \gg |D_{AB}|$, $|D_A|$, $|D_B|$) can be treated by combining the local and pair-interaction tensors into the molecular-state tensors $\bar{\bar{g}}_S$ and $\bar{\bar{D}}_S$ using, for instance, Eqs. (3.23) and (3.25) for a binuclear system. Then the effect of the asymmetric exchange + local anisotropy refers to a small perturbation with respect to the isotropic exchange. The level-splitting for each S-multiplet is analogous to the mononuclear systems.
6. In the weak-exchange limit the isotropic exchange, asymmetric exchange, and the local anisotropy effects strongly interfere. The level-splitting needs be evaluated by the diagonalization of the interaction matrix.
7. For ferromagnetically coupled systems the effect of the ZFS can be well determined from the low-temperature data of the magnetic susceptibility. For antiferromagnetically coupled systems this effect superimposes the decrease of the magnetic susceptibility on temperature lowering.

4. Experimental data on ZFS

4.1. Data analysis

Several experimental techniques allow one to measure the ZFS parameters (D, E, a, F) directly: (a) magnetic susceptibility measurements on single crystals, (b) magnetization measurements, (c) calorimetric measurements on Schottky anomalies, (d) electron spin resonance, (e) magnetic circular dichroism, (f) far infrared spectroscopy, (g) inelastic neutron scattering.

The two ZFS parameters (D and E) are a measure of the magnetic anisotropy. When $E = 0$, the x- and y-directions are equivalent. Also, when the D-parameter vanishes, the system becomes isotropic and is well modeled by a Curie paramagnet (its magnetization is reproduced by the Brillouin function and the magnetic susceptibility follows the Curie law).

In terms of the spin-Hamiltonian the set of magnetic parameters (g_x, g_y, g_z, D, E and χ_{TIP}) are interrelated through the Λ-tensor components (the sign convention is important hereafter) as compiled in Table 3. Thus the Λ-tensor represents a more fundamental magnetic quantity. The D-parameter

$$D \sim \lambda \sim (\Delta E_{0\to K})^{-1} \sim \kappa \langle 0|\vec{L}|K\rangle \tag{4.1}$$

could increase in the following circumstances:

(i) the spin–orbit coupling constant ξ_d entering the spin–orbit splitting parameter $\lambda = \pm\xi_d/2S$ increases with the proton number;
(ii) the spin value entering the splitting parameter $\lambda = \pm\xi_d/2S$ is small, e.g. $S = 1$;
(iii) the Λ-tensor components are rather big owing to the synergy effect of the ligand field asymmetry;
(iv) the d-d transition energies entering the denominator of the Λ-tensor components are rather small (less than $10\,000\,\mathrm{cm}^{-1}$);
(v) the covalency is small so that the orbital reduction factor $\kappa \to 1$;
(vi) asymmetry of the covalency is large, i.e. $\kappa_\parallel \neq \kappa_\perp$.

With the condition $\Lambda_{zz} < \Lambda_{xx}$ the angular momentum distribution can be represented through an oblate ellipsoid giving rise to a positive D-parameter; while in the reverse case of $\Lambda_{zz} > \Lambda_{xx}$ a prolate ellipsoid matches the angular momentum distribution and consequently $D < 0$ applies.

The interpretation of the recorded data (temperature dependence of the magnetic susceptibility measured at low fields) is usually done within the *spin-Hamiltonian formalism*

$$\hat{H}_a = \hbar^{-2} D(\hat{S}_z^2 - \tfrac{1}{3}\hat{S}^2) + \hbar^{-2} E(\hat{S}_x^2 - \hat{S}_y^2) + \hbar^{-1} g_a \mu_B B \hat{S}_a \tag{4.2}$$

(for Cartesian components $a = x, y, z$) as reviewed in Section 2. In this way, the free parameters fixed by the optimization routine are: D, g_z, (synonym for the parallel component $g_\parallel$) and g_x (synonym for the perpendicular component $g_\perp$). Rarely the E-parameter is also determined (very exceptionally also g_y) using the magnetic data. Sometimes the correction to the molecular field created by the nearest neighbors (zj) is applied in the form

$$\hat{H} = \hat{H}^{\mathrm{zfs}} - (zj)\bar{h}^{-1}\langle S_z\rangle \hat{S}_z \tag{4.3}$$

(the convention for the numerical prefactor -1 is important as commonly -2 is also applied). This leads to the formula for the corrected magnetic susceptibility

$$\chi^{\mathrm{cor}} = \frac{\chi_{\mathrm{av}}}{(1 - Z \cdot \chi_{\mathrm{av}})} \tag{4.4}$$

where

$$Z = \frac{zj}{(N_{\mathrm{A}}\mu_0\mu_{\mathrm{B}}^2/k)g_{\mathrm{av}}^2} \tag{4.5}$$

The average is usually as simple as

$$\chi_{\mathrm{av}} = \tfrac{1}{3}(\chi_x + \chi_y + \chi_z) \tag{4.6}$$

but a more advanced powder average can also be applied.

The fitting procedure can be based on a more general spin-Hamiltonian that utilizes the operator equivalent approach, where in addition to the usual bilinear ZFS the biquadratic ZFS correction is also considered.

The value of the ZFS energy can be read off directly by knowing the lowest energy levels of the system. The calculation can be performed at different levels of sophistication:

(a) by utilizing the crystal field theory as outlined by König and Kremer [68,69],

(b) within the angular overlap model of Gerloch and Slade [71,72].

Having the energy levels reconstructed (by an appropriate parametrization) calculation of the magnetization, magnetic susceptibility and the heat capacity proceeds through the partition function.

4.2. Magnetic susceptibility

A modeling of the temperature variation of the magnetic susceptibility components for a set of spins is shown in Fig. 15. The following observations can be withdrawn.

1. With D-positive:
   (a) The parallel components approach zero for $S = 1$ and $S = 2$. This happens because the ground state is then non-magnetic, $|S, M_S = 0\rangle$.
   (b) For $S = 3/2$ and $S = 5/2$ the ground state is a Kramers doublet $|S, M_S = \pm 1/2\rangle$. With decrease in temperature, the magnetically more productive states $|S, M_S = \pm 3/2\rangle$ and eventually $|S = 5/2, M_S = \pm 5/2\rangle$ are depopulated and thus the parallel susceptibility tends to reach a plateau. However, at a low enough temperature the $|S, M_S = +1/2\rangle$ state also becomes depopulated so that the only remaining contributing level is $|S, M_S = -1/2\rangle$ which is now saturated. The parallel susceptibility rises abruptly.
   (c) The perpendicular component increases rapidly on cooling because the ground level possesses a large negative 2nd-order van Vleck coefficient in (2.29), i.e. $\varepsilon^{(2)}_{\mathrm{ground}}/(\mu_{\mathrm{B}}^2 g_x^2) = -3/8D$, $-3/D$ and $-1/D$ for $S = 3/2$, 2, and 5/2 (see Table 5).

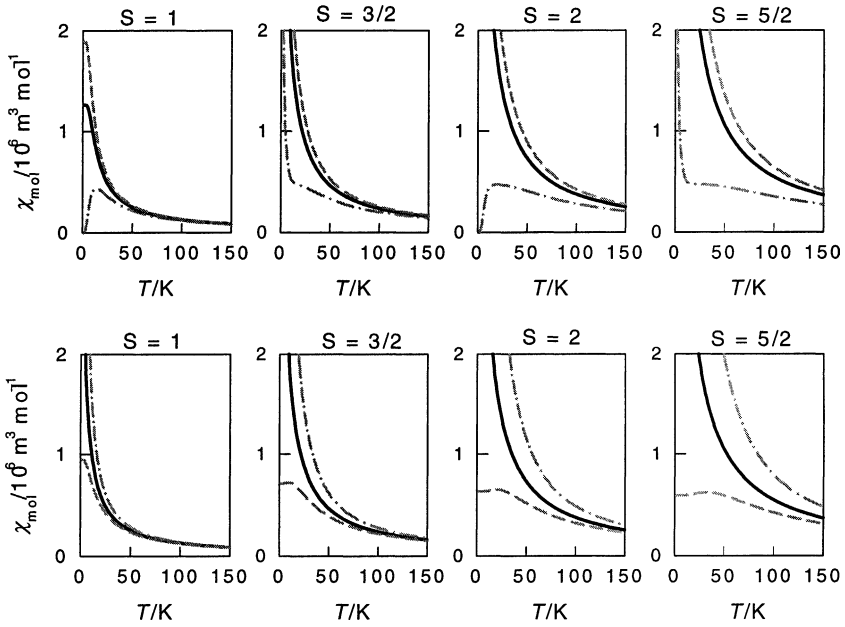

Fig. 15. Modeling the molar magnetic susceptibility for ZFS systems ($E = 0$); top panel: $D/k = 20$ K; bottom panel: $D/k = -20$ K; parallel component ($\chi_\parallel$)—dot-dashed, perpendicular component ($\chi_\perp$)—short dashed, and the average (χ_{av})—solid.

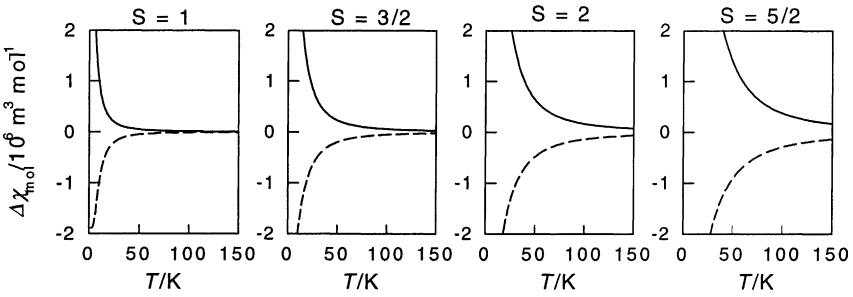

Fig. 16. Modeling of the susceptibility anisotropy: solid—$D/k = 20$ K; dashed—$D/k = -20$ K.

(d) Consequently the averaged susceptibility follows the Curie-Weiss law (the negative Weiss constant accounts for the *D*-parameter).

2. With *D*-negative:
   (e) The ground state is always a Kramers doublet with the maximum spin projection, $|S, M_S = \pm S\rangle$. Therefore, the parallel susceptibility on cooling increases rapidly and is not influenced by the depopulation of the magnetically less productive states.
   (f) The perpendicular energy levels possess small positive the 2nd-order van Vleck coefficients in Eq. (2.29), i.e. $\varepsilon^{(2)}_{\text{ground}}/(\mu_B^2 g_x^2) = +3/8\text{D}$, $+(1/3)D$ and $+(5/16)D$ for $S = 3/2$, 2, and 5/2 (see Table 5). The corresponding susceptibility component on cooling reaches a plateau.

The measurements of the susceptibility anisotropy

$$\Delta\chi = \chi_{\parallel} - \chi_{\perp} \tag{4.7}$$

clearly distinguishes between the signs of the *D*-parameter at relatively high temperature as modeled at Fig. 16. The definition of the local coordinate system at which the magnetic parameters, the *g*- and the *D*-tensor, are evaluated, however, remains a bit questionable. It is frequently assumed that their principal axes coincide and, moreover, that they are represented by the crystal directions: *z*- or $l_{\parallel} = (0\,0\,1)$.

The magnetic anisotropy measurements on oriented single crystals are capable of directly distinguishing the parallel and the perpendicular magnetic susceptibilities [73]. Such measurements were done, for instance, for $[C(NH_2)_3]V(SO_4)_2{\cdot}6H_2O$ salt between 1.5 and 20 K [74,75]. It was found that on lowering the temperature, the perpendicular component of the magnetic susceptibility increases whereas the parallel component passes through a maximum at ca 4 K and then approaches zero. Such a situation indicates that $D > 0$. Some more experimental data are collected in Table 21.

These data show rather moderate values of the axial ZFS parameter bracketed with the interval of ca. $D = \pm 10\,\text{cm}^{-1}$. With the exception of $HgCo^{II}(NCS)_4$ the complexes listed are hexa- (penta-) coordinate. In terms of the formal pertur-

Table 21
ZFS parameters based upon the single-crystal susceptibility data

System	Experimental	Magnetic parameters (cm^{-1})	Reference
$[C(NH_2)_3]V^{III}(SO_4)_2{\cdot}6H_2O$, $S = 1$	$T = 1.5$–20 K	$D = 3.74$, $g_z = 1.94$, $g_x = 1.66$	[74,75] Y
$Cs_3V^{III}Cl_6{\cdot}4H_2O$, $S = 1$	$T = 1.5$–20 K	$D = 8.05$, $g_z = 1.93$, $g_x = 1.74$	[76] Y
$[V^{III}(\text{urea})_6]I_3$, $S = 1$	$T = 1.5$–300 K	$B_2^0 = -162$, $B_4^0 = -99$, $B_4^3 = 2595$, $\lambda = 45$, $\lambda/\lambda_0 = 0.43$, $\kappa = 0.40$; $D^* = 5.86$	[77] O
	$T = 80$–300 K	$\lambda = 45$, $\Delta = 450$, $\kappa = 0.50$	[77] O
$[Cr^{III}(NH_3)_6](ClO_4)_2Br{\cdot}CsBr$, $S = 3/2$	$T = 0.04$–4.2 K	$D = 0.18$, $g_z = 1.985$, $g_x = 1.995$, $zj = -0.049$	[78] #N
$[Mn^{III}(TPP)Cl]{\cdot}2C_6H_6$, cn = 5, $S = 2$	$T = 80$–300 K	$D = -2.3$, $g = 2$	[79] O
$[Mn^{III}(TPP)Cl(py)]{\cdot}C_6H_6$, $S = 2$	$T = 80$–300 K	$D = -3.0$, $g = 2$	[79] O
$[Fe^{III}(TPP)Cl]$, cn = 5, $S = 5/2$	$T = 80$–300 K	$D = 5.9$, $g = 2$	[80] O
$[Fe^{III}(acac)_3]$, $S = 5/2$	$T = 80$–300 K	$D = -0.11$	[81] O
$K_3[Fe^{III}(ox)_3]{\cdot}3H_2O$, $S = 5/2$	$T = 80$–300 K	$D = -0.55$	[81] O
$HgCo^{II}(NCS)_4$, cn = 4, $S = 3/2$	$T = 1.7$–300 K, $B = 0.5$ T	$D_{(z)} = +10.2$, $g_z = 2.168$, $D_{(x)} = +10.8$, $g_x = 2.251$, $zj = -0.19$	[82] #Y
$[Ni^{II}(pyO)_6](ClO_4)_2$, $S = 1$	$T = 1.5$–20 K	$D = +4.35$, $g_z = 2.32$, $g_x = 2.33$, $zj = -2.08$	[83] #Y
$[Ni^{II}(pyO)_6](NO_3)_2$, $S = 1$		$D = +3.95$, $g_z = 2.25$, $g_x = 2.29$	[84] Y
$[Ni^{II}(H_2O)_6]SO_4$, $S = 1$	$T = 0.4$–4.2 K, $B = 0$–9 T	$D = +4.74$, $g_z = 2.216$, $g_x = 2.249$	[85] Y
$[Ni^{II}(H_2O)_6][SnCl_6]$, $S = 1$	$T = 0.35$–4.2 K, $M(B \to 4\,\text{T}, T = 1.3$–4.2 K)	$D = 0.45$, $g = 2.25$	[86] O
$Ni^{II}Cl_2.4H_2O$, $S = 1$	$T = 1.5$–20 K	$D = -7.99$, $E = 0.07$, $g = 2.28$, $zj = -7.30$	[87] #O

General notes: The symbol '#' shows that a different definition of the *J*-parameter has been applied in the original source whereas here $-zj$ and/or $-J$ constants precede the spin operators; the coordination number (cn) is displayed when different from 6. The consistency criterion $D/\lambda = (g_z - g_x)/2$: Y—fulfilled, N—violated, O—cannot be judged.

Table 22
ZFS parameters (cm^{-1}) based upon the powder susceptibility data for Ni(II) compounds, $S = 1$

System	Experimental	D	E	g_z	g_x	Other	Reference
$[Ni(iz)_4(\kappa^1{:}ac)_2]$	$T = 4.2$–$140\,K$, $B_{AC} \approx 0$, $M(B \rightarrow 6\,T, T = 4.3\,K)$	−22.34		2.181	2.039		[101] Y
$[Ni(dmiz)_2(\kappa^2{:}ac)_2]$	$T = 4.2$–$140\,K$, $B_{AC} \approx 0$	−9.94		2.263	2.175		[102] Y
Ni(dien)(mea)$Ni(CN)_4$, chain structure	$T = 4.2$–$140\,K$, $B_{AC} \approx 0$	−6.98		2.145	2.101		[103] Y
$[Ni(terpy)_2](PF_6)_2$	$T = 1.5$–$250\,K$, $B = 0.5 \rightarrow 5.5\,T$	−6.10	0.12	2.095			[104] O
	$M(B \rightarrow 5\,T, T = 1.9\,K)$	−6.25		2.15			[104] O
$[Ni(aepn)_2]Ni(CN)_4{\cdot}H_2O$	$T = 4.2$–$140\,K$, $B_{AC} \approx 0$	−1.90		2.156	2.144		[103] Y
		+1.77		2.140	2.151		
$[Ni(tren)(NCS)_2]$, $S_i = 1$	$T = 4.2$–$289\,K$	−0.76		2.181		*zj*, −1.52	[160] #O
$[Ni(bipy)_3]Cl_2{\cdot}5.5H_2O$	$T = 2$–$300\,K$	Small		2.12			[105] O
$[Ni(teta)(\mu\text{-}N(CN)_2)]{\cdot}(ClO_4)$, chain structure	$T = 4.2$–$40\,K$, $B_{AC} \approx 0$	Small		2.066		J_{chain}, 0	[106] O
$[Ni(iz)_2(\mu\text{-}NCS)_2]$, chain structure	$T = 2$–$290\,K$, $B = 1\,T$	0.2		2.18		J_{chain}, 8	[107] #O
$Ni(tn)_2Ag_2(CN)_4$, chain structure $S(Ag^I) = 0$	$T = 2$–$10\,K$, $B = 0.1\,T$;	2.36		2.11			[108] O
		2.33	0.52	2.11		J_{chain}, 0	[108] O
	$M(B \rightarrow 5\,T, T = 2\,K)$	−1.77	0.97	2.11		J_{chain}, 0	[108] O
$[Ni(NH_3)_4(NO_2)_2]$	$T = 2$–$300\,K$	~~10.4~~		2.18			[88]
	$M(B \rightarrow 5\,T, T = 4.2\,K)$	<2		2.18		*zj*, −5.4	[89] #
$Ni(NO_3)_2{\cdot}6H_2O$	$T = 1.5$–$20\,K$	4.46	1.13	2.25		*zj*, −0.43	[109] O
$[Ni\{L^{15}_{NNNSSS}\}ZnCl]$ $S(Zn^{II}) = 0$	$T = 2$–$300\,K$	4.9		2.2			[110] O
$Ni(en)_2Ni(CN)_4$ chain structure	$T = 0.05$–$20\,K$, $M(B \rightarrow 6\,T, T = 4.27\,K)$	6.6		2.24		J_{chain}, −0.06	[111] O
$[Ni(pz)_4Br_2]$	$T = 2$–$30\,K$, $B = 0.5\,T$	5.5		2.12	2.20		[112] Y
$[Ni(pz)_4Cl_2]$	$T = 2$–$30\,K$, $B = 0.5\,T$	7.2		2.14	2.21		[112] Y
$[Ni(mpz)_4I_2]$	$T = 2$–$80\,K$, $B = 0.5\,T$ $M(B \rightarrow 5.2\,T)$	2.5		2.16	2.13	0.60	[114] N
$[Ni(mpz)_4Br_2]$	$T = 2$–$80\,K$, $B = 0.5\,T$, $M(B \rightarrow 5.2\,T)$	5.3		2.16	2.13	0.65	[114] N
$[Ni(mpz)_4Cl_2]$	$T = 2$–$80\,K$, $B = 0.5\,T$, $M(B \rightarrow 5.2\,T)$	7.4		2.19	2.13	0.85	[114] N
$[Ni\{L^6{}_{NNOO}\}_2(H_2O)_2]$	$T = 2$–$160\,K$, $B = 0.1\,T$	+9.47	1.54	2.067	2.125 g_y, 2.145	*zj*, −2.03	[113] Y
		D^*		ξ	κ		[a]
$[Ni(py)_4Cl_2]$	$T = 4.3$–$300\,K$	4.8		480	0.74		[115] O
$[Ni(py)_4Br_2]$	$T = 4.3$–$300\,K$	6.9		475	0.90		[115]
$[Ni(pz)_4Cl_2]$	$T = 4.3$–$300\,K$	7.7		540	0.95		[115]
$[Ni(pz)_4Br_2]$	$T = 4.3$–$300\,K$	6.0		420	0.90		[115]
$[Ni(miz)_4Cl]Cl$, cn = 5	$T = 4.3$–$300\,K$	11.0		400	0.95	J_{chain}, −2.2	[115] #
$[Ni(miz)_4Br]Br$, cn = 5	$T = 4.3$–$300\,K$	8.2		380	0.85	J_{chain}, −2.6	[115] #
$[Ni(en)_2(NO_2)_2]$	$T = 4.3$–$300\,K$	−1.6		550	0.90	J_{dim}, 0.9	[115] #
cn = 4 or 10		D		g_z	g_x		
Ni(azurin), cn = 4	$T = 5$–$120\,K$, $B = 0.1\,T$	17.7		1.98			[116] O
$[Ni\{L^1_{NNSS}\}]$, cn = 4	$T = 4.2$–$300\,K$, $B = 1\,T$	36		2.09			[117] O
$[Ni\{L^2_{NNSS}\}]$, cn = 4	$T = 4.2$–$300\,K$, $B = 1\,T$	53		2.09			[117] O
$[Ni(Cp)_2]$, cn = 10	$T = 4.2$–$200\,K$	33.6		2.00	2.11		[118] Y

General notes: The symbol '#' marks that a different definition of the *J*-parameter has been applied in the original source whereas here $-zj$ and/or $-J$ constants precede the spin operators; the coordination number (cn) is displayed when different from 6. The consistency criterion $D/\lambda = (g_z - g_x)/2$: Y—fulfilled, N—violated, O—cannot be judged. D^* refers to the difference of the lowest energy levels.

[a] AOM parameters optimized to electron spectra.

bation theory the *g*-factor asymmetry should be consistent with the sign of the *D*-parameter as the simple PT theory says

$$D = \tfrac{1}{2}\lambda(g_z - g_x) \tag{4.8}$$

With one exception this prediction is fulfilled.

The magnetic susceptibility measurements on powder samples where the *D*-values have been reported are reviewed

Table 23
Selected *D*-values for Ni(II) complexes

Compound	Cl	Br	I	Reference
$[Ni(pz)_4X_2]$	7.2	5.5		[112]
$[Ni(mpz)_4X_2]$	7.4	5.3	2.5	[114]
$[Ni(py)_4X_2]$	4.8	6.9		[115], D^*
$[Ni(pz)_4X_2]$	7.7	6.0		[115], D^*
$[Ni(miz)_4X]X$	11.0	8.2		[115], D^*

Table 24
ZFS parameters based upon the powder susceptibility data for Mn(III) compounds, $S = 2$

System	Experimental	D	g_z	g_x	J_{dim}	Reference
cn = 6						
$[Mn(acac)_3]$	$T = 2$–$20\,K$, $B = 0.1\,T$	+3.1	2			[119]
$[Mn(trop)_3]$	$T = 2$–$20\,K$, $B = 0.1\,T$	−2.6	2		−0.18	[119]
$Na_5[Mn(tar)_2(H_2O)_2]\cdot 9H_2O$	$T = 1.3$–$26\,K$	−3.5	1.96	1.99		[120]
$[Mn(dedtc)_3]$	$T = 4.2$–$300\,K$, $B = 0.3\,T$	Small				[121]
$[Mn(sal\text{-}N\text{-}Ph)_3]$	$T = 4.2$–$300\,K$, $B = 1\,T$, $M(B \rightarrow 5\,T, T = 4.2$–$20\,K)$	−2.1	1.99		0	[122] #
$[Mn(sal\text{-}N\text{-}Benz)_3]$	$T = 4.2$–$300\,K$, $B = 1\,T$, $M(B \rightarrow 5\,T, T = 4.2$–$20\,K)$	−2.6	1.99		−0.16	[122] #
[Mn(salen)SCN], cn = 6, assumed dimer	$T = 4.2$–$300\,K$, $B = 1\,T$	−3.8	1.97		−0.88	[122] #
[Mn(salen)Br], cn = 6, assumed dimer	$T = 4.2$–$300\,K$, $B = 1\,T$	−1.0	1.95		−3.68	[122] #
$[Mn(TPP)(miz)_2]ClO_4\cdot THF$	$T = 1.2$–$300\,K$, $M(B \rightarrow 1.5\,T, T = 4.2\,K)$	−2.5	2.00			[123]
$[Mn(TPP)Cl(py)].C_6H_6$	$T = 4$–$300\,K$	−3.5	2.00			[79]
	$M(B \rightarrow 5\,T, T = 2$–$20\,K)$	−3.0	2.00		0	[124]
cn = 5						
[Mn(acen)Cl]	$T = 4.2$–$300\,K$, $B = 1\,T$, $M(B \rightarrow 5\,T, T = 4.2$–$20\,K)$	−1.6	2.00		−0.20	[122] #
$[Mn(TPP)Cl]\cdot 2C_6H_6$	$T = 4$–$300\,K$	−2.5	2.00			[79]
	$M(B \rightarrow 5\,T, T = 2$–$20\,K)$	−1.9	2.00		*zj*, −0.05	[124] #
$[Mn(TPP)ClO_4]$	$T = 1.2$–$300\,K$, $M(B \rightarrow 1.5\,T, T = 4.2\,K)$	−2.0	2.00			[123]
$[Mn(OEP)Cl]\cdot H_2O$	$T = 4.2$–$300\,K$, $B = 1\,T$	−1.6	2.02		−0.06	[125] #
$[Mn(OEP)Br]\cdot H_2O$	$T = 4.2$–$300\,K$, $B = 1\,T$	−1.0	2.02		−0.08	[125] #
$[Mn(OEP)(OAc)]\cdot H_2O$	$T = 4.2$–$300\,K$, $B = 1\,T$, $M(T, B \rightarrow 5\,T)$	−1.9	1.97		0	[125] #
$[Mn(OEP)ClO_4]\cdot H_2O$	$T = 4.2$–$300\,K$, $B = 1\,T$, $M(T, B \rightarrow 5\,T)$	−2.3	1.96		−0.34	[125] #
		+3.0	1.96		−0.38	
$[Mn(TPP)ClO_4]\cdot H_2O$	$T = 4.2$–$300\,K$, $B = 1\,T$	−2.3	2.00		−0.14	[125] #
$[Mn(TTP)Cl]\cdot C_6H_6$	$T = 4.2$–$300\,K$, $B = 1\,T$, $M(T, B \rightarrow 5\,T)$	−1.8	2.01		−0.04	[125] #
$[Mn(TTP)Cl]\cdot H_2O$	$T = 4.2$–$300\,K$, $B = 1\,T$	−1.8	2.00		−0.08	[125] #
Chain structures, cn = 6		D	g_z	g_x	J_{chain}	
$\{K_2[Mn(mal)_2(EtOH)_2][Mn(mal)_2]\}_n$	$T = 4.2$–$100\,K$, $B = 1\,T$	−7.9	1.99	1.98	−0.36	[126] #
$\{(NH_4)_2[Mn(mal)_2(EtOH)_2][Mn(mal)_2]\}_n$	$T = 4.2$–$100\,K$, $B = 1\,T$	−7.6	2.09	2.03	−0.18	[126] #
$\{Na_2[Mn(mal)_2][Mn(mal)_2EtOH]\cdot EtOH\}_n$	$T = 4.2$–$100\,K$, $B = 1\,T$	−7.8	1.96	2.02	−0.48	[126] #
$\{K_2[Mn(sal)_2(EtOH)_2][Mn(sal)_2]\}_n$	$T = 4.2$–$300\,K$, $B = 1\,T$	−9.0	2.00	2.00	−0.46	[127] #
$\{(NH_4)_2[Mn(sal)_2(EtOH)_2][Mn(sal)_2]\}_n$	$T = 4.2$–$300\,K$, $B = 1\,T$	−7.0	2.09	2.03	−1.40	[127] #
$\{Na_2[Mn(sal)_2][Mn(sal)_2EtOH]\cdot EtOH\}_n$	$T = 4.2$–$300\,K$, $B = 1\,T$	−20.3	2.00	2.00	−0.46, *zj*, −1.62	[127] #

General notes: The symbol '#' marks that a different definition of the J-parameter has been applied in the original source whereas here $-zj$ and/or $-J$ constants precede the spin operators; the coordination number (cn) is displayed when different from 6. The consistency criterion $D/\lambda = (g_z - g_x)/2$: Y—fulfilled, N—violated, O—cannot be judged.

separately in Tables 22–25. A few critical notes follows:

1. The magnetic field at which the data were taken should be small enough to avoid features due to magnetic saturation at low temperature. This is not always the case. The choice of $B = 0.1\,T$ with the SQUID apparatus (that scans the static magnetization) is a good setting. Errors could result using a Faraday balance and a field of $B = 1.5$ because the measured force

$$F_z = \frac{1}{\mu_0}\frac{m}{M_r}\frac{d}{dz}\left[\int_0^{B_z}\tilde{\chi}_{mol}(B_z)B_z dB_z\right] \approx \frac{1}{\mu_0}\frac{m}{M_r}\bar{\chi}_{mol}\frac{d}{dz}\left[\frac{1}{2}B_z^2\right] = \frac{1}{\mu_0}\frac{m}{M_r}\bar{\chi}_{mol}\left[B_z\frac{dB_z}{dz}\right] \quad (4.9)$$

   is no longer proportional to susceptibility and a calibration coefficient $B_z(dB_z/dz)$. The best method is to collect data with an alternating current susceptometer which scans the differential magnetic susceptibility directly at low fields ($B_{AC} \approx 0.001\,T$).
2. To report large values of the D-parameter without accounting for the g-factor anisotropy can lead to error because both effects have the same origin. The sign of the D-parameter should be consistent with the g-factor anisotropy, i.e. positive D appears when $g_z > g_x$ for shells less than half full ($\lambda > 0$) and, negative D appears when $g_z < g_x$ for shells more than half full ($\lambda < 0$).
3. The D-values are meaningful only when the ground state is orbitally non-degenerate, i.e. when there in a guarantee that the magnetic angular momentum is absent within the ground state.
4. Usually, the issue of whether using the opposite sign of D would yield a similar fit, is not tested.

Table 25
ZFS parameters based upon the powder susceptibility data

Compound	Experimental	Magnetic parameters (cm^{-1})	Reference
d^2			
$[V^{III}(urea)_6](ClO_4)_3$, $S = 1$	$T = 1.75$–$300\,K$	$B_2^0 = -163$, $B_4^0 = -99$, $B_4^3 = 2595$, $\lambda = 47$, $\lambda/\lambda_0 = 0.45$, $\kappa = 0.40$, $D^* = 5.86$	[77] O
$[V^{III}(acac)_3]$, $S = 1$	$B = 0.1\,T$	$D = 7.7$, $g_z = 1.96$, $g_x = 1.78$	[119] Y
d^3			
$[Cr^{III}(dedtc)_3]$, $S = 3/2$	$T = 2.2$–$300\,K$, $B = 0.3\,T$	$D = 0.6$	[121] O
$[Cr^{III}(\{L^{15}_{NNNSSS}\}Fe^{II})_2]PF_6$, $S = 3/2$	$T = 2$–$300\,K$, $B = 1.0\,T$	$D = 1.0$, $g = 1.97$, EPR: $D = 1.0$, $g_z = 1.976$, $g_x = 1.973$	[129] Y
d^5			
$[Mn^{II}(Me_6tren)Br]Br$, $S = 5/2$	$T = 4$–$300\,K$, $B = 1.2\,T$	$D = 0.24$, $g_z = 1.97$, $g_x = 2.07$	[130] O
$[Mn^{II}(bzimpy)Cl_2].0.5MeOH$, cn = 5, $S = 5/2$	$T = 4$–$300\,K$, $B = 1.4\,T$	$D = -2.73$, $E = 2.23$, $zj = 0.385$ $g_z = 1.944$, $g_x = 2.057$, $g_y = 1.880$	[131] O
$[Fe^{III}(Pydtc)_3]$, $S = 5/2$	$T = 2.2$–$300\,K$, $B = 0.3\,T$	$D = -2.14$; $B_2^0 = -0.72$, $B_4^0 = -0.24$, $B_4^3 = \pm 1.4$	[121] O
			[132] O
$[Fe^{III}(hemin)]$, $S = 5/2$	$T = 2$–$200\,K$, $B = 1.8\,T$	$D = 12$; $B_2^0 = 4.84$, $B_4^0 = -2.71$, $B_4^4 = -5.78$	[133] O
			[134]
$[Fe^{III}(TPP)(SCN)]$, cn = 5, $S = 5/2$	$T = 2$–$200\,K$, $B = 1.8\,T$	$D = 10$	[133] O
$[Fe^{III}(TPP)Cl]$, cn = 5, $S = 5/2$	$T = 2$–$200\,K$, $B = 1.8\,T$	~~$D = 12$~~	[133] O
		$D = 6$	[135] O
$[Fe^{III}(TPP)Br]$, cn = 5, $S = 5/2$	$T = 2$–$200\,K$, $B = 1.8\,T$	$D = 5$	[133] O
	$T = 2$–$100\,K$, $B = 1\,T$, $M(B \to 5\,T, T = 2$–$20\,K)$	$D = 13$, $g = 2$	[135] O
$[Fe^{III}\{L^{13}{}_{NNOO}\}Cl]\cdot CH_3CN$, cn = 5, $S = 5/2$	$T = 4$–$300\,K$, $B = 1\,T$	$D = 10.2$, $E = 3.4$, $g = 2.0$	[136] O
$[Fe^{III}\{L^{14}{}_{NNOO}\}Cl(H_2O)]\cdot 1/3CH_3Cl$, $S = 5/2$	$T = 4$–$300\,K$, $B = 1\,T$	$D = 7.2$, $E = 2.4$, $g = 2.0$, $zj = 1.0$	[136] #O
cis-$[Fe^{III}$(cyclam)(NO)I]I, $S = 3/2$	$T = 4$–$300\,K$, $B = 1\,T$	$D = +12.6$, $g = 2.0$	[147] O
$[Fe^{III}\{L^{19}{}_{NNN}\}(NO)(N_3)_2]$, $S = 3/2$	$T = 4$–$300\,K$, $B = 1\,T$	$D = +13.6$, $g = 2.1$	[147] O
d^6			
$[Fe^{II}(H_2O)_6]SiF_6$, $S = 2$		$D = 10.9$, $g_z = 2.00$, $g_x = 2.12$	[203,204]
$[Fe^{II}(py)_4(CF_3SO_3)_2]$, $S = 2$	$T = 4.2$–$310\,K$	$D = 6.1$, $g = 2.15$	[205] O
$[Fe^{II}(py)_4(CH_3SO_3)_2]$, $S = 2$	$T = 4.2$–$310\,K$	$D = 3.4$, $g = 2.08$	[205] O
$[Fe^{II}(py)_4(p\text{-}tolSO_3)_2]$, $S = 2$	$T = 4.2$–$310\,K$	$D = 3.9$, $g = 2.09$	[205] O
$[Fe^{II}(bpy)Cl_2]$, orange isomer, cn = 5, $S = 2$	$T = 4.2$–$300\,K$, $B = 0.51\,T$	$D = -2$	[206] O
$[Fe^{II}(TMC)(N_3)]BF_4$, cn = 5, $S = 2$	$T = 4.2$–$267\,K$	$D = 2.1$, $g_z = 2.39$, $g_x = 2.01$	[207] N
$[Fe^{II}(TMC)(NCMe)](BF_4)_2$, cn = 5, $S = 2$	$T = 4.2$–$267\,K$	$D = 3.4$, $g_z = 2.63$, $g_x = 2.00$	[207] N
$[Fe^{II}(TMC)(NCS)]BF_4$, cn = 5, $S = 2$	$T = 4.2$–$267\,K$	$D = 5.4$, $g_z = 2.58$, $g_x = 1.96$	[207] N
$[Fe^{II}(TMC)(Br)]Br$, cn = 5, $S = 2$	$T = 4.2$–$267\,K$	$D = 5.7$, $g_z = 2.32$, $g_x = 1.95$	[207] N
$[Fe^{II}(TMC)(Cl)]BF_4$, cn = 5, $S = 2$	$T = 4.2$–$267\,K$	$D = 6.2$, $g_z = 2.03$, $g_x = 2.00$	[207] N
$[Fe^{II}(1,7\text{-}CT)(Cl)]PF_6$, cn = 5, $S = 2$	$T = 4.2$–$267\,K$	$D = 8.8$, $g_z = 2.28$, $g_x = 1.94$	[207] N
$[Fe^{II}(1,3,7,10\text{-}CT)(Cl)]PF_6$, cn = 5, $S = 2$	$T = 4.2$–$267\,K$	$D = 3.1$, $g_z = 2.22$, $g_x = 2.01$	[207] N
$BaFe^{II}Si_4O_{10}$, cn = 4, $S = 2$	$T = 4.2$–$298\,K$, $B = 0.51\,T$	$D = 11.9$, $g_z = 1.979$, $g_x = 2.082$	[208] Y
$[Fe^{II}(biq)(NCS)_2]$, cn = 4, $S = 2$	$T = 1.5$–$303\,K$, $B = 0.51\,T$	$D = 5$, $g_z = 2.41$, $g_x = 2.24$	[209] N
$(NMe_4)_2[Fe^{II}Cl_4]$, cn = 4, $S = 2$	$T = 1.5$–$20\,K$, $B = 0.51\,T$	$D = 9.0$, $g_z = 2.05$, $g_x = 2.27$	[210] Y
$[Fe^{II}(PTC)]$, cn = 4, $S = 1$	$T = 1.25$–$300\,K$	$D = 70$, $g_z = 1.93$, $g_x = 2.86$	[137] Y
$[Fe^{II}(pdca)_2]\cdot 3H_2O$, cn = 6, $S = 2$	$T = 6$–$300\,K$	$D = 8.76$, $g = 2.16$	[138] O
$(NBu_4)[Co^{III}(bdt)_2]$, cn = 4, $S = 1$	$T = 2$–$100\,K$, $B = 1.07\,T$	$D = 37.4$, $g_z = 2.19$, $g_x = 2.31$	[139] Y
$(Nbu_4)[Co^{III}(tdt)_2]$, cn = 4, $S = 1$	$T = 2$–$100\,K$, $B = 1.07\,T$	$D = 39.4$, $g_z = 2.09$, $g_x = 2.27$	[139] Y
$K[Co^{III}(3\text{-}Prbi)_2]$, cn = 4, $S = 1$	$T = 4.2$–$300\,K$, $B = 1.66\,T$	$D = 40.9$, $g = 2$	[140] O
$[Co^{I}Cp^*_2]^+[Co^{III}\{L^4_{NNOO}\}]^-$, cn = 4, $S = 1$	$T = 1.9$–$300\,K$	$D = 45$, $g_z = 2.5$, $g_x = 2.2$	[141] N
$[Fe^{I}Cp^*_2][Co^{III}\{L^4_{NNOO}\}]$, cn = 4, $S = 1$	$T = 1.9$–$300\,K$	Co: $D = 45$, $g_z = 2.4$, $g_x = 2.2$, Fe: $J = +7$, $g_z = 4.40$, $g_x = 1.41$	[141] N
d^7			
$HgCo^{II}(NCS)_4$, cn = 4, $S = 3/2$,	$T = 1.7$–$300\,K$, $B = 0.5\,T$	$D = +10.6$, $g = 2.220$	[82] O
$(Net_4)_2[Co^{II}\{L^3_{SSOO}\}]$, cn = 4, $S = 3/2$	$T = 2$–$300\,K$, $B = 1\,T$, $0.005\,T$	$D = 5.4$, $g_z = 2.20$, $g_x = 2.29$	[142] #Y
$[Co^{II}\{L^5_{NNNOO}\}]$, cn = 5, $S = 3/2$	$T = 4.2$–$300\,K$, $B = 1.4\,T$	$D = -38.9$, $E = 1.7$, $zj = -1.0$, $g_z = 3.21$, $g_x = 1.67$, $g_y = 1.89$	[143] Y

Table 25 (*Continued*)

Compound	Experimental	Magnetic parameters (cm^{-1})	Reference
$[Co^{II}(bzimpy)Cl_2]$, cn = 5, $S = 3/2$	$T = 2$–150 K, $B = 0.1$ T	$D = 73.4$, $E = 3.28$, $zj = -0.205$, $g_z = 1.506$, $g_x = 2.501$, $g_y = 2.622$	[131] Y
$(NEt_4)_2[Co^{II}\{L^3_{SSOO}\}].2H_2O$, $S = 3/2$	$T = 2$–300 K, $B = 1$ T, 0.005 T	$A = 1.4$, $\kappa = 1$, $\lambda = -160$, $\delta = 800$	[142] O
$[Co^{II}(iphos)_2(H_2O)_2]$, $S = 3/2$	$T = 1.7$–260 K, $B = 0.6$ T, $M(B \rightarrow 7\,T, T = 1.8, 3, 5\,K)$	$D = 52$, $E = 17$, $g_z = 1.70$, $g_x = 2.53$	[144] Y
$[Co^{II}(acac)_2(H_2O)_2]$, $S = 3/2$		$D^* = 82.7$; $B = 980$, $\xi = 435$, $10Dq = 9300$, $-\delta = 550$	[145] O
$[Co^{II}(pyO)_6](ClO_4)_2$	$T = 4.2$–300 K, $B = 1$ T	$D^* = 25.5$; $B = 780$, $C = 3030$, $\xi = 525$, $10\Delta q = 8900$, $\Delta e_p = -665$	[146] O

General notes: The symbol '#' marks that a different definition of the *J*-parameter has been applied in the original source whereas here $-zj$ and/or $-J$ constants precede the spin operators; the coordination number (cn) is displayed when different from 6. The consistency criterion $D = (\lambda/2)(g_z - g_x)$: Y—fulfilled, N—violated, O—cannot be judged.

5. A reliable determination of the *D*-parameter requires a low-temperature data set ($T < D/k$); otherwise the values reported will be highly uncertain.
6. In some cases the powder susceptibility data are pathologically insensitive to the sign of the *D*-parameter. This is exactly the case of $S = 3/2$ where the modeling is presented in Fig. 17.
7. The overall effect of the *D*-parameter is a reduction of the effective magnetic moment from its temperature-independent value as the temperature decreases. The same effect is obtained from the negative molecular field correction which accounts for the isotropic exchange interaction with nearest neighbors ($zj < 0$). Evidently, these two effects interfere. Therefore it is risky to interpret the experimental data discussing only the sizable *D*-values without checking the paramagnetic anisotropy by independent measurements on oriented single crystals. An example of such a failure is the $[Ni(NH_3)_4(NO_2)_2]$ complex as reported by Figgis et al. [88,89].
8. In dealing with an increasing number of free parameters (D, g_z, g_x, zj) their mutual dependence might be questioned. Such a correlation analysis is rather rare [90].
9. The retrieved parameter set could depend upon the optimization technique applied. For example, the widely used *simplex method* is rather primitive; the *simulated annealing method* or the *genetic algorithms* are more advanced and capable of reaching the global minimum of the optimized functional [91–100].
10. The final parameter set also depends on the definition of the functional to be optimized. The least-squares functional on the magnetic susceptibility better fits the low-temperature data whereas such a functional on the effective magnetic moment reproduces better the high-temperature window of the data set.
11. The reported *D*-values are model-dependent: they were derived by analyzing the experimental data set in terms of the spin-Hamiltonian only. An alternative procedure is to employ all the spin–orbital basis functions leading to all the terms (e.g. 45 functions for the Ni(II) complexes instead only of the three pure spin states) and look for the energy differences between the lowest states. This could be performed either within the crystal-field theory or the angular overlap model [68–72]. It is better to delineate these differently derived values by a different symbol and D^* is used hereafter for the entire spin–orbital basis set derivation.
12. At small fields (when the Zeeman term can be considered as a perturbation) an approximate analytical formula of the type $\chi_a = f(D, g_a)$ could be applied; these suffer from the condition $|D| \gg \mu_B BgS$. As an alternative, the eigenvalue problem could be solved within the framework of the linear variation method; this approach

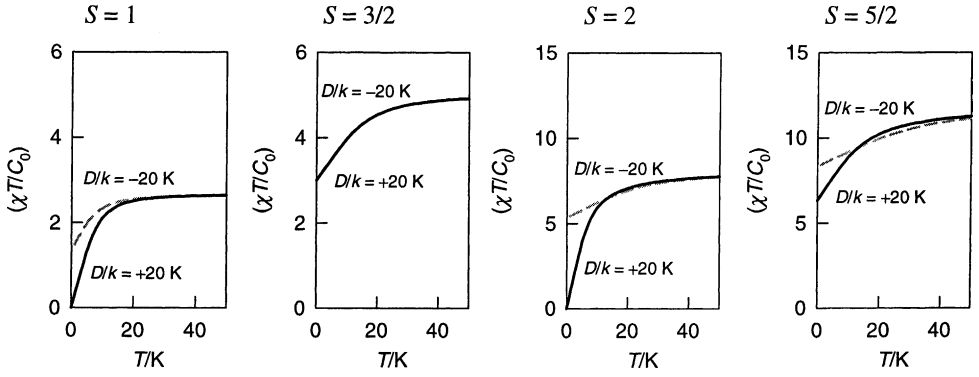

Fig. 17. The two product functions for $S = 1$, 3/2, 2, and 5/2 obtained with $D/k = \pm 20$ K. These are identical for $S = 3/2$.

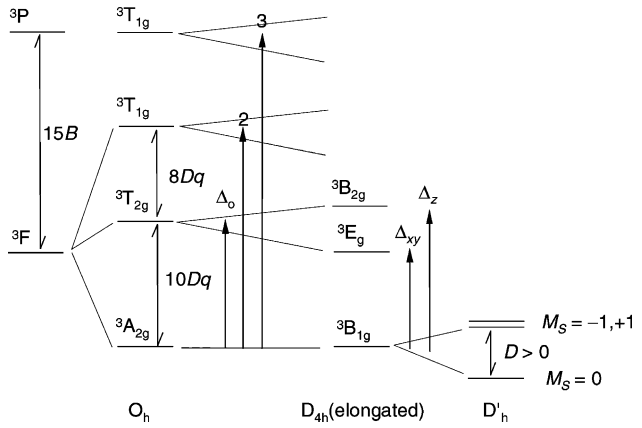

Fig. 18. Effect of the spin–orbit interaction leading to a positive D on tetragonal distortion in $S = 1$ d^8-complexes.

is preferable. However, the result will depend upon the selection of the size of the basis set.

4.2.1. Ni(II) complexes

The data compiled for the hexacoordinate Ni(II) compounds (Table 22) show that the D-parameters adopt values between -22 and $+12\,cm^{-1}$. This interval is rather broad. All the g-factors exceed the spin-free value of 2.0023 and typically lie between 2.1 and 2.2.

For tetracoordinate Ni(II) complexes, as well as nickelocene, the D-values are much larger but note that now the ground term is ^3T with non-zero orbital angular momentum. A few chain-structure compounds have also been included and they show only moderate D-values.

A frequent claim is [115] that the positive D-parameter is associated with a weakening of the axial bonds: the D-parameter is increased with axial elongation of the octahedron (geometry of the elongated square bipyramid) or when the axial ligand is weaker in its crystal field than the in-plane ligand (Fig. 18). Such a prediction is only partly valid as seen from the selected data where the increased crystal field strength over the series X = Cl, Br, and I is not always followed by a decrease of D (Table 23).

For chelate complexes the positive D-values prevail irrespective of whether the axial bonds are longer or shorter and the axial ligands possess a stronger or weaker crystal field. The chelate effect is associated with a considerable in-plane covalency leading to a significant drop in the orbital reduction factor $\kappa_x \ll 1$.

A simple formula for an octahedral reference system

$$D = \lambda^2(\Lambda_{xx} - \Lambda_{zz}) = \lambda^2 4\frac{(\kappa_x^2 - \kappa_z^2)}{\Delta_o(^3A_{2g} \rightarrow {}^3T_{2g})} \tag{4.10}$$

will predict negative D when $\kappa_x < \kappa_z(\approx 1)$. Therefore, it can be concluded that several factors come into the competition and they influence the final sign and value of the D-parameter:

1. the geometric distortion which could be influenced by the crystal packing;
2. the crystal-field strength of the individual ligands;
3. the covalency (orbital reduction factors).

For an elongated tetragonal bipyramid the above formula relaxes to [101]

$$D = \lambda^2 4\left[\frac{\kappa_x^2}{\Delta_x(^3B_{1g} \rightarrow {}^3E_g)} - \frac{\kappa_z^2}{\Delta_z(^3B_{1g} \rightarrow {}^3B_{2g})}\right] \tag{4.11}$$

Within the formal perturbation theory we have interrelationships (the positive sign convention for the L-tensor) $g_z = g_e - 2\lambda\Lambda_{zz}$ and $g_x = g_e - 2\lambda\Lambda_{xx}$, and for $\lambda < 0$ as in the case of Ni(II) complexes ($\lambda/hc = -315\,cm^{-1}$) there is

$$D = \frac{\lambda}{2}(g_z - g_x) = \begin{cases} < 0, & \text{when } g_z > g_x \\ > 0, & \text{when } g_z < g_x \end{cases} \tag{4.12}$$

as sketched in Fig. 19.

4.2.2. Mn(III) complexes

The g-factor anisotropy is very small for Mn(III) compounds and difficult to be detected on the magnetic susceptibility data alone (the EPR technique is helpful in this respect). The averaged g-values range between 1.95 and 2.09. The D-values are, also, quite small and they vary between

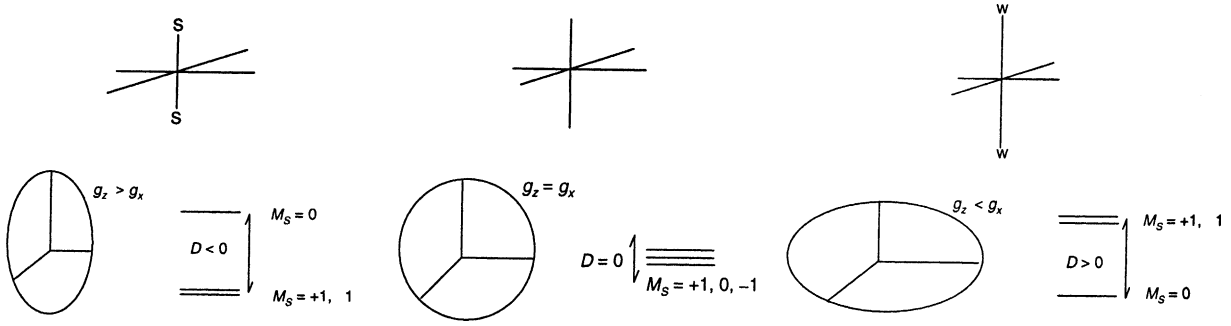

Fig. 19. Relationships between the g-tensor componenets and the D-parameter for an $S = 1$ system with $\lambda < 0$; s (w) means a stronger (weaker) crystal field or compressed (elongated) tetragonal bipyramid.

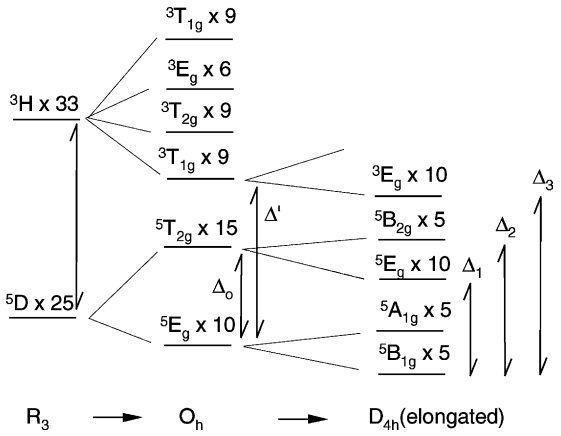

Fig. 20. The lowest energy levels in octahedral Mn(III) complexes.

-3.8 and $+3.1\,\mathrm{cm}^{-1}$ for mononuclear species (Table 24). These features have an obvious root: small spin–orbit splitting parameter $\lambda = \xi_{\mathrm{Mn(III)}}/2S$ which is $\lambda/hc = 89\,\mathrm{cm}^{-1}$.

An expression for the D-parameter has been derived from perturbation theory [128]

$$D = \pm\lambda^2\left[\frac{3}{\Delta_o(^5\mathrm{E_g} \rightarrow {}^5\mathrm{T_{2g}})} + \frac{4}{\Delta'(^5\mathrm{E_g} \rightarrow {}^3\mathrm{T_{1g}})}\right] \quad (4.13)$$

where $\Delta_o = 10Dq$ is the octahedral crystal field splitting (Fig. 20). The positive sign applies when the ground state is $^5\mathrm{A_{1g}}$ (a compressed tetragonal bipyramid) whereas the negative sign appears when the ground state is $^5\mathrm{B_{1g}}$ (an elongated tetragonal bipyramid). Considering the tetragonal symmetry lowering explicitly, the perturbation theory yields a refined expression in the form [123]

$$D = \frac{\xi}{16}^2\left[\frac{1}{\Delta_1(^5\mathrm{B_{1g}} \rightarrow {}^5\mathrm{E_g})} - \frac{4}{\Delta_2(^5\mathrm{B_{1g}} \rightarrow {}^5\mathrm{B_{2g}})} - \frac{4}{\Delta_3(^5\mathrm{B_{1g}} \rightarrow {}^3\mathrm{E_g})}\right] \quad (4.14)$$

The analysis of magnetic data for Mn(III) complexes is frequently carried out by assuming a pair-wise weak antiferromagnetic exchange interaction (Table 24). The zero-field Hamiltonian is then postulated as follows

$$\hat{H} = -J(\vec{S}_1 \cdot \vec{S}_2) + D_1[\hat{S}_{z1}^2 - \tfrac{1}{3}S(S+1))] + D_2[\hat{S}_{z2}^2 - \tfrac{1}{3}S(S+1))] \quad (4.15)$$

and this form (with small negative exchange coupling constant J) reduces the D-parameter to an acceptable range. Omitting J, the D-values would be too negative.

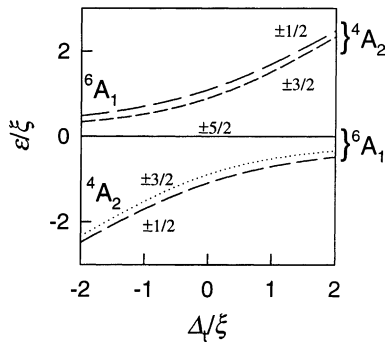

Fig. 21. Energy levels of a spin admixed system $^6\mathrm{A_1}$–$^4\mathrm{A_2}$ in the zero field.

4.2.3. V(III) complexes

As evident from Tables 21 and 25 the hexacoordinate V(III) complexes exhibit rather sizable values of the D-parameter spanning positive values up to $8\,\mathrm{cm}^{-1}$. All the g-factors lie below 2.0 and are highly anisotropic: $g_x \ll g_z < g_e$.

The ligand sphere of the complexes investigated was represented by six unidentate ligands (in one case three bidentate ones). As the ground state $^3\mathrm{T_{1g}}$ is subject to the Jahn-Teller effect, either tetragonal or trigonal distortion of the coordination polyhedron is expected. With the compressed tetragonal bipyramid, by setting the crystal field parameters $F_4(\mathrm{ax}) > F_4(\mathrm{eq})$, the ground state becomes $^3\mathrm{A_{2g}}$. This is the case when the ZFS philosophy is legitimate. On the contrary, when the axial crystal field is weaker (a geometry of elongated tetragonal bipyramid) the ground CF term is $^3\mathrm{E_g}$ and this is split in a more complex manner where the spin-Hamiltonian is not appropriate any longer. With $\lambda/hc = +105\,\mathrm{cm}^{-1}$ there is

$$D = \tfrac{1}{2}\lambda(g_z - g_x) > 0, \quad \text{when} \quad g_z > g_x \quad (4.16)$$

and the situation is opposite to the case of Ni(II) when looking for the g-tensor ellipsoid: now the prolate form is associated with the positive D-value for V(III). Notice that this prolate form applies when the interatomic distance ellipsoid exhibits an oblate form (a compressed tetragonal bipyramid).

4.2.4. Cr(III) complexes

The ground CF term for hexacoordinate Cr(III) complexes is $^3\mathrm{A_{1g}}$ and it represents a typical ZFS system. The recorded D-values are small owing to the small spin–orbit splitting parameter $\lambda/hc = +92\,\mathrm{cm}^{-1}$. The g-factors are a bit below 2.0 and slightly anisotropic. Positive D-values are consistent with $g_z > g_x$.

Table 26
Lowest energy levels for d^5 systems [66]

State	$E(^6\mathrm{A_1}, \pm1/2, \mathrm{a_1})$	$E(^6\mathrm{A_1}, \pm3/2, \mathrm{a_1})$	$E(^6\mathrm{A_1}, \pm5/2, \mathrm{a_1})$
Energy for O_h	$-2\xi^2/\Delta_o$	$-2\xi^2/\Delta_o$	$-2\xi^2/\Delta_o$
Energy for D_{4h}	$-(6/5)\xi^2/\Delta_t = -6D$	$-(4/5)\xi^2/\Delta_t = -4D$	0

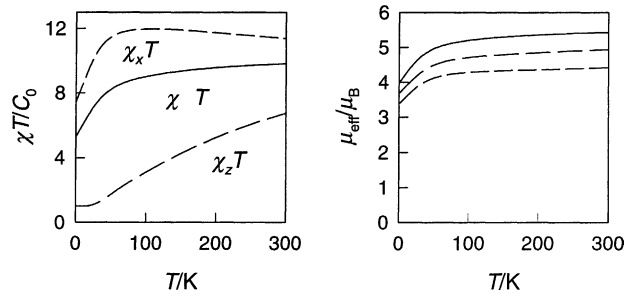

Fig. 22. Temperature variation of the magnetic susceptibility functions (left) and the effective magnetic moment (right) for the spin admixed system $^6A_1$–$^4A_2$, $\xi/hc = 460\,cm^{-1}$, $g_x = g_z = 2.0$: left—individual curves show magnetic anisotropy for $\Delta/hc = 500\,cm^{-1}$; right—different energy gap $\Delta/hc = +500\,cm^{-1}$ (solid), $\Delta/hc = 0$ (long dashed), $\Delta/hc = -500\,cm^{-1}$ (medium dashed).

4.2.5. Fe(III) and Mn(II) complexes

The majority of studies on Fe(III) complexes were done for the porphine-type complexes with coordination number five. A few hexacoordinate complexes represent typical $^6A_{1g}$ systems having the spin–orbit splitting parameter λ undefined as the $^6A_{1g}$ term is not split by the SOI. The energy levels are only shifted and this shift is interpreted in terms of the true spin–orbit coupling constant ξ and the energy gap $\Delta_o = E(^4T_1) - E(^6A_1)$ between the ground and the first excited state as shown in Table 26.

On tetragonal distortion the levels are split: the axial zero−field splitting parameter is $D = \xi^2/5\Delta_t$ and its sign is determined by the sign of the energy gap $\Delta_t = E(^4A_2) - E(^6A_1)$. The energy gap Δ_t is assumed to be large in absolute value in order for the perturbation theory to be applicable. For a small energy gap perturbation theory is not applicable and one has to diagonalize the 10×10 zero−field matrix (Fig. 21). This situation refers to the spin admixed states.

The modelling of the magnetic susceptibility shows that with decreasing energy gap the effective magnetic moment decreases (Fig. 22). For a positive enough value of Δ_t the effective magnetic moment refers to the $^6A_1$ state and D—positive. On the contrary, for large negative values of Δ_t the effective magnetic moment refers to the $^4A_2$ state and $D < 0$.

A more detailed analysis gave the expressions that recognize the covalency effects (orbital reduction factors κ) in the form [57b]

$$D = \frac{\xi^2}{10}\left[\frac{2\kappa_z^2}{\Delta_z(^6A_1 \rightarrow {}^4T_{1z})} - \frac{\kappa_y^2}{\Delta_y(^6A_1 \rightarrow {}^4T_{1y})} - \frac{\kappa_x^2}{\Delta_x(^6A_1 \rightarrow {}^4T_{1x})}\right] \quad (4.17)$$

$$E = \frac{\xi^2}{10}\left[\frac{\kappa_y^2}{\Delta_y(^6A_1 \rightarrow {}^4T_{1y})} - \frac{\kappa_x^2}{\Delta_x(^6A_1 \rightarrow {}^4T_{1x})}\right] \quad (4.18)$$

Inspection of Table 25 shows that the D-values for hexacoordinate Fe(III) and Mn(II) complexes are rather small and the g-factors are close to 2.0. The D-values increase with ligand sphere asymmetry or with a coordination number of 5 [136].

4.2.6. Co(III) and Fe(II) complexes

These d^6 systems could exist in various spin states: low-spin ($S = 0$), high-spin ($S = 2$), and with distorted chromophore or with cn = 4 also in the intermediate-spin state ($S = 1$). Often a spin crossover (transition from the low-spin to the high-spin state) is observed for this class of compounds. The D-values reported for the tetracoordinate-planar Co(III) complexes ($S = 1$) are really large: up to $+45\,cm^{-1}$. The g-factors are larger than 2.0 and are substantially anisotropic (Table 25).

For nearly octahedral Fe(II) complexes two situations can occur. With elongated tetragonal bipyramidal geometry the ground CF-term is $^5B_{2g}$ and this situation matches the positive ZFS. Consequently the axial ZFS parameter is expressed as

$$D = \lambda^2/\Delta_{ax}(^5B_{2g} \rightarrow {}^5E_g) > 0 \quad (4.19)$$

For a compressed tetragonal bipyramid the ground CF-term is ^5E_g and this is further split by the spin–orbit interaction into five equally spaced doublets.

4.2.7. Co(II) complexes

In tetrahedral geometry the ground CF term state is non-degenerate $^4A_2$ and represents a typical ZFS system. The D-values adopt sizable values of $+10\,cm^{-1}$; the g-factors are larger than 2.0 and are anisotropic. The D-values are influenced by the lowest excitation energies as perturbation theory predicts

$$D = 4\lambda^2\left[\frac{1}{\Delta_x(^4B_1 \rightarrow {}^4E)} - \frac{1}{\Delta_z(^4B_1 \rightarrow {}^4B_2)}\right] \quad (4.20)$$

with $\lambda/hc = -172\,cm^{-1}$, D is rather large.

The situation is different for octahedral Co(II) complexes The magnetic angular momentum present in the T-terms significantly affects the energy levels and consequently the magnetic properties. In a regular octahedral crystal field the 12-fold degenerate $^4T_1$ term splits into multiplets according to the total quantum number $|L - S| \leq J \leq L + S$. With the negative splitting parameter λ the ground state has $J = 5/2$ and the irreducible representations (Γ_7, Γ_8) of the double group O' are accidentally degenerate. However, this degeneracy is partly lifted through off-diagonal (interaction) matrix elements.

With reduction of symmetry to D_{4h}, further splitting occurs. First, the $^4T_{1g}$ CF-term splits into ^4E_g and $^4A_{2g}$ where $^4A_{2g}$ is the ground state when the tetragonal field parameter Δ_{ax} is positive. When spin orbit coupling is switched on, the ground state further splits into Kramers doublets Γ_6 and Γ_7. The difference between these states can be written as $2D$. Also, the upper CF-term ^4E_g splits into four Kramers

Table 27
Range of D-values (cm^{-1}) in mononuclear complexes based on susceptibility data[a]

	V^{III}, $S=1$	Cr^{III}, $S=3/2$	Mn^{III}, $S=2$	Fe^{III}, $S=5/2$	Mn^{II}, $S=5/2$	Fe^{II}, $S=2$	Co^{III}, $S=1$	Co^{II}, $S=3/2$	Ni^{II}, $S=1$
λ/hc	+105	+92	+89	–; $\xi=460$	–; $\xi=300$	−100	−290	−172	−315
cn = 6									
O_h-term	$^3T_{1g}$,*	$^4A_{2g}$	^5E_g,*	$^6A_{1g}$	$^6A_{1g}$	$^5T_{2g}$,*		$^4T_{1g}$,*	$^3A_{2g}$
D_{4h}-term	$^3A_{2g}$/c	$^4B_{1g}$	$^5A_{1g}$/c, $^5B_{1g}$/e	$^6A_{1g}$	$^6A_{1g}$	$^5B_{2g}$/e		$^4A_{2g}$/c	$^3B_{1g}$
Minimum	+3.7	+0.2	−3.0	−2.1		−5		+25	−22.3
Maximum	+8.0	+1.0	+3.1	+7.2	+0.2	+12		+83	+9.5
cn = 5 and 4									
Minimum			−2.5	+5	−2.7	+2	+37	−38	+18
Maximum			−1.0	+13		+12	+45	+73	+53

[a] Systems obeying the Jahn–Teller effect (through which the octahedral geometry is spontaneously distorted) are marked with a star (*); c—commpressed bipyramid, e—elongated bipyramid.

doublets (CF-multiplets). The D-values are very large, up to 83 cm^{-1} and the g-factor anisotropy is also large.

The range of D-values reported so far on the basis of magnetic susceptibility data is reviewed in Table 27.

4.2.8. Dinuclear complexes

In dinuclear complexes two kinds of the spin–spin interaction are met:

(a) the local $D-$tensors contributing from each centre

$$\hat{H}_A^{ZFS} + \hat{H}_B^{ZFS} = \overline{h}^{-2}(\vec{S}_A \cdot \bar{\bar{D}}_A \cdot \vec{S}_A + \vec{S}_B \cdot \bar{\bar{D}}_B \cdot \vec{S}_B) \quad (4.21)$$

(b) the pair−interaction $D-$tensor belonging to the asymmetric exchange

$$\hat{H}_{AB}^{asym} = \overline{h}^{-2}(\vec{S}_A \cdot \bar{\bar{D}}_{AB} \cdot \vec{S}_B) \quad (4.22)$$

These can be combined into a single molecular−state term $\bar{\bar{D}}_S$. At the same time the local g-tensors are also combined to $\bar{\bar{g}}_S$ (Chapter 3.2). All the $D-$tensors involved are symmetric and traceless, each having five independent components. For a diagonal form only two parameters survive:

(1) the axial zero−field splitting parameter

$$D = \tfrac{1}{2}(-D'_{xx} - D'_{yy} + 2D'_{zz}) = \tfrac{3}{2}D_{zz} \quad (4.23)$$

(2) the rhombic zero−field splitting parameter

$$E = \tfrac{1}{2}(D'_{xx} - D'_{yy}) \quad (4.24)$$

The spin-Hamiltonian appropriate to the binuclear system contains the isotropic exchange term, the asymmetric exchange term, the local ZFS terms, and the local spin Zeeman terms so that it involves these magnetic parameters: J_{AB}, D_{AB}, D_A, D_B, g_A, and g_B. The remaining parameters E_{AB}, E_A, and E_B are usually neglected. For a sizable local ZFS parameter D_A, the g-factor anisotropy should be also considered, i.e. g_{Az} and g_{Ax} and analogously for the centre B. To this end one has 8 magnetic parameters and this set can be eventually enriched by the molecular field correction zj. This is too much in order to be fixed unambiguously on the basis of the temperature dependence of the magnetic susceptibility alone. (We also assumed that all the g-tensors and D-tensors are collinear; otherwise angles between them should be considered.)

The set of magnetic parameters can be reduced taking into account the results of the formal perturbation theory: the components of the Λ-tensor determine the components of the g- and D-tensors.

The magnetic parameters for binuclear complexes which involve non-zero D-parameter values are collected in Tables 28 and 29. In addition to twelve notes presented along with the mononuclear complexes, some additional remarks follow.

1. Three effects reduce the magnetic productivity at low temperature: (i) the intramolecular antiferromagnetic exchange, (ii) the intramolecular antiferromagnetic exchange treated within the molecular field correction, (iii) the ZFS. Their correct separation is a difficult task and without a parameter correlation analysis, the reported data for D are very uncertain.
2. With ferromagnetic exchange the identification of magnetic impurities is problematic as the magnetic contribution of the impurity (S_i) is lower than those of the pure exchange-coupled substance ($S_1 + S_2$).
3. The asymmetric exchange (D_{AB}) is usually omitted and only the local ZFS effects (D_A, D_B) are considered.

4.2.9. Trinuclear complexes

In trinuclear complexes, a new aspect appears as the geometry spans several classes:

(a) an equilateral triangle, all three sides equal;
(b) an isosceles triangle, two sides equal;
(c) a general triangle;
(d) an (almost) linear assembly (the most frequent case).

The geometrical topology defines possible constraints among the exchange coupling constants (e.g. all equal for the equilateral triangle). Moreover, the Jahn-Teller effect can apply. This means that the geometry for which the ground electronic state is orbitally degenerate is unstable (it

Table 28
ZFS parameters in homobimetalic complexes

System	Experimental	D_M	g_z	g_x	J_{M-M}	Reference
d^4, Mn^{III}						
$[Mn^{III}(salen)(H_2O)]_2(ClO_4)_2$, $S_i = 2$	$T = 4$–$300\,K$, $B = 1.0\,T$	−1.70	2.0		+12.6	[148]#
$[Mn^{III}(salen)(NO_3)]_n$, chain structure, $S_i = 2$	$T = 4$–$300\,K$, $B = 1.0\,T$	−0.43	2.0		−1.01	[148]#
$[Mn^{III}_2(nsalpro)_2(H_2O)]\cdot 3H_2O$, $S_i = 2$	$T = 2$–$300\,K$	−2.59	2.076	2.006	−3.86	[149]#
$[Mn^{III}_2(nsalpro)_2]\cdot 2DMF$, $S_i = 2$	$T = 2$–$300\,K$	−2.51	2.098	2.041	−3.24	[149]#
$[Mn^{III}(3\text{-MeO-salen})Cl]_2$, $S_i = 2$	$T = 2$–$300\,K$	−0.96	2.105	1.980	0.66	[149]#
d^5, Mn^{II}						
$[Mn^{II}(tren)(NCO)]_2(BPh_4)_2$, $S_i = 5/2$	$T = 4$–$300\,K$, $B = 1.2\,T$	3.8	2.20	1.91		[130]#[a]
		−0.29	2.0		−0.30	
$[Mn^{II}(tren)(NCS)]_2(BPh_4)_2$, $S_i = 5/2$	$T = 4$–$300\,K$, $B = 1.2\,T$	2.89	2.20	1.84		[130]#[a]
		−0.001	2.0		−0.26	
$[Mn^{II}(tren)(CN)]_2(BPh_4)_2$, $S_i = 5/2$	$T = 4$–$300\,K$, $B = 1.2\,T$	0.60	2.04			[130]#
d^6, Fe^{II}						
$(PPh_4)_2[Fe^{II}_2Cl_6]$, $S_i = 2$	$T = 2$–$300\,K$, $B = 0.1\,T$, $M(B \to 5\,T,\ T = 2,\ 5\,K)$	4.9	2.25	2.20	0.14	[150]#
$(NEt_4)_2[Fe^{II}_2Cl_6]$, $S_i = 2$	$T = 2$–$300\,K$, $B = 0.1\,T$	5.2	2.31	2.23	0.20	[150]#
$(ppn)_2[Fe^{II}_2Cl_6]$, $S_i = 2$	$T = 2$–$300\,K$, $B = 0.1\,T$	6.3	2.24		0.14	[150]#
$(AsPh_4)_2[Fe^{II}_2Cl_6]$, $S_i = 2$	$T = 2$–$300\,K$, $B = 0.1\,T$	4.5	2.30	2.00	−0.10	[150]#
$(H\text{-TMPP})_2[Fe^{II}_2Cl_6]$, $S_i = 2$	$T = 2$–$300\,K$, $B = 0.1\,T$	3.7	2.20	2.00	−1.48	[150]#
$[(bpym)\{Fe^{II}Cl_2(bpym)\}_2]$, $S_i = 2$	$T = 2$–$300\,K$, $B = 0.1\,T$	−17.0	2.24		−2.2	[150]#
$[(bpym)\{Fe^{II}Cl_2(MeOH)_2\}_2]\cdot(NEt_4)Cl$, $S_i = 2$	$T = 2$–$300\,K$, $B = 0.1\,T$	−16.3	2.07		−2.0	[150]#
$[Fe^{II}(alaw)_2(MeOH)]$, dimer, $S_i = 2$	$T = 1.6$–$300\,K$	4.9	2.296	2.023	−3.2	[151]#
$[Fe^{II}\{L^{10}{}_{NNNO(O)}\}(MeOH)]_2\cdot(ClO_4)_2$, $S_i = 2$	$T = 2$–$300\,K$	3.2	1.980	2.168	−3.4	[152]#
$[Fe^{II}\{L^{11}{}_{NO}\}_2(MeOH)_2Cl]_2$, $S_i = 2$	$T = 2$–$300\,K$	11.1	2.029	1.997	−4.2	[153]#
d^7, Co^{II}						
$(ppn)_2[Co^{II}_2Cl_6]$, $S_i = 3/2$	$T = 2$–$300\,K$, $B = 0.1\,T$	29.0	2.25		−11.6	[150]#
$[Co^{II}_2(bhmp)(ac)_2]BPh_4$, $S_i = 3/2$	$T = 4.5$–$300\,K$, $B = 0.5\,T$	κ, 0.77, D^*, 37	λ, −116, g_z^*, 2.11	Δ, 572, g_x^*, 4.73	−0.44	[154]
$[Co^{II}_2(bhmp)(bz)_2]BPh_4$, $S_i = 3/2$	$T = 4.5$–$300\,K$, $B = 0.5\,T$	κ, 0.96, D^*, 35	λ, −93, g_z^*, 2.09	Δ, 616, g_x^*, 4.91	−0.33	[154]
$[Co^{II}_2(bomp)(ac)_2]BPh_4$	$T = 1.8$–$300\,K$	κ, 0.98, D^*, 60	λ, −134, g_z^*, 2.18	Δ, 749, g_x^*, 4.99	−0.55	[155]
$[Co^{II}_2(bomp)(bz)_2]BPh_4$	$T = 1.8$– $300\,K$	κ, 0.84, D^*, 72	λ, −138, g_z^*, 2.45	Δ, 440, g_x^*, 4.84	−0.70	[155]
$[Co^{II}(sal\text{-}tabp)]_2\cdot 0.5H_2O$, $S_i = 3/2$, cn = 4	$T = 4$–$290\,K$	−2.0	2.60	2.20	−1.2	[156]#
		D	g	zj	J	
d^8, Ni^{II}						
$[Ni^{II}(sal\text{-}tabp)]_2\cdot H_2O$, $S_i = 1$, cn = 4	$T = 4$–$290\,K$	0.84	2.22	−2.4	−0.98	[156] #
$[Ni^{II}(sal\text{-}m\text{-}phen)]_2\cdot 3H_2O$, $S_i = 1$, cn = 4	$T = 4$–$290\,K$	0.72	2.36	−3.0	−3.2	[156] #
	$T = 4$–$300\,K$, $B = 1.8\,T$	0.8	2.19		−2.8	[157]
$[Ni^{II}(sal\text{-}2,4\text{-}tol)]_2\cdot 3H_2O$, $S_i = 1$, cn = 4	$T = 4$–$300\,K$, $B = 1.8\,T$	1.2	2.20		−2.7	[157]
$[Ni^{II}(sal\text{-}2,6\text{-}tol)]_2$, $S_i = 1$, cn = 4	$T = 4$–$300\,K$, $B = 1.8\,T$	1.0	2.18		−2.9	[157]
$[Ni^{II}_2(en)_4Cl_2]Cl_2$, $S_i = 1$	$T = 1.5$–$300\,K$	+6.5	2.14	−0.33	19.7	[90][b] #
		−11	2.12	−0.04	20.8	
$[Ni^{II}_2(en)_4Br_2]Br_2$, $S_i = 1$	$T = 1.5$–$300\,K$	+6.6	2.12	−0.56	17.2	[90][b] #
		−7.6	2.12	−0.32	15.1	
$[Ni^{II}_2(en)_4(SCN)_2]I_2$, $S_i = 1$	$T = 1.5$–$300\,K$	+4.7	2.14	−0.36	9.7	[90][b] #
		−3.3	2.14	−0.31	9.0	
$[Ni^{II}(CH_2(dmpz)_2)Cl_2]_2$, dimer, $S_i = 1$	$T = 4.2$–$90\,K$, $B = 0.38\,T$	2.17	2.310	−0.78	+5.16	[158] #
$[\mu\text{-BiIm}(Ni^{II}(tren))_2](BPh_4)_2$, $S_i = 1$	$T = 4.2$–$286\,K$	53 (problematic)	2.082	+2.50	−5.8	[159] #
$[Ni^{II}(tren)(NCO)]_2(BPh_4)_2$, $S_i = 1$	$T = 4.2$–$289\,K$	−10.1	2.282	1.42	−8.8	[160] #
$[Ni^{II}(tren)(NCS)]_2(BPh_4)_2$, $S_i = 1$	$T = 4.2$–$289\,K$	−0.45	2.255	−0.32	+4.8	[160] #
$[Ni^{II}(tren)(NCSe)]_2(BPh_4)_2$ $S_i = 1$	$T = 4.2$–$289\,K$	−0.49	2.247	−0.14	+3.2	[160] #
$[Ni^{II}(tren)(N_3)]_2(BPh_4)_2$ $S_i = 1$	$T = 4.2$–$300\,K$, $B = 1.48\,T$	+6.8	2.325	0.50	−70.2	[199] #
$[\mu\text{-}(N_3)(Ni^{II}(macro)(N_3))_2]I$, $S_i = 1$	$T = 4.2$–$300\,K$, $B = 1.48\,T$	4.9	2.233	−2.4	−24.6	[199] #
$[Ni^{II}(terpy)(NCO)(H_2O)]_2(PF_6)_2$, $S_i = 1$	$T = 2$–$300\,K$, $B = 0.2\,T$	−12.2	2.21	0.40	+9.2	[200] #
$[Ni^{II}(terpy)(N_3)_2]_2(PF_6)_2\cdot 2H_2O$, $S_i = 1$	$T = 2$–$100\,K$	−12.5	2.26	0.76	+40.2	[201] #
$[\mu\text{-}(NCSe)_2(Ni^{II}(medpt)_2(NCSe))_2](PF_6)_2$, $S_i = 1$	$T = 4$–$300\,K$, $B = 1.5\,T$	1.5	2.15	0.22	+17.6	[202] #
$[\mu\text{-}(NCS)_2(Ni^{II}(terpy)(NCS))_2]$, $S_i = 1$	$T = 2$–$300\,K$, $B = 0.2\,T$	−4.3	2.10	0.02	+9.8	[161] #
$[\mu\text{-}(NCS)_2(Ni^{II}(terpy)(NCSe))_2]$, $S_i = 1$	$T = 2$–$300\,K$, $B = 0.2\,T$	−10.0	2.15	0.01	+20.2	[161] #
$[\mu\text{-}(NCS)_2(Ni^{II}_2(mepn)_3(NCS)_2]_2[Ni^{II}(mepn)_2(NCS)_2]\cdot H_2O$, $S_i = 1$	$T = 4$–$300\,K$, $B = 1.5\,T$	−20.0	2.13	0.20	+8.6	[162] #
$[\mu\text{-}(NCS)_2(Ni^{II}(mepn)_2(NCS))_2](PF_6)_2$, $S_i = 1$	$T = 4$–$300\,K$, $B = 1.5\,T$	−2.0	2.14	−0.14	+12.7	[162] #

General notes: The symbol '#' markes that a different definition of the J-parameter has been applied in the original source as here $-zj$ and/or $-J$ constants precede the spin operators; the coordination number (cn) is displayed when different from 6.

[a] The first set obtained by fitting the effective magnetic moment, the second-magnetic susceptibility.

[b] Two sets of magnetic parameters differing in the sign of the D-parameter.

Table 29
ZFS parameters in heterobimetalic and mixed-valence complexes

System	Experimental	D_M	g_z	g_x	J_{M-M}	Reference
$[\{L^{15}_{NNNSSS}\}Fe^{III}Cr^{III}Fe^{II}\{L^{15}{}_{NNNSSS}\}](PF_6)_2$, $S(Fe^{III}) = 1/2$, $S(Cr^{III}) = 3/2$, $S(Fe^{II}) = 0$	$T = 2$–300 K, $B = 1.0$ T	D_{Cr}, 2.0	g_{Cr}, 1.80, g_{Fe}, 2.00		+52	[129] #
$[\{L^{15}_{NNNSSS}\}Fe^{III}Co^{III}Fe^{III}\{L^{15}_{NNNSSS}\}](PF_6)_3$, $S(Fe^{III}) = 1/2$, $S(Co^{III}) = 0$	$T = 2$–300 K, $B = 1.0$ T	D_{Fe}, 1.5	g_{Fe}, 2.07		+83	[129] #
$[Fe^{III}Fe^{II}\{L^{12}_{N3O3N2O4}\}(mpdp)_2].(BPh_4)$, $S_1 = 5/2$, $S_2 = 2$	$T = 2$–300 K, $B = 0.5$–5 T	D_2, −13	g_1, 2	g_2, 2.09	−8.0	[163] #
$[Fe^{III}Fe^{II}\{L^{19}_{NONNON}\}(\mu\text{-ac})_2]ClO_4$, $S_1 = 5/2$, $S_2 = 2$	$T = 4.3$–300 K, $B = 0.5$ T	3	1.73	2.11	−10 *B*, 820	[164] #
$[Fe^{III}Fe^{II}L^{19}_{NONNON}\}(\mu\text{-bz})(bz)(H_2O)]ClO_4$, $S_1 = 5/2$, $S_2 = 2$	$T = 4.3$–300 K, $B = 0.5$ T	4	1.93	1.99	−44 *B*, 600	[164] #
$[Fe^{III}OFe^{IV}\{L^{18}_{ONNO}R_1R_2\}_2]I_3$.sol, $S_1 = 5/2$, $S_2 = 2$	$T = 4.2$–300 K, $B = 0.6$ T			*zj*	*J*	
sol = $I_2{\cdot}CHCl_3$, R_2 = Et		11.9			−35.4	[165] #
sol = $I_2{\cdot}CHCl_3$, R_2 = *n*-Pr		11.5		9.8	−46.2	[165] #
sol = $I_2{\cdot}CHCl_3$, R_2 = *n*-Bu		10.8		6.0	−41.0	[165] #
sol = $1.5I_2$, $R_1 = R_2$ = Me		16.1		3.2	−43.4	[165] #
sol = I_2, R_1 = Me, R_2 = Et		9.0		4.8	−39.0	[165] #
sol = I_2, R_1 = Me, R_2 = *n*-Pr		10.7		1.7	−42.0	[165] #
$[Fe^{III}(OH)_2Fe^{IV}\{L^{18}_{ONNO}R_1R_2\}_2]BF_4$, R_2=*n*-Pr		10.3		6.0	−31.2	[165] #
$[Fe^{III}(OEP^{\bullet})Cl]_2(SbCl_6)_2$, $S(Fe^{III}) = 5/2$, $s(OEP^{\bullet}) = 1/2$, cn = 5	$T = 2$–300 K, $B = 0.2$, 1 T	10		$J_{Fe\text{-}r}$, −63	$J_{R\text{-}R}$, −4	[166] #
$[Fe^{III}(OEP^{\bullet})Br]_2(SbCl_6)_2$, $S(Fe^{III}) = 5/2$, $s(OEP^{\bullet}) = 1/2$, cn = 5	$T = 2$–300 K, $B = 0.2$, 1 T	10		$J_{Fe\text{-}r}$, −83	$J_{R\text{-}R}$, −4	[166] #
$[(phen)_2Cr^{III}(\mu\text{-}OH)_2Ni^{II}(Me_2\text{-tpa})](ClO_4)_3{\cdot}2H_2O$, $S(Cr^{III}) = 3/2$, $S(Ni^{II}) = 1$	$T = 4.2$–300 K	$D_{5/2}$, 0.051	g_{Ni}, 2.09	g_{Cr}, 2.0	+4.07	[167]
$[(phen)_2Cr^{III}(\mu\text{-}OH)_2Ni^{II}(Me_3\text{-tpa})](ClO_4)_3{\cdot}3H_2O$, $S(Cr^{III}) = 3/2$, $S(Ni^{II}) = 1$	$T = 4.2$–300 K	$D_{5/2}$, 0.065	g_{Ni}, 2.06	g_{Cr}, 2.0	+7.58	[167]
$[\{L^{16}_{NNOOO(O)}\}Fe^{II}(MeOH)\ Gd^{III}(NO_3)_3](MeOH)_2$, $S(Fe^{II}) = 2$, $S(Gd^{III}) = 7/2$	$T = 2$–300 K, $B = 0.7$ T, $M(B \rightarrow 5\,T,\ T = 2\,K)$	D_{Fe}, 2.06	g_{Fe}, 2.18	g_{Gd}, 2.00	1.00	[168] #
$[\{L^{16}_{NNOOO(O)}\}Fe^{II}(Me_2CO)Gd^{III}(NO_3)_3$, $S(Fe^{II}) = 2$, $S(Gd^{III}) = 7/2$	$T = 2$–300 K, $B = 0.7$ T	D_{Fe}, 3.22	g_{Fe}, 2.01	g_{Gd}, 2.00	0.82	[168] #
$[\{L^{17}_{NNOOO(O)}\}Fe^{II}(Me_2CO)Gd^{III}(NO_3)_3$, $S(Fe^{II}) = 2$, $S(Gd^{III}) = 7/2$	$T = 2$–300 K, $B = 0.7$ T	D_{Fe}, 4.43	g_{Fe}, 2.10	g_{Gd}, 2.00	0.16	[168] #
$[Ru^{II}ClRu^{III}(\mu\text{-}O_2C{\cdot}Et)_4]$, $S_i(Ru_2) = 3/2$	$T = 2$–300 K, $B = 0.3$, 1.0 T	47	1.90		−16.1	[169] #[a]
		21	1.66		−14.8	
$[Ru^{II}ClRu^{III}(\mu\text{-}O_2C{\cdot}C(Me){=}CHEt)_4]$, $S_i(Ru_2) = 3/2$	$T = 2$–300 K, $B = 0.3$, 1.0 T	48	2.04		−14.9	[169] #[a]
		19	1.84		−14.4	
$[Ru^{II}ClRu^{III}(\mu\text{-}O_2C{\cdot}CMePh_2)_4]$, $S_i(Ru_2) = 3/2$	$T = 2$–300 K, $B = 0.3$, 1.0 T	38	2.06		−26.6	[169] #[a]
		35	1.82		−24.0	
$[Mn^{II}\{L^{15}_{NNNSSS}\}Co^{II}Cl]$	$T = 2$–300 K	D_{Mn}, 3.0, D_{Co}, 10	g_{Mn}, 2.0, g_{Co}, 2.48		−114	[110] #
$[Mn^{II}\{L^{15}_{NNNSSS}\}Ni^{II}Cl]$	$T = 2$–300 K	D_{Mn}, 3.7, D_{Ni}, 7.0	g_{Mn}, 2.0, g_{Ni}, 2.17		−98	[110] #
$[Ni^{II}\{L^{15}_{NNNSSS}\}Ni^{II}Cl]$	$T = 2$–300 K	D_o, 5, D_t, 7	g_o, 2.2, g_t, 2.2		−270	[110] #
$[Cu^{II}(fsa)_2enCr^{III}(H_2O)_2]Cl{\cdot}3H_2O$, $S(Cr^{III}) = 3/2$, $S(Cu^{II}) = 1/2$	$T = 4.2$–300 K, $B = 0.2$ T	+4.5	g_2, 1.98	g_3, 1.95	105	[170][b]
		−5	g_2, 1.98	g_3, 1.95	105	
$[(MeOH)Cu^{II}(fsa)_2enFe^{III}Cl(H_2O)]{\cdot}MeOH$, $S(Fe^{III}) = 5/2$, $S(Cu^{II}) = 1/2$	$T = 4.2$–300 K, $B = 0.2$ T	+7.8	g_2, 1.99	g_3, 1.97	−78,	[170][b]
		−8.7	g_2, 2.00	g_3, 2.00	−84	
$[Ni^{II}(fsa)_2enFe^{III}Cl(MeOH)]{\cdot}H_2O$, $S(Fe^{III}) = 5/2$, $S(Ni^{II}) = 0$	$T = 4.2$–300 K, $B = 0.2$ T	D_{Fe}, 11.8	g_{Fe}, 1.99			[170]
$\{Co^{II}{}_2Cu^{II}{}_2\text{-SOD}\}$, cn = 4, $S(Co^{II}) = 3/2$, $S(Cu^{II}) = 1/2$	$T = 6$–300 K, $B = 0.8$ T	D_1, 2.2	g_1, 2.54	g_2, 2.08	−16.5	[171]
$\{E_2Co^{II}{}_2\text{-SOD}\}$, cn = 4, $S(Co^{II}) = 3/2$	$T = 6$–300 K, $B = 0.8$ T	D_1, 11.5	2.24			[171]

General notes: The symbol '#' markes that a different definition of the *J*-parameter has been applied in the original source as here $-zj$ and/or $-J$ constants precede the spin operators; the coordination number (cn) is displayed when different from 6.

[a] The first set obtained by fitting the effective magnetic moment, the second-magnetic susceptibility.

[b] Two sets of magnetic parameters differing in the sign of the *D*-parameter.

Table 30
ZFS parameters in trinuclear complexes

System M_t–M_c–M_t[a]	Experimental		D	g_c	g_t	J_{c-t}	Reference
$[Mn^{III}_2Mn^{II}(sal)_2(salH)_2(H_2O)_4(mpy)_6]^+[Mn^{III}(sal)_2(mpy)_2]^-$, $S_c = 2$, $S_t = 5/2$, $S_1 = 2$	T = 4–300 K, B = 5 T		−3.50	2	2	−1.06	[172] #
$[Co^{II}_3(HAT)(N(CN)_2)_6(H_2O)_2]$, monomer-like, $S = 3/2$	T = 2–300 K		38.9	2.01			[173]
Ni–M–Ni complexes, $S_t = 1$		D_{Ni}	$g_{Ni,z}$	$g_{M,z}$	J_{M-Ni}		
		D_{Ni-M}	$g_{Ni,x}$	$g_{M,x}$			
		D_M					
Ni–Cr–Ni complex, $S_c = 3/2$ $[Cr(CN)_4\{(CN)Ni(trenen)\}_2](BF_4)\cdot H_2O$	T = 2–300 K, B = 0.1 T		−22.2	2.24	1.99	+9.02	[174][b]
			+21.8	2.10	1.99		
			0				
			−9.2	2.16	1.99	+9.65	[174][b]
			+13.4	2.10	1.99		
			0				
Ni–Mn–Ni complex, $S_c = 5/2$, $[Mn^{II}\{Ni(NO_2)(L^{2-})(dmf)\}_2]$	T = 4.2–300 K, B = 1.5		+8.38	1.99	2.00	−1.98	[175]
			−0.64	2.04	2.00		
			0				
Ni–Co–Ni complex, $S_c = 3/2$, $[Co^{II}\{Ni(NO_2)(L^{2-})(dmf)\}_2]$	T = 4.2–300 K, B = 1.5		+6.11	2.36	2.68	−2.11	[175]
			−15.71	2.39	2.66		
			−1.65				
Ni–Ni–Ni complex, $S_c = 1$, $[Ni^{II}\{Ni(NO_2)(L^{2-})(dmf)\}_2]$	T = 4.2–300 K, B = 1.5		+11.52	2.14	2.14	−13.45	[175]
			+4.22	2.22	2.22		
			+11.52				
Ni–Cu–Ni complex, $S_c = 1/2$, $[Cu^{II}\{Ni(NO_2)(L^{2-})(dmf)\}_2]$	T = 4.2–300 K, B = 1.5		+43.1	2.34	2.23	−15.27	[175]
			−43.6	2.61	2.23		
			0				
Ni–Cu–Ni complexes, $S_t = 1$, $S_c = 1/2$			D_{Ni}	g_{Ni}	g_{Cu}	J_{Cu-Ni}	
$[Cu\{L^8_{NNNN}\}(H_2O)(Ni(hfac)_2(H_2O)_2)_2]$	T = 4.2–300 K, B = 1.5 T		±4.0	2.07	2.01	−25.4	[176]
$[Cu(pbaOH)(Ni(cth))_2](ClO_4)_2$	T = 4–300 K, B = 1.5 T		±4.1	2.20	2.29	−90.0	[177]
$[Cu(Me_2pba)(Ni(cth))_2](ClO_4)_2$	T = 4–300 K, B = 1.5 T		±8.3	2.13	2.10	−99.4	[177]
$[Cu(pbaOH)(Ni(Me_3[12]N_3))_2](ClO_4)_2$	T = 4–300 K, B = 1.5 T		±15.1	2.20	2.14	−118.7	[177]
$[Cu(Me_2pba)(Ni(Me_3[12]N_3))_2](ClO_4)_2$	T = 4–300 K, B = 1.5 T		±11.7	2.32	2.30	−110.0	[177]
$[Cu(pbaOH)(Ni(Me_4[12]N_3))_2](ClO_4)_2$	T = 4–300 K, B = 1.5 T		±14.8	2.21	2.20	−115.0	[177]
$[Cu(Me_2pba)(Ni(Me_4[12]N_3))_2](ClO_4)_2$	T = 4–300 K, B = 1.5 T		±17.1	2.19	2.16	−130.0	[177]
$[Cu(pba)(Ni(cth))_2](ClO_4)_2$	T = 2–300 K		±2.4	2.24	2.18	−124.5	[178]
$[Cu(pba)(Ni(cth))_2](ClO_4)_2$	T = 4.2–300 K		±1.6	2.13	2.15	−109.2	[179]
$[Cu(opba)(Ni(cth))_2](ClO_4)_2\cdot H_2O$	T = 4.2–300 K		±3.8	2.13	2.18	−104.2	[179]
$[Cu(pba)(Ni(bispictn))_2](ClO_4)_2\cdot 2.5H_2O$	T = 4.2–300 K		±3.3	2.15	2.19	−107.2	[179]
$[Cu(pbaOH)(Ni(bispictn))_2](ClO_4)_2\cdot H_2O$	T = 4.2–300 K		±2.7	2.13	2.15	−102.0	[179]
Cu^{II}–Fe^{III}–Cu^{II} complexes, $S_t = 1/2$, $S_c = 5/2$							
$[Fe(acac)(Cu(Mesalen))_2](NO_3)_2$	T = 30–300 K			2.05		−63	[180]
	T = 4.2–30 K		$D_{3/2}$, 7.2	2.08			[180]
Cu^{II}–Cu^{II}–Cu^{II} complexes, $S_t = 1/2$, $S_c = 1/2$			D_{Cu}[c]	g_{Cu}	J_{t-t}	J_{c-t}	
$[Cu_3EtBz\cdot 2MeOH]$	T = 2–300 K, B = 0.03 T; $M(B \to 2.5\,T,\ T = 2)$, 4, 8, 15 K		1 (2)	2.07	−4.4	38.6	[181] #
$[Cu_3BuBz\cdot 2EtOH]$	T = 2–300 K, B = 0.004,0.03 T; $M(B \to 2.5\,T,\ T = 2)$, 4, 8, 15 K		1.6 (3)	2.05	0	44	[181] #
$[Cu_3BuNaEs\cdot 2MeOH]$	T = 2–300 K, B = 0.2 T; $M(B \to 2.5\,T,\ T = 2)$, 4, 8, 15 K		1.2 (1.3)	2.02	−12	94	[181] #
$[Cu_3EtBz\cdot H_2O]$	T = 2–300 K, B = 0.2 T; $M(B \to 2.5\,T,\ T = 2)$, 13 K		0	2.08	−14	72	[181] #
$[Cu_3BuBz\cdot H_2O]$	T = 2–300 K, B = 0.2 T; $M(B \to 2.5\,T,\ T = 2)$, 13 K		0	2.06	−11	92	[181] #

General notes: The symbol '#' markes that a different definition of the J-parameter has been applied in the original source as here $-zj$ and/or $-J$ constants precede the spin operators.

[a] S_t: terminal, S_c: central ion.

[b] Data set-1: perturbation theory; data set-2: variation method (matrix diagonalization).

[c] First value—from magnetization, second—from susceptibility.

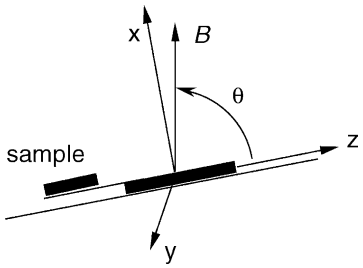

Fig. 23. Side view of the cantilever torquemeter.

does not refer to a minimum of the adiabatic potential surface). Consequently a distortion mode removes the orbital degeneracy.

Magnetic data which involve *D*-values are collected in Table 30.

4.3. Magnetization studies

Magnetization measurements at low temperature are capable of identifying the steps on the magnetization curve (see Fig. 5) which directly reflect the magnitude of *D*. For negative *D*, the ground state possesses either $M_S = 0$ or $M_S = -1/2$. With increasing B it is crossed by the state $M_S = -1$ or $M_S = -3/2$ and consequently a magnetization step occurs. Such experiments were done in large (pulsed) fields, for instance, for $FeSiF_6{\cdot}6H_2O$ [182,183]. Some more data are compiled in Table 31.

In common experiments the magnetization vector is measured along the direction of the applied magnetic field. There exists an alternate version of magnetometry that records a torque when the sample is exposed to the magnetic field. The torque $\vec{T}$ experienced by a magnetically anisotropic substance in a uniform magnetic field is

$$\vec{T} = \vec{M} \times \vec{B} \tag{4.25}$$

In the usual configuration (Fig. 23) the rotation axis of the torquemeter is set parallel to y while $\vec{B}$ is applied in the xz-plane (at an angle ϑ from z). Then the y-component of the torque vector becomes expressed as

$$T_y = B^2(\chi_{zz} - \chi_{xx})\sin\vartheta\cos\vartheta \tag{4.26}$$

and this directly measures the in-plane anisotropy; the signal is increased greatly in large magnetic fields. The torque vanishes when the magnetic field is applied along one of the principal directions (x, y, z) of the susceptibility tensor. The torque operator is obtained by differentiating the spin Zeeman term with respect to the angular variable

$$\hat{T}_y = -\left(\frac{\partial \hat{H}^Z}{\partial\vartheta}\right)_B = -\frac{\partial}{\partial\vartheta}\left[\hbar^{-1}\mu_B g B\sum_{i=1}^{N}\vec{S}_i\right]$$
$$= -\hbar^{-1}\mu_B g B\sum_{i=1}^{N}(\hat{S}_{i,x}\cos\vartheta - \hat{S}_{i,z}\sin\vartheta) \tag{4.27}$$

A combined study of $\chi = f(T,[B])$ and $M = f(B,[T])$ is much more informative and is capable of unambiguously fixing the sign of the axial ZFS parameter, even for powder samples. Such studies have recently appeared with increasing frequency since progress in experimental technique have offered such parallel studies in a single apparatus operating in different modes (SQUID- and AC-susceptometers/magnetometers). Even better, however, would be (dense) three-dimensional functions $\chi = f(T, B)$ and $M = f(T, B)$.

The analysis of the two data sets commonly proceeds as if they were independent. These combined studies have become quite common for *high-nuclearity clusters* in recent years as shown in Table 32. There is a possibility to fit all experimental scans in one run according to the scheme in Fig. 24. The weighted functional being optimized, for instance, reads

$$F = w_1\frac{\sum_{i=1}^{n}|\chi_i^{\mathrm{obs}} - \chi_i^{\mathrm{calc}}|}{(1/n)\sum_{i=1}^{n}|\chi_i^{\mathrm{obs}}|} + w_2\frac{\sum_{j=1}^{m}|M_j^{\mathrm{obs}} - M_j^{\mathrm{calc}}|}{(1/m)\sum_{j=1}^{m}|M_j^{\mathrm{obs}}|} \tag{4.28}$$

A procedure such as this has recently been published [101] and the result is displayed in Fig. 25. The procedure can easily be extended to any number of input streams which can involve more scans of the magnetization (at different temperatures) or more scans of the susceptibility (at different

Table 31
ZFS parameters for mononuclear complexes based upon single-crystal and powder magnetization data

System	Experimental	Magnetic parameters (cm^{-1})	Reference
$Cs_3V^{III}Cl_6{\cdot}4H_2O$, $S = 1$	B → 15 T, pulsed	$D = +7.85$, $g_z = 1.94$, $g_x = 1.80$	[184]
$(Zn{:}Cr^{II})Te$, $S = 2$	$T = 4.2$ K, $\nu = 20$ GHz,	EPR: $D = +2.30$, $a = 0.14$, $g_z = 1.97$, $g_x = 1.99$	[185]
	$x = 0.001$, $T = 0.6$ K, $B \rightarrow 16$ T	Consistent magnetization steps	[186]
$Fe^{II}SiF_6{\cdot}6H_2O$, $S = 2$	$B \rightarrow 45$ T, pulsed	$D = +12.3$	[182,183]
$(Cd{:}Co^{II})S$, $S = 3/2$	$x = 0.005$, $T = 30$ mK	$D = 0.66$, $g_z = 2.269$	[187]
$(Cd{:}Co^{II})Se$, $S = 3/2$	$x = 0.005$, $T = 30$ mk	$D = 0.47$, $g_z = 2.295$	[188]
$[Ni^{II}(H_2O)_6][SnCl_6]$, $S = 1$	$T = 1.35$, 2.16, 4.18 K, $B \rightarrow 4$ T	$D = +0.45$, $g = 2.25$	[86]
$[Ni^{II}(terpy)_2](PF_6)_2$, $S = 1$	$T = 1.9$ K, $B \rightarrow 5$ T	$D = -9$ K, $E = 0$, $g = 2.15$	[104]
$[Cu(salen)Ni^{II}(hfa)_2]$, $S = 1$	$T = 1.42$, 4.2 K, $B \rightarrow 20$ T, powder	$D = +12.5$, $E = 0.75$, $\vartheta_{g(Cu)-D(Ni)} = 67^\circ$, $g_{Ni} = 2.26$, $g_{Cu,z} = 2.24$, $g_{Cu,x} = 2.025$, $J_{Ni\text{-}Cu} = -23.6$	[189]
$[Ni^{II}(ac)_2(iz)_4]$, $S = 1$	$T = 4.2$ K, $B \rightarrow 6$ T, powder	$D = -22.34$, $g_z = 2.181$, $g_x = 2.175$	[101]

Table 32
ZFS parameters in polynuclear complexes (clusters)

System	Experimental	Magnetic parameters	Reference
$\{Mn^{III}_6$-ring$\}$ cluster, $S = 12$	M-powder, $B \rightarrow 7$ T, $T = 2$, 4 K	$D = -0.12$, $g = 1.80$	[190]
$\{Mn^{IV}_4Mn^{III}_8$-cubane-ring$\}$ cluster, $S = 10$		$D = -0.50$	[191]
$\{Mn^{IV}_4Mn^{III}_8$-cubane-ring$\}$ cluster, $S = 10$	M-powder, $B \rightarrow 7$ T, $T = 1.9$–4.5 K	$D = -0.63$, $g = 1.92$	[192]
$\{Fe^{III}_4$-cubane$\}$ cluster, $S_i = 5/2$	χ-powder, $T = 2$–300 K, $B = 0.1$–5 T; $M(B \rightarrow 5\,T)$, $T = 2$, 5 K	$J_1 = 0$, $J_2 = -2.6$, $J_3 = 9.2$, $D = 6.4$, $g = 2.21$	[193] #
$\{Fe^{III}_4$-cubane$\}$ cluster, $S_i = 5/2$	χ-powder, $T = 2$–300 K, $B = 0.1$–5 T; $M(B \rightarrow 5\,T)$, $T = 2$, 5 K	$J_1 = 5.2$, $J_2 = 5.0$, $J_3 = -11.2$, $D = 4.5$, $g = 2.09$	[193] #
$\{Fe^{III}_4$-bis-dimer$\}$ cluster, $S_i = 5/2$	χ-powder, $T = 2$–300 K, $B = 0.1$–5 T; $M(B \rightarrow 5\,T)$, $T = 2$, 5 K	$J_1 = 3.0$, $J_2 = 0.4$, $g = 2.14$, $D_{cn=5} = -5.6$, $D'_{cn=6} = 4.5$	[193] #
$\{Fe^{III}_4$-bis-dimer$\}$ cluster, $S_i = 5/2$	χ-powder, $T = 2$–300 K, $B = 0.1$–5 T; $M(B \rightarrow 5\,T)$, $T = 2$, 5 K	$J_1 = -5.2$, $J_2 = 1.6$, $g = 2.18$, $D_{cn=5} = 6.3$, $D'_{cn=6} = 1.6$	[193] #
$\{Fe^{III}_6$-ring$\}$ cluster, $S_i = 5/2$	χ-powder, $T = 2.3$–280 K, $B = 1$ T	$j'_{eff} = -13.69$, $g = 2.00$	[194] #
	χ-crystal, $T = 2.3$–280 K, $B = 1$ T	$j'_{eff} = -13.69$, $g_z = 1.965$, $g_x = 2.020$, $D_a = -0.050$, $D_{ab} = 0.055$	
	$M(B \rightarrow 20\,T)$, $T = 0.7$, 1.5 K pulsed $B \rightarrow 52$ T, $T = 1.5$ K	$j'_{eff} = -15.4$, $g = 2.00$, $D_a = -0.050$, $D_{ab} = 0.055$	
	Crystal cantilever torque magnetometry, $B \rightarrow 23$ T, $T = 0.45$–4.3 K	$\Delta_1 = 15.28$ (singlet-triplet gap), $D_1 = 4.32$, $\vartheta_0 = -1.6^\circ$, $g = 2.0$	[195]
$\{Fe^{III}_{10}$-ring$\}$ cluster	χ-powder, $T = 2.5$–300 K, $B = 0.3$, 0.9 T, $M(B \rightarrow 20\,T)$, $T = 0.6$, 4.2 K, pulsed $B \rightarrow 50$ T, $T = 0.6$ K	$J = -9.6$, $g = 2.0$	[196] #
	Crystal cantilever torque magnetometry, $B \rightarrow 23$ T, $T = 0.45$–4.3 K	$\Delta_1 = 4.48$ (singlet-triplet gap), $D_1 = 2.24$, $\vartheta_0 = 7.7^\circ$, $g = 2.0$	[195] *
$[Ni^{II}_4\{L^9_{NNNNNN}\}_4](PF_6)_8$, 2 × 2 grid cluster	χ-powder, $T = 1.5$–250 K, $B = 0.1$ to 5.5 T	$J = -5.56$, $g = 2.05$	[104]
	χ-crystal, $T = 1.5$–50 K, $B = 1$, 3, 5.5 T	Set-1: $J = -5.56$, $g = 2.05$; Set-2: $J = -5.73$, $D = -4.25$, $g_z = 2.104$, $g_x = 2.023$	[104]
$\{Ni^{II}_4$-cubane$\}$ cluster	χ-powder, $T = 2$–300 K, $B = 1$ T, $M(B \rightarrow 5\,T)$, $T = 2$, 5 K	$J_1 = -5.96$, $J_2 = 29.94$, $J_3 = 21.8$, $D = 0.011$, $g = 2.23$	[197] #
$\{Ni^{II}_{21}(cit)_{12}\}$ cluster	χ-powder, $T = 2$–300 K	D(ac) $= -0.32$, $g = 2.26$	[198]
	M-crystal, $T = 140$, 180 mK, $B \rightarrow 8$ T	$S_{eff} = 3$	[198]

General notes: The symbol '#' markes that a different definition of the J-parameter has been applied in the original source as here $-zj$ and/or $-J$ constants precede the spin operators.

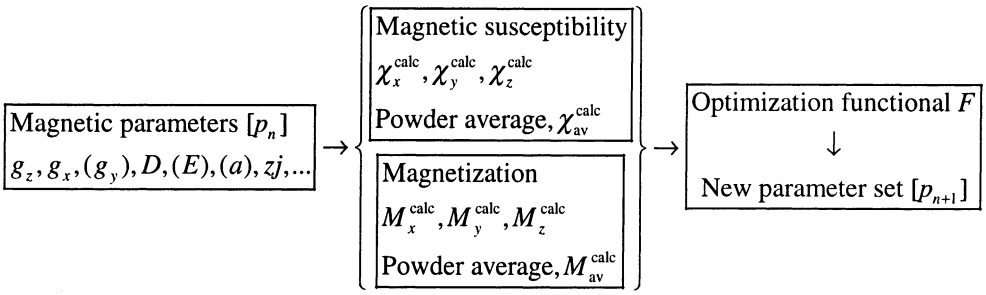

Fig. 24. A scheme of the multifunctional fitting procedure.

magnetic fields). Obviously, other experimental techniques could be involved such as calorimetry etc.

4.4. Electron paramagnetic resonance

EPR is a spectroscopic method which measures *differences* between magnetic energy levels (Table 33). This is the principal difference from the magnetic susceptibility measurements which measures the Boltzmann occupation of all energy levels.

The structure of the EPR spectrum depends upon [35–43]

1. the $g-$tensor anisotropy,
2. the presence of the hyperfine interaction of the central atom nuclear spin with the electron spin (the A^M-tensor),
3. the presence of the super−hyperfine interaction of the ligand donor atom nuclear spins with the electron spin (the A^L-tensors),
4. the appearance of satellites among which the forbidden transitions may occur,
5. the nuclear quadrupole effects,
6. the zero−field splitting,
7. the exchange (spin−spin) interactions of the magnetic centers.

Either a manual analysis of the important points of the spectrum or preferably computer simulations of the entire spectrum are capable of subtracting the magnetic parameters.

Let us focus ourselves on determination of the zero−field splitting parameter D on the basis of EPR spectra for a mononuclear transition metal complex.

For an $S = 1$ system (e.g. a complex of Ni^{2+}) with $D = 0$ the Zeeman term causes the energy levels to be equally spaced. The two allowed EPR transitions occur at the same energy (Fig. 26)

$$-1 \leftrightarrow 0 : \Delta E = h\nu = g_{\parallel}\mu_B B_z \tag{4.29}$$

$$0 \leftrightarrow +1 : \Delta E = h\nu = g_{\parallel}\mu_B B_z \tag{4.30}$$

so that a single, doubly degenerate line is observed. For $D \neq 0$ the energy levels are modified and consequently two separate lines appear

$$-1 \leftrightarrow 0 : \Delta E = h\nu = g_{\parallel}\mu_B B_z - |D| \tag{4.31}$$

$$0 \leftrightarrow +1 : \Delta E = h\nu = g_{\parallel}\mu_B B_z + |D| \tag{4.32}$$

The inclusion of the rhombic zero−field splitting parameter $E \neq 0$ alters the energy levels and consequently the EPR transitions occur at

$$-1 \leftrightarrow 0 : \Delta E = h\nu = g_{\parallel}\mu_B B_z - |D| + \frac{E^2}{2g_{\parallel}\mu_B B_z} \tag{4.33}$$

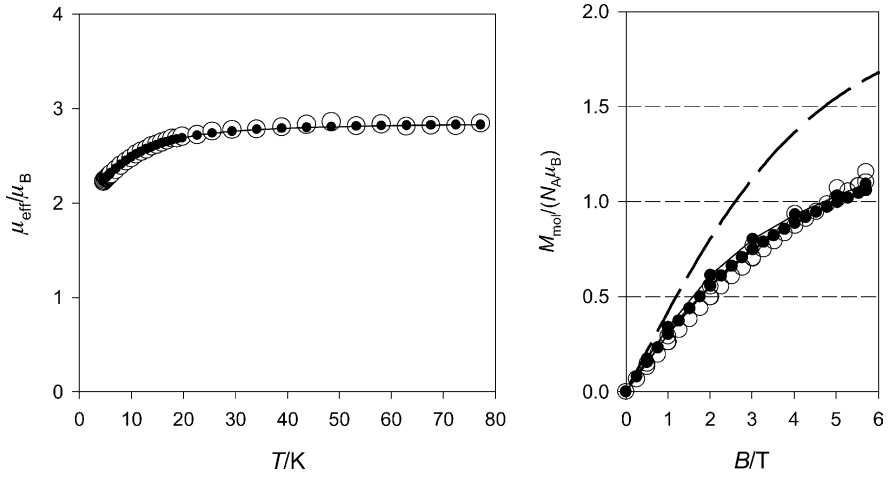

Fig. 25. Temperature dependence of the effective magnetic moment (left) and field dependence of the magnetization (right) for $[Ni(ac)_2(iz)_4]$. Experimental data—open circles, theoretical fit—filled circles. Dashed curve—the averaged magnetization according to Brillouin function for $S = 1$.

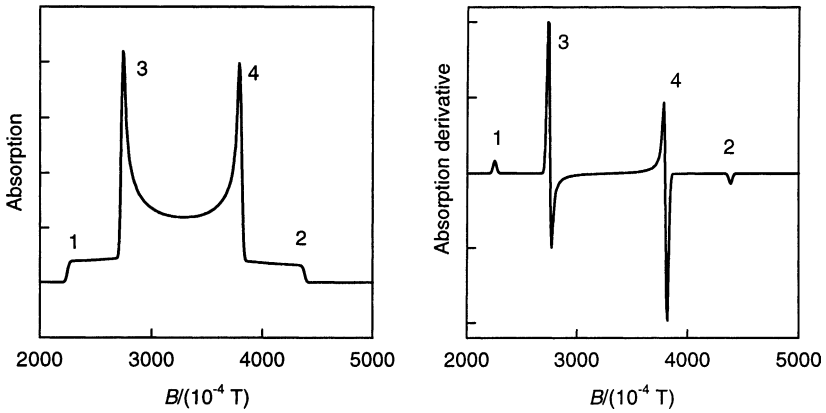

Fig. 26. Simulated powder X-band EPR spectrum for $S = 1$ with $D/hc = 0.1\,\mathrm{cm}^{-1}$.

$$0 \leftrightarrow +1 : \Delta E = h\nu = g_{\parallel}\mu_{\mathrm{B}}B_z + |D| - \frac{E^2}{2g_{\parallel}\mu_{\mathrm{B}}B_z} \quad (4.34)$$

The absorptions in the perpendicular direction are much more intense relative to those in the parallel direction. This effect originates in the geometrical factor $\mathrm{d}B = B\sin\vartheta\mathrm{d}\vartheta$ where ϑ is the angle in polar coordinates that describes deviation from the z-direction.

For an $S = 3/2$ system (e.g. a complex of Co^{2+}) with $D = 0$ only one triply degenerate line is observed at $\Delta E = h\nu = g_{\parallel}\mu_{\mathrm{B}}B_z$. This corresponds to the allowed transitions $-3/2 \leftrightarrow -1/2$, $-1/2 \leftrightarrow +1/2$ and $+1/2 \leftrightarrow +3/2$. For $D \neq 0$, however, the energy levels in zero field are split into two doublets separated by $2D$. The addition of the Zeeman term requires that the allowed transitions occur at the energies:

$$-3/2 \leftrightarrow -1/2 : \Delta E = h\nu = g_{\parallel}\mu_{\mathrm{B}}B_z - 2|D| \quad (4.35)$$

$$-1/2 \leftrightarrow +1/2 : \Delta E = h\nu = g_{\parallel}\mu_{\mathrm{B}}B_z \quad (4.36)$$

$$+1/2 \leftrightarrow +3/2 : \Delta E = h\nu = g_{\parallel}\mu_{\mathrm{B}}B_z + 2|D| \quad (4.37)$$

The model EPR spectrum, when the magnetic field is parallel to the axis of quantization, will have a central absorption band surrounded by two lines at $\pm 2|D|$.

The sign of the $D-$parameter cannot be determined via this simple experiment; its determination requires intensity data collected at variable temperature. At X−band, with a frequency of the microwave radiation of some 9 GHz, the absorption occurs at ca $B_z = 0.34\,\mathrm{T}$ and the energy separation involved is approximately $0.3\,\mathrm{cm}^{-1}$. At Q−band the measured energy separation spans the order of $1\,\mathrm{cm}^{-1}$. Therefore EPR absorption cannot be observed between energy levels whose splitting is large than these values. This can happen with non-Kramers ions ($S = 1$ or 2): the zero−field splitting leaves a spin−singlet ground state.

A frequent task is comparison of the D (or eventually E) parameters obtained by magnetic measurements and by the EPR method. The magnetochemical D-values are not restricted by the experimental method and values of $|D|/hc =$ 1 to $70\,\mathrm{cm}^{-1}$ can be determined. However, the reliable determination of values less than $1\,\mathrm{cm}^{-1}$ suffers from the lack of low-temperature data. On the contrary, the EPR resonance is absent for D-values large enough.

Table 33
Key features of the EPR spectra

Microwave source	X-band: $\nu = 9.3\,\mathrm{GHz}$; $\tilde{\nu} = 0.31\,\mathrm{cm}^{-1}$ Q-band: $\nu = 35\,\mathrm{GHz}$ W-band: $\nu \sim 100\,\mathrm{GHz}$ The microwave source is oriented perpendicular to the magnetic field The magnetic field is swept for a constant microwave frequency
Energy levels	$E(M_S, M_I) = \mu_{\mathrm{B}}gBM_S + AM_IM_S$
Fundamental resonance condition	$\Delta E = h\nu = g_z\mu_{\mathrm{B}}B_z(\Delta M_S)$
Allowed (intense) transitions	$\Delta M_S = \pm 1$, $\Delta M_I = 0$ The quantization along the z-axis holds true only for the parallel magnetic field; for the perpendicular field the quantum number M_S is not operative. In very large fields the z-axis becomes that which is parallel to the field.
Forbidden (low-intensity) transitions	$\Delta M_S = \pm 2$ or 0
Shape of the spectrum	Predominantly the first derivative of the absorption curve vs. the ramping magnetic field B_z is scanned; the absorption curve matches to a Lorenzian shape
Randomly oriented sample	For polycrystalline samples a random orientation is provided by integrating the field direction over a sphere

Table 34
EPR of zero-field splitting systems

Energy levels and allowed (intense) EPR transitions ($\Delta M_S = \pm 1$);	Simulated powder X-band EPR spectrum with $\nu = 9.3$ GHz and all $g = 2.0023$
$S = 1,\ D < h\nu;\ D/hc = 0.1\,\mathrm{cm}^{-1}$	Transition fields, B (10^{-4} T): 1: 2248; 2: 4388; 3: 2732–2766; 4: 3785–3819
$S = 1,\ D > h\nu,\ D/hc = 0.5\,\mathrm{cm}^{-1}$	Transition fields, B (10^{-4} T): 2: 8666; 3: 4890–4923
$S = 3/2,\ 2D < h\nu,\ D/hc = 0.1\,\mathrm{cm}^{-1}$	Transition fields, B (10^{-4} T): 1: 1178; 2: 3319; 3: 5458; 4: 2240–2274; 5: 3052–3086; 6: 4362–4396; 5′: 3751–3787
$S = 3/2,\ 2D > h\nu,\ D/hc = 0.5\,\mathrm{cm}^{-1}$	Transition fields, B (10^{-4} T): 2: 3318; 6: 8641–8675

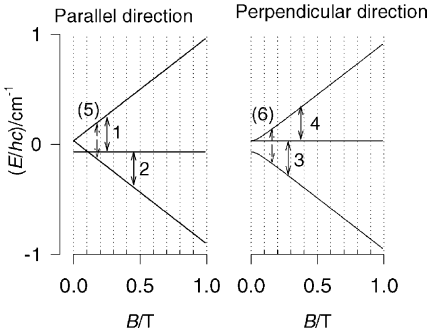

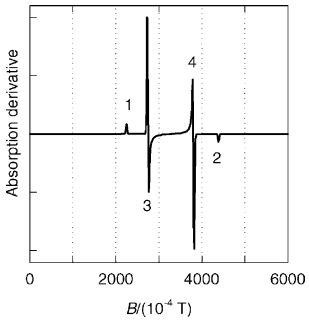

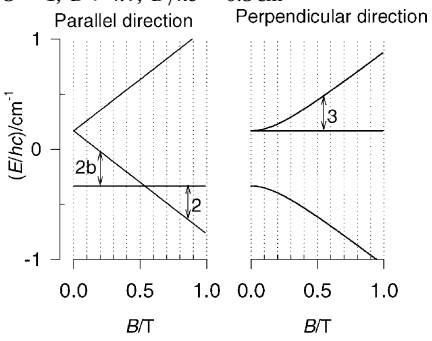

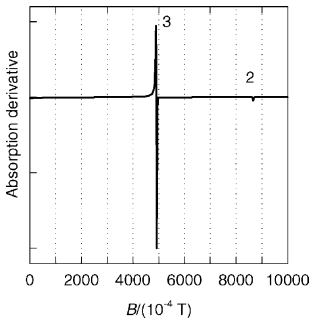

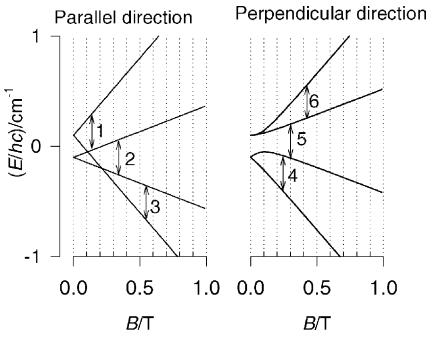

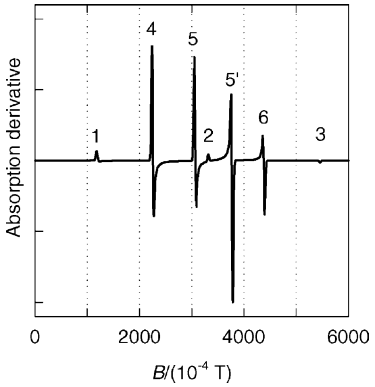

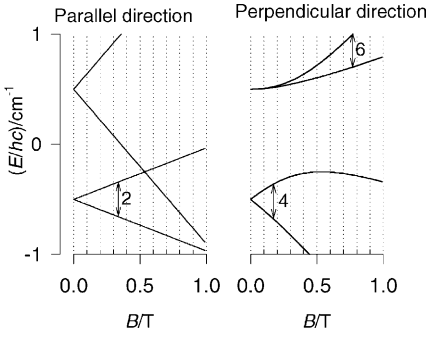

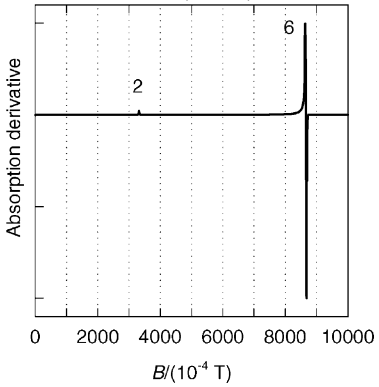

Table 34 (*Continued*)

Energy levels and allowed (intense) EPR transitions ($\Delta M_S = \pm 1$);	Simulated powder X-band EPR spectrum with $\nu = 9.3$ GHz and all $g = 2.0023$
$S = 2$, $4D < h\nu$, $D/hc = 0.05\,\mathrm{cm}^{-1}$	Transition fields, B (10^{-4} T): 1: 1713; 2: 2784; 3: (3852); 4: 4923; 5: 2540–2574; 6: 2945–2980; 7: 3471–3501; 8: 4127–4161; 7′: 3816–3855
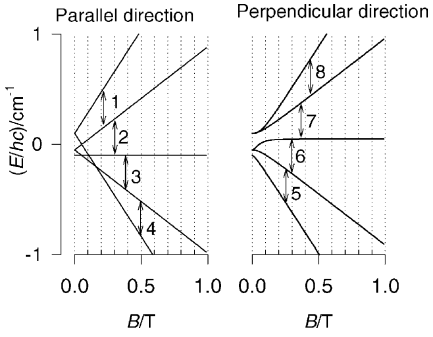	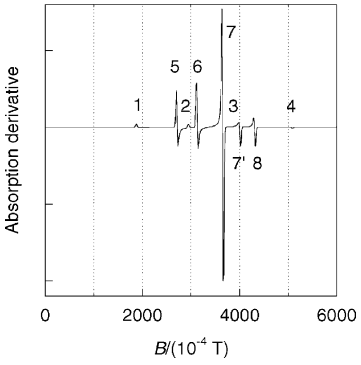
$S = 2$, $4D > h\nu$, $D/hc = 0.5\,\mathrm{cm}^{-1}$	Transition fields, B (10^{-4} T): 4b: (2035); 4: 8667
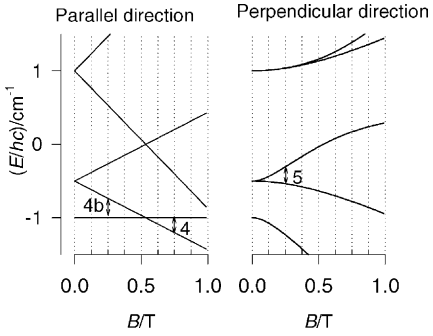	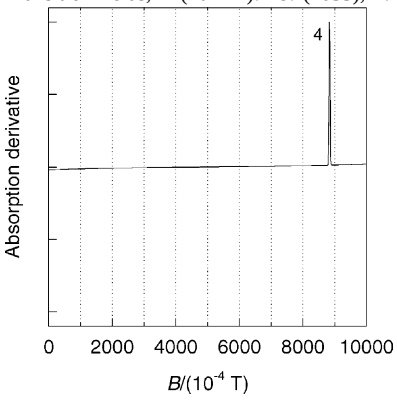
$S = 5/2$, $6D < h\nu$, $D/hc = 0.05\,\mathrm{cm}^{-1}$	Transition fields, B (10^{-4} T): 1: 1177; 2: 2249; 3: 3319; 4: 4387; 5: 5458; 6: 2326–2358; 7: 2667–2701; 8: 3137–3171; 9: 3599–3633; 10: 4448–4482; 9′: 3719–3754
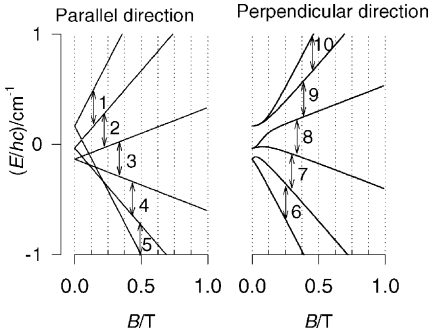	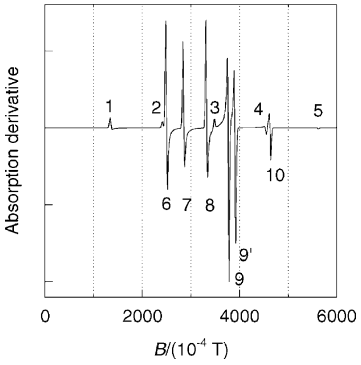
$S = 5/2$, $6D > h\nu$, $D/hc = 0.5\,\mathrm{cm}^{-1}$	Transition fields, B (10^{-4} T): 3: 3318; 6: 1250; 8: 6732

Table 34 (*Continued*)

Energy levels and allowed (intense) EPR transitions ($\Delta M_S = \pm 1$);	Simulated powder X-band EPR spectrum with $\nu = 9.3$ GHz and all $g = 2.0023$
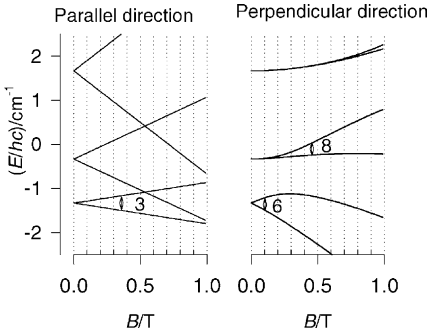	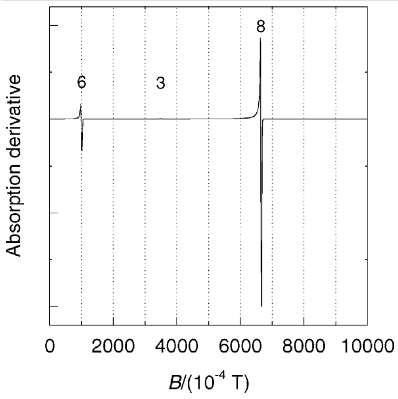
	$S = 3,\ 9D < h\nu,\ D/hc = 0.04\,\mathrm{cm}^{-1}$ 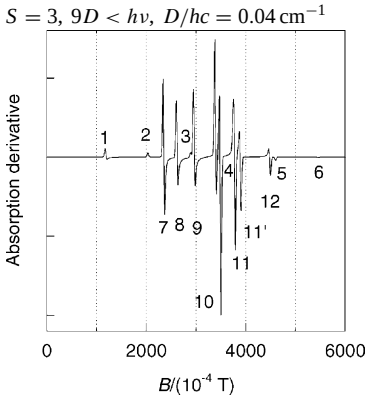
	$S = 7/2,\ 12D < h\nu,\ D/hc = 0.04\,\mathrm{cm}^{-1}$ 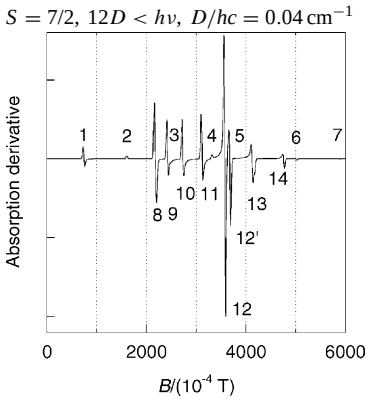

Key features of the EPR spectra are modeled in Table 34 for individual spin systems.

Magnetic parameters derived from EPR data in high-field/high-frequency experiments, for species with relatively large values of D are compiled in Table 35. These data do not include extensive tabulations from earlier investigations which can be found in EPR books, such as [35]. Moreover, the basic source of EPR data on exchange coupled systems is a book by Bencini and Gatteschi [42]. Makinen et al. [228,229] utilized the spin lattice relaxation time as a basis for the determination of the lowest energy gap in a series of Co(II) complexes with cn = 4, 5, and 6. His tabulations are also not reproduced here.

4.5. Calorimetry

Calorimetric measurements on Schottky anomalies were introduced in Chapter 2.7. Some data which involve D values are reviewed in Table 36. A disadvantage of the calorimetric measurements is that a large amount of the sample (several grams) is required by common apparatus.

Table 35
ZFS parameters based upon the high-field/high-frequency EPR

System	Experimental	Magnetic parameters (cm^{-1})	Reference
$Cs[(Ga:V^{III})(H_2O)_6](SO_4)_2{\cdot}6H_2O$, $S=1$	$T=5$–20 K, $x=0.01$, crystal, $\nu=95$, 190, 285 GHz, $B\rightarrow 12$ T	$D=4.86$, $g_z=1.950$, $g_x=1.866$, deuteriated sample, $D=4.77$, $g_z=1.955$, $g_x=1.869$	[211]
$[Cr^{II}(H_2O)_6]^{2+}$(aq)	$T=10$ K, $\nu=90$–440 GHz, $B\rightarrow 14.5$ T	$D=-2.20$, $g=1.98$	[216]
$[Mn^{III}(TPP)Cl]$, cn $=5$, $S=2$	$T=5$, 10 K, $\nu=109$, 280, 374 GHz, $B\rightarrow 15$ T	$D=-2.29$, $g_z=1.98$, $g_x=2.005$	[212]
$[Mn^{III}(PC)Cl]$, cn $=5$, $S=2$	$T=5$ K, $\nu=220$–550 GHz, $B\rightarrow 15$ T	$D=-2.31$, $g_z=2.00$, $g_x=2.005$	[212]
$[Mn^{III}(cor)]$, cn $=4$, $S=2$	$T=4.2$ K, $\nu=291$–544 GHz, $B\rightarrow 15$ T	$D=-2.64$, $E=0.015$, $g_z=2.00$, $g_x=2.02$	[212]
$[Mn^{III}(cor)py]$, cn $=5$, $S=2$	$T=4.2$ K, $\nu=97.7$, 277 GHz, $B\rightarrow 15$ T	$D=-2.78$, $E=0.030$, $g_z=2.00$, $g_x=2.02$	[212]
$[Mn^{III}(tpfc)(OPPh_3)]$, cn $=5$, $S=2$	$T=5$, 30 K, $\nu=285$, 345 GHz, $B\rightarrow 12$ T	$D=-2.69$, $E=0.030$, $g_z=1.980$, $g_x=1.994$	[213]
$[Mn^{III}(dbm)_3]$, $S=2$	$T=4.2$–30 K, $\nu=245$, 349 GHz, $B\rightarrow 12$ T	$D=-4.35$, $E=0.26$, $g_z=1.97$, $g_x=1.99$	[214]
$[Mn^{III}(terpy)(N_3)_2]$, $S=2$	$T=5$–15 K, $\nu=190$–475 GHz, $B\rightarrow 12$ T	$D=-3.29$, $E=0.48$, $g_z=2.010$, $g_x=2.000$, $g_y=1.980$	[215]
$TiO_2:Mn^{III}$	crystal, $T=4.2$ K, $\nu=2$–70 GHz	$D=-3.4$, $E=0.116$, $g_z=1.99$, $g_x=2.00$	[128]
$[(Mg:Mn^{II})(pyO)_6](ClO_4)_2$, $S=5/2$	$x=0.005$, crystal, $\nu=9.45$, 35.09 GHz, $T=77$, 300 K	$D=0.038$, $g=2.002$	[217]
$[(Zn:Mn^{II})(acac)_2(H_2O)_2]$, $S=5/2$	$x=0.005$, crystal, $\nu=9.4$, 35.1 GHz, $T=77$, 300 K	$D=0.065$, $E=0.019$, $g=1.98$	[217]
$(Cd:Co^{II})S$, $S=3/2$	$x=0.016$, crystal, $\nu=96$ GHz, $T=4.2$ K	$D=0.64$, $g=2.269$	[187]
$(Cd:Co^{II})Se$, $S=3/2$	$x=0.004$, crystal, $\nu=9.56$, 9.25 GHz, $T=4$–35 K	$D=0.47$, $g_z=2.295$, $g_x=2.294$	[188]
$[(Fe:Ni^{II})(H_2O)_6]SiF_6$, $S=1$	$T=1.5$, 4.2 K, $x\sim 0.0001$, crystal, $\nu=14.0$–16.5 GHz	$D=-3.05$, $E=0.17$, $g=2.255$	[218]
$[(Zn:Ni^{II})(H_2O)_6]SiF_6$, $S=1$	$T=4.2$–302 K, $x=0.005$, crystal $\nu=12$–18 GHz	$T=4.2$: $D=-0.13$, $g=2.233$ $T=77$: $D=-0.19$, $g=2.235$ $T=201$: $D=-0.47$, $g=2.25$ $T=302$: $D=-0.64$, $g=2.26$	[219]
$[Ni^{II}(H_2O)_6]SnCl_6$, $S=1$	$T=4.2$–370 K, X-band, crystal	$T=4.2$: $D=0.46$, $g_z=2.26$, $g_x=2.19$ $T=77$: $D=0.40$, $g_z=2.27$, $g_x=2.17$ $T=195$: $D=0.25$, $g_z=2.35$, $g_x=2.38$ $T=273$: $D=0.25$, $g_z=2.33$, $g_x=2.35$ $T=298$: $D=0.078$, $g_z=2.28$, $g_x=2.30$ $T=338$ K, $D=0$, $g=2.33$	[220]
$[Ni^{II}(H_2O)_6]SO_4$, $S=1$	$T=300$ K, crystal	$D=4.85$, $E=0.06$, $g=2.25$	[221]
$[Ni^{II}(H_2O)_6](BrO_3)_2$, $S=1$	$T=4.2$	$D=-2$, $g=2.29$	[222]
$[(Zn:Ni^{II})(dmiz)_2\mu\text{-}(ox)]_\infty$, $S=1$, zig-zag chain	$T=5$–40 K, $x=0.07$, 0.09, $\nu=110$–440 GHz, $B\rightarrow 13$ T	$D=1.87$, $E=0.38$, $g_z=2.230$, $g_x=2.220$, $g_y=2.215$	[223]
$[Ni^{II}(en)_2\mu\text{-}(NO_2)]_\infty(ClO_4)$, $S=1$, chain	$T=4.2$ K, $\nu=160$–1042 GHz, $B\rightarrow 21$ T	Zero-field Haldane gaps at $q=\pi$: $\Delta_y=9.45$, $\Delta_x=10.9$, $\Delta_z=20.1$	[224]
$[Ni^{II}(iz)_6](NO_3)_2$		$D=0.88$, $g=2.19$	[225]
$[Ni^{II}(iz)_6](ClO_4)_2$	$\nu=9.5$, 33–35 GHz	$D=0.46$, $g=2.20$	[226]
$[Ni^{II}(pz)_6](ClO_4)_2$	$\nu=9.5$, 33–35 GHz	$D=0.07$, $E=0$, $g=2.19$	[226]
$[Ni^{II}(CH_3CN)_6](GaCl_4)_2$	$\nu=9.5$, 33–35 GHz	$D=0.19$, $E=0$, $g=2.195$	[226]
$[Ni^{II}(4\text{-Cl-pz})_6](ClO_4)_2$	$\nu=9.5$, 33–35 GHz	$D=0.26$, $E=0$, $g=2.180$	[226]
$[Ni^{II}(CH_3CN)_6](SbCl_6)_2$	$\nu=9.5$, 33–35 GHz	$D=0.26$, $E=0.026$, $g=2.190$	[226]
$[Ni^{II}(CH_3CN)_6](InBr_4)_2$	$\nu=9.5$, 33–35 GHz	$D=0.27$, $E=0.046$, $g=2.198$	[226]
$[Ni^{II}(CH_3CN)_6](ClO_4)_2$	$\nu=9.5$, 33–35 GHz	$D=0.38$, $E=0.018$, $g=2.195$	[226]
$[Ni^{II}(5\text{-Me-pz})_6](ClO_4)_2$	$\nu=9.5$, 33–35 GHz	$D=0.40$, $E=0$, $g=2.178$	[226]
$[Ni^{II}(5\text{-Me-pz})_6](BF_4)_2$	$\nu=9.5$, 33–35 GHz	$D=0.47$, $E=0$, $g=2.175$	[226]
$[Ni^{II}(4\text{-Me-pz})_6](ClO_4)_2$	$\nu=9.5$, 33–35 GHz	$D=0.51$, $E=0.17$, $g=2.190$	[226]
$[Ni^{II}(N\text{-Me-iz})_6](BF_4)_2$	$\nu=9.5$, 33–35 GHz	$D=0.82$, $E=0$, $g=2.180$	[226]
$[Ni^{II}(N\text{-Me-iz})_6](ClO_4)_2$	$\nu=9.5$, 33–35 GHz	$D=0.90$, $E=0$, $g=2.185$	[226]
$[\{L^{20}_{NNNSSS}\}Co^{III}Cu^{III}Co^{III}\{L^{20}_{NNNSSS}\}](ClO_4)_3{\cdot}2Me_2CO$, $S=1$	$T=10$ K, $\nu=9.65$ GHz	$D=0.20$, $g=2.051$	[227]

Table 36
ZFS parameters based upon calorimetry

System	Experimental[a]	Magnetic parameters (cm^{-1})	Reference
$[V^{III}(urea)_6]Br_3·3H_2O$, $S = 1$	T = 1–19 K	$D = 5.84$	[236]
$NH_4V^{III}(SO_4)_2·12H_2O$, $S = 1$	T = 1.3–21.7 K	$D = 4.9$	[237]
$Cd_{1-x}Co^{II}{}_xS$, $S = 3/2$	T = 0.4–4 K	$D = 0.67$	[238]
$Cd_{1-x}Co^{II}{}_xSe$, $S = 3/2$	T = 0.4–4 K	$D = 0.50$	[238]
$Ni^{II}SO_4·6H_2O$, $S = 1$	T = 1.1–20.8 K	$D = +4.76$, $E = 0.28$	[239]
$[Ni^{II}(H_2O)_6][SnCl_6]$, $S = 1$	T = 0.37–4.2 K	$D = 0.45$	[86]
$Ni^{II}Cl_2·4H_2O$, $S = 1$	T = 0.85–25 K	$D = -7.99$, $E = 0.07$	[87]
$Ni^{II}(NO_3)_2·6H_2O$, $S = 1$	T = 0.55–11.9 K	$D = +4.46$, $E = 1.13$	[109]
$[Ni^{II}pz_4Cl_2]$, $S = 1$	T = 1–80 K	$D = 7.2$	[112]
$[Ni^{II}pz_4Br_2]$, $S = 1$	T = 1–80 K	$D = 5.4$	[112]
$[Ni^{II}(en)_2(NCS)_2]$, $S = 1$	T = 0.3–20 K	Set-1: $D = +6.24$, $E = 1.13$ Set-2: $D = -4.81$, $E = 2.55$	[240]
$[Ni^{II}(Cp)_2]$, cn = 10, $S = 1$	T = 6.8–50 K	INS: $D = 31.6$[a]	[118]

[a] INS: inelastic neutron scattering.

Table 37
ZFS parameters based upon FIR

System	Experimental[a]	Magnetic parameters (cm^{-1})[a]	Reference
$Al_2O_3:V^{III}$	$T = 4.2$ K, $B \rightarrow 5.5$ T	$D = 8.25$, $g_z = 1.92$, $g_x = 1.74$	[230]
$[Fe^{II}(H_2O)_6]SiF_6$, $S = 2$	$T = 6$, 20 K, $B \rightarrow 7$ T	$D = 11.78$, $E = 0.67$	[231]
		MS: $D = 11.8$, $E = 0.85$	[232]
$(PPh_4)_2[Fe^{II}(SPh)_4]$, cn = 4, $S = 2$	$T = 6$, 20 K, $B \rightarrow 7$ T	$D = 5.98$, $E = 1.42$	[231]
		MS: $D = 7.55$, $E = 1.69$	[233]
$[Fe^{III}(DP)F]$, $S = 5/2$	$T = 4.2$ K, $B \rightarrow 5$ T	$2D = 11.1$	[234]
$[Fe^{III}(DP)Cl]$, $S = 5/2$	$T = 4.2$ K, $B \rightarrow 5$ T	$2D = 17.9$	[234]
$[Fe^{III}(DP)Br]$, $S = 5/2$	$T = 4.2$ K, $B \rightarrow 5$ T	$2D = 23.6$	[234]
$[Fe^{III}(DP)I]$, $S = 5/2$	$T = 4.2$ K, $B \rightarrow 5$ T	$2D = 33$	[234]
$[Fe^{III}(DP)(OMe)]$, $S = 5/2$	$T = 4.2$ K, $B \rightarrow 5$ T	$2D = 9.3$	[234]
$[Fe^{III}(DP)(OPh)]$, $S = 5/2$	$T = 4.2$ K, $B \rightarrow 5$ T	$2D = 10.9$	[234]
$[Fe^{III}(DP)(ac)]$, $S = 5/2$	$T = 4.2$ K, $B \rightarrow 5$ T	$2D = 13.8$	[234]
$[Fe^{III}(DP)N_3]$, $S = 5/2$	$T = 4.2$ K, $B \rightarrow 5$ T	$2D = 14.8$	[234]
$[Fe^{III}(PP)Cl]$, $S = 5/2$	$T = 4.2$ K, $B \rightarrow 5$ T	$2D = 13.9$	[234]
$[Fe^{III}(daDP)Cl]$, $S = 5/2$	$T = 4.2$ K, $B \rightarrow 5$ T	$2D = 15.78$	[234]
Fe^{III} in Ferrichrome-A, $S = 5/2$	$T = 4.2$ K, $B \rightarrow 5$ T	$D = -0.27$, $E/D = -0.25$, $g = 2.0$	[235]
$[Fe^{III}(S_2CNR_2)_3]$, NR_2 = pyrrolidyl, $S = 5/2$	$T = 4.2$ K, $B \rightarrow 5$ T	$D = -2.14$, $E/D = -0.10$	[235]
$[Fe^{III}(S_2CNR_2)_2Br]$, NR_2 = pyrrolidyl, cn = 5, $S = 3/2$	$T = 4.2$ K, $B \rightarrow 5$ T	$D = +8.17$	[235]
$[Fe^{III}(S_2CNR_2)_2Cl]$, NR_2 = pyrrolidyl, cn = 5, $S = 3/2$	$T = 4.2$ K, $B \rightarrow 5$ T	$D = +2.60$	[235]
$[Fe^{III}(S_2CNMe_2)_2Br]$, cn = 5, $S = 3/2$	$T = 4.2$ K, $B \rightarrow 5$ T	$D = +7.30$	[235]
$[Fe^{III}(S_2CNMe_2)_2Cl]$, cn = 5, $S = 3/2$	$T = 4.2$ K, $B \rightarrow 5$ T	$D = -2.10$	[235]
$[Fe^{III}(S_2CNEt_2)_2Br]$, cn = 5, $S = 3/2$	$T = 4.2$ K, $B \rightarrow 5$ T	$D = +7.50$, $E/D = 0.067$	[235]
$[Fe^{III}(S_2CNEt_2)_2Cl]$, cn = 5, $S = 3/2$	$T = 4.2$ K, $B \rightarrow 5$ T	$D = -1.93$	[235]
$[Fe^{III}(S_2CN\textit{i}\text{-}Pr_2)_2Cl]$, cn = 5, $S = 3/2$	$T = 4.2$ K, $B \rightarrow 5$ T	$D = -2.35$, $E/D = 0.036$	[235]
$[Fe^{III}(PP)F]$, $S = 5/2$	$T = 4.2$ K, $B \rightarrow 5$ T	$D = 5.0$	[235]
$[Fe^{III}(PP)Cl]$, $S = 5/2$	$T = 4.2$ K, $B \rightarrow 5$ T	$D = 6.95$	[235]
$[Fe^{III}(PP)N_3]$, $S = 5/2$	$T = 4.2$ K, $B \rightarrow 5$ T	$D = 9.10$, $E/D = 0.085$	[235]
$[Fe^{III}(DP)F]$, $S = 5/2$	$T = 4.2$ K, $B \rightarrow 5$ T	$D = 5.55$	[235]
$[Fe^{III}(DP)Cl]$, $S = 5/2$	$T = 4.2$ K, $B \rightarrow 5$ T	$D = 8.95$	[235]
$[Fe^{III}(DP)Br]$, $S = 5/2$	$T = 4.2$ K, $B \rightarrow 5$ T	$D = 11.8$	[235]
$[Fe^{III}(DP)I]$, $S = 5/2$	$T = 4.2$ K, $B \rightarrow 5$ T	$D = 16.4$	[235]
$[Fe^{III}(DP)N_3]$, $S = 5/2$	$T = 4.2$ K, $B \rightarrow 5$ T	$D = 7.32$, $E/D = 0.036$	[235]
Ferrimyoglobin-H_2O	$T = 4.2$ K, $B \rightarrow 5$ T	$D = 9.5$	[235]
Ferrimyoglobin-F	$T = 4.2$ K, $B \rightarrow 5$ T	$D = 5.94$	[235]
Ferrihemoglobin-F	$T = 4.2$ K, $B \rightarrow 5$ T	$D = 6.30$	[235]
$[Mn^{III}(DP)Cl]$, $S = 2$	$T = 4.2$ K, $B \rightarrow 5$ T	$D = -2.53$	[235]
$[Mn^{III}(DP)Cl]$, $S = 2$	$T = 4.2$ K, $B \rightarrow 5$ T	$D = -1.10$	[235]
$[Mn^{III}(DP)N_3]$, $S = 2$	$T = 4.2$ K, $B \rightarrow 5$ T	$D = -3.08$	[235]

[a] MS: Mössbauer spectroscopy.

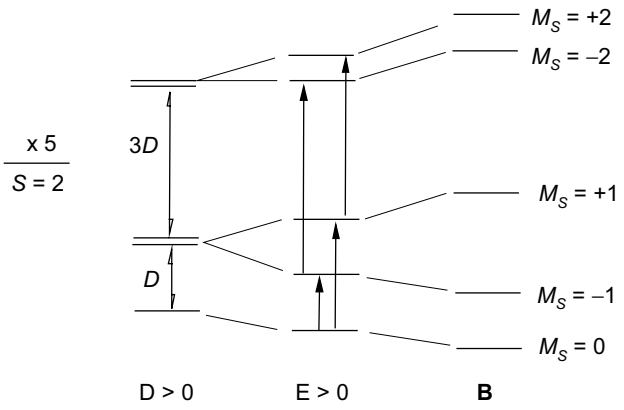

Fig. 27. Energy levels for an $S = 2$ system showing some infrared transitions that could be observed.

The data analysis requires a subtraction of the lattice (Debye) part of the heat capacity. For this purpose a simple polynomial function, some more advanced theoretical model functions, or the measured line for an isomorphous, Schottky-silent (e.g. the Zn) crystal, are applied.

As with other techniques, the calorimetric data do not provide a unambiguous determination of the sign of the *D*-parameter as tested by Murakawa et al. [240].

4.6. Far infrared spectroscopy

Far infrared spectroscopy is another technique which can be used to measure the energy gap − the zero−field splitting parameter *D*, directly. In order to identify *magnetic dipole transitions*, the magnetic field (up to several T) is applied: the Zeeman effect modifies the energy levels and systematically alters the allowed transitions, $\Delta M = \pm 1$ (Fig. 27). Experimental data are collected in Table 37. A key reference to this technique, which involves transition probabilities, is Brackett et al. [235].

The absorption coefficient (the power absorbed per unit length) between the initial electronic state $|a_n\rangle$ and the final state $|b_n\rangle$ may be written

$$\alpha_n(\nu) = \left(\frac{4\pi^2 e^2 N_0}{\hbar m_e^2 c^3}\right) \nu\rho(\nu - \nu_n)|\langle a_n|\vec{k} \times \vec{\pi} \cdot \vec{S}|b_n\rangle|^2 \tag{4.38}$$

where N_0—the concentration of paramagnetic ions, ρ—a line-shape function, $\vec{k}$—unit vector in the direction of propagation, $\vec{\pi}$—unit vector in the direction of electric field polarization, ν_n—the frequency corresponding to the difference of the eigenvalues of the initial and final states. The temperature average is

$$\alpha(\nu) = \sum_n \alpha_n(\nu) \cdot P_n(T) \tag{4.39}$$

where $P_n(T)$—is the difference in the thermal population of the two states. For unpolarized radiation the average over $\vec{\pi}$ and $\vec{k}$ is done analytically

$$\bar{\alpha}(\nu) = \left(\frac{\pi e^2 N_0 \nu}{\hbar m_e^2 c^3}\right) \sum_n \int_{\vartheta=0}^{\pi} \int_{\varphi=0}^{2\pi} \rho(\nu - \nu_n) P_n(T) \times \frac{1}{3}[\langle a_n|\hat{S}_x|b_n\rangle^2 + \langle a_n|\hat{S}_y|b_n\rangle^2 + \langle a_n|\hat{S}_z|b_n\rangle^2](\sin\vartheta \mathrm{d}\vartheta\, \mathrm{d}\varphi) \tag{4.40}$$

and the remaining average is over the magnetic field $B(\vartheta, \varphi)$ in polar coordinates for a polycrystalline sample. Consequently:

1. high-frequency transitions are increased as an effect of *n*;
2. the solid angle enhances transitions perpendicular to the field (*x*,*y*),
3. transitions from states elevated more than *kT* are suppressed by $P_n(T)$,
4. all transitions are suppressed at high temperature when $D \ll kT$.

This technique is also called "Far-Infrared Magnetic Resonance". However, the magnetic field here is kept constant and the frequency of the radiation is varied. Typically the Fourier-transform technique combined with the Michelson interferometer, low-temperature (helium-cooling) unit and the high-sensitive detector (Ge bolometer) are used. There are also some limitations to the character of the sample (absorption yield, background transmission) [235].

There is a considerable progress in new technique termed the "frequency domain spectroscopy". In fact this is the infrared spectroscopy using tunable lasers in the magnetic field; with the constant frequency and sweep field, however, it could be considered as a terra-hertz electron spin resonance. This technique allows a direct determination of the ZFS gap [263–266].

4.7. Inelastic neutron scattering

Thermal neutrons provided by nuclear reactors can be exploited for inelastic neutron scattering—INS. (Due to the large incoherent scattering contribution of ^{1}H, undeuteriated samples are not well suited for the study of magnetic excitations by thermal neutrons.) The magnetic moment of a neutron interacts with the magnetic moment of an electron and the electron transition is induced. The differential cross section of a transition $|S\rangle \rightarrow |S'\rangle$ in an INS experiment is

$$\frac{\mathrm{d}^2\sigma}{\mathrm{d}\Omega \mathrm{d}\omega} = \left(\frac{\gamma e^2}{m_e c^2}\right)^2 \left(\frac{1}{2} g F(\vec{Q})\right)^2 \frac{k_{\mathrm{out}}}{k_{\mathrm{in}}} \exp[-2W(\vec{Q})] \times \left[\sum_{a=x,y,z} (1 - Q_a^2/Q^2) \sum_{\lambda,\lambda'} \exp\left(\frac{-E_\lambda}{kT}\right) \times \langle\lambda|\hat{S}_a|\lambda'\rangle^2 \delta(\hbar\omega + E_\lambda - E_{\lambda'})\right] \tag{4.41}$$

with $\vec{Q}$—the scattering vector; k_{in} and k_{out} the wavevectors of the incoming and outgoing neutrons, respectively; $g =$

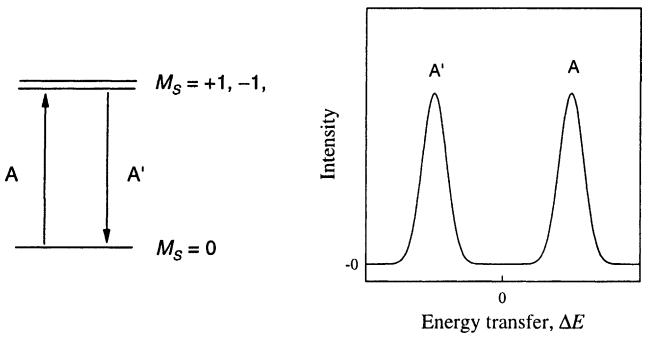

Fig. 28. Allowed energy gain (A) and energy loss (A′) transitions for the $S = 1$ system in the zero magnetic field (left) and a hypothetical neutron-energy loss and gain spectrum (right).

-1.913 is the gyromagnetic ratio of the neutron (the neutron magnetic moment in units of the nuclear magneton); g—the Landé factor, $|\lambda\rangle$ and $|\lambda'\rangle$—the initial and final electronic states with energies E_λ and $E_{\lambda'}$; $\exp[-2W(\vec{Q})]$ is the Debye-Waller factor; $F(\vec{Q})$—the magnetic form factor. The allowed transitions are restricted to $\Delta M = 0, \pm 1$ (Fig. 28).

There is an analogy between the INS and Raman spectroscopy (inelastic photon scattering): the neutron is scattered at a higher or lower energy than that of the incident (monochromated) beam. The INS discriminates unambiguously between transitions of vibrational and magnetic origin: for magnetic excitations, with increasing modulus of the scattering vector $\vec{Q}$ the intensity of the scattered neutrons decreases as $F^2(\vec{Q})$. The INS offers an unique information that is the energy function $E(\vec{k})$. The usual record is represented by I vs. ΔE functions (I—intensity, ΔE—energy transfer, or energy loss/gain). Unfortunately, several grams of the (deuteriated) sample are required for the INS experiment.

4.8. Nuclear magnetic relaxation dispersion

The magnetic moment associated with the unpaired electrons of a paramagnetic particle interacts strongly with the nuclear magnetic moments through the hyperfine interaction. In solution this interaction provides a highly efficient relaxation mechanism for nuclear spins leading to a *paramagnetic relaxation enhancement* (PRE) [261,262]. In the *nuclear magnetic relaxation dispersion* (NMRD) the PRE is studied as a function of the magnetic field using an NMR apparatus equipped with a relaxometer. The nuclear spin—lattice relaxation rate of ligand nuclei bound to the paramagnetic site depends analytically upon several contributions [241,242]. These also involve the *static ZFS* interaction which represents an average over fast processes (like vibrations, collisions). Additionally, the *transient ZFS* interaction contributes; it originates in the distortion of the paramagnetic particle because of collisions with surrounding solvent molecules.

4.9. Magnetic circular dichroism

Circular dischroism (CD) spectra show a difference between absorption of the left (L) and right (R) circularly polarized light, $\Delta\varepsilon = \varepsilon_L - \varepsilon_R$, during the electron excitation. The molar extinction coefficients (ε [$\mathrm{cm^{-1}\,mol^{-1}\,dm^3}$]) are obtained from absorbance (A), molar concentration (c [$\mathrm{mol\,dm^{-3}}$]) and the path length (l [cm]) as usual: $\kappa l(\log e) = \varepsilon cl = \log(I_0/I) = A$. (Right circularly polarized light (RCP) corresponds to light propagating towards an observer with its electric vector rotating in a clockwise direction; left circularly polarized light (LCP)—in an anticlockwise direction.) The CD feature is natural for chiral centers in the absence of a magnetic field.

Magnetic circular dichroism (MCD) involves a longitudinal magnetic field (applied parallel to the direction of propagation of the CP light). The selection rules for allowed transitions are $\Delta M = -1$ for RCP and $\Delta M = +1$ for LCP (Fig. 29). Such transitions occur for any substance having energy levels split by the magnetic field. There are a number of key references to MCD [243–247]. A consistent convention is also of great importance as discussed elsewhere [245].

The profile of the MCD spectrum depends upon temperature and applied magnetic field. The usual presentation is the function [245]

$$\frac{\Delta A}{E} = cl\frac{\varepsilon_{\mathrm{L}} - \varepsilon_{\mathrm{R}}}{E} = cl\frac{\log e}{1000}N_{\mathrm{A}}\left(\frac{8\pi^3\alpha^2}{hcn}\right)\sum_I\sum_J \frac{N_I - N_J}{N}\left[\left|\langle I|\hat{m}_-|J\rangle\right|^2 - \left|\langle I|\hat{m}_+|J\rangle\right|^2\right] f_{IJ}(E) \tag{4.42}$$

where a—electric permeability, n—index of refraction, $E = h\nu$—energy of the light, $f(E)$—absorption bandshape (e.g., a Gaussian-shaped function); the rest of the symbols adopt their usual meaning. The difference in the number of molecules between the ground and excited state (N_I and N_J, per $\mathrm{cm^3}$) collapses to N_I since at room temperature and below $N_J \sim \exp[-(E_J - E_I)/kT] \approx 0$. The electric dipole operators in electric dipole transitions are defined with the convention

$$\hat{m}_{\pm 1} = \frac{\mp(\hat{m}_x \pm i\hat{m}_y)}{\sqrt{2}} = \mp\hat{m}_\pm \tag{4.43}$$

where

$$\vec{m}(\hat{m}_x, \hat{m}_y, \hat{m}_z) = \sum_k e_k\vec{r}_k(x, y, z) \tag{4.44}$$

Under certain approximations (Born-Oppenheimer approximation, Franck-Condon principle, rigid-shift approximation) three contributing terms ($\tilde{A}$, $\tilde{B}$, $\tilde{C}$) appear

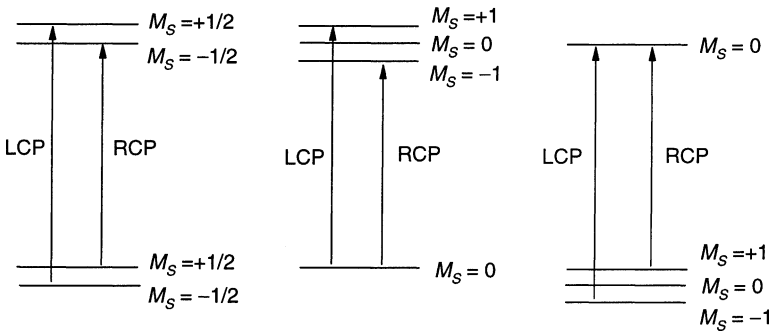

Fig. 29. Examples of the MCD transitions.

$$\frac{\Delta A}{E} = cl\frac{8N_A\pi^3\alpha^2\log e}{1000\,hcn}\mu_B B \times \left[\tilde{A}\left(-\frac{\partial f(E)}{\partial E}\right) + \left(\tilde{B} + \frac{\tilde{C}}{kT}\right) f(E)\right] \quad (4.45)$$

The three MCD terms depend upon the electronic and magnetic structure of the system under investigation. For the electronic transition from the I-th electronic state (with i-th componente when degenerate) to the excited state J (with the componente j) the transition energy equals $E_{Ii\rightarrow Jj} = E_J - E_I$ and the three MCD terms are expressed as follows

$$\tilde{A} = +\frac{1}{d_I}\sum_{i,j}[|I_i\langle|\hat{m}_{-1}|J_j\rangle|^2 - |I_i\langle|\hat{m}_{+1}|J_j\rangle|^2] \times [\langle J_j|\hat{\mu}_z|J_j\rangle - \langle I_i|\hat{\mu}_z|I_i\rangle] \quad (4.46)$$

$$\tilde{B} = +\frac{2}{d_I}\mathrm{Re}\sum_{i,j}\left\{\sum_{K_k\neq J}[\langle I_i|\hat{m}_{-1}|J_j\rangle\langle K_k|\hat{m}_{+1}|I_i\rangle - \langle I_i|\hat{m}_{+1}|J_j\rangle\langle K_k|\hat{m}_{-1}|I_i\rangle]\frac{\langle J_j|\hat{\mu}_z|K_k\rangle}{E_K - E_J} + \sum_{K_k\neq I}[\langle I_i|\hat{m}_{-1}|J_j\rangle\langle J_j|\hat{m}_{+1}|K_k\rangle - \langle I_i|\hat{m}_{+1}|J_j\rangle\langle J_j|\hat{m}_{-1}|K_k\rangle]\frac{\langle K_k|\hat{\mu}_z|I_i\rangle}{E_K - E_I}\right\} \quad (4.47)$$

$$\tilde{C} = -\frac{1}{d_I}\sum_{i,j}[|\langle I_i|\hat{m}_{-1}|J_j\rangle|^2 - |\langle I_i|\hat{m}_{+1}|J_j\rangle|^2]\langle I_i|\hat{\mu}_z|I_i\rangle \quad (4.48)$$

Here, d_I—degeneracy of the ground state (number of the components i), $|K_k\rangle$ is another electronic state not involved in the transition but being mixed either with the ground or the excited state in the magnetic field. The magnetic perturbation is given by the Zeeman term which is exhibited by a magnetoactive (paramagnetic) particle

$$\hat{H}' = \hat{\mu}_z B = \mu_B\bar{h}^{-1}(\hat{L}_z + 2\hat{S}_z)B \quad (4.49)$$

Another form of the basic MCD equation reads [249]

$$\Delta\varepsilon = -\frac{K}{\sum_I \exp(-E_I/kT)}\sum_{i,j,k}\varepsilon_{ijk}A_{zk} \times \sum_I\sum_J \mathrm{Im}[\langle I|\hat{m}_i|J\rangle\langle J|\hat{m}_j|I\rangle]\exp\left(\frac{-E_I}{kT}\right) f_{IJ}(E) \quad (4.50)$$

where K contains all the constants, ε_{ijk} is the Levi-Civita antisymmetric tensor ($\varepsilon_{xyz} = \varepsilon_{yzx} = \varepsilon_{zxy} = 1$, $\varepsilon_{yxz} = \varepsilon_{zyx} = \varepsilon_{xzy} = -1$, and zero otherwise). The band-shape function can be expanded into a Taylor series where only the linear terms are kept. The directional parameters (in polar coordinates) $A_{zx} = \sin\vartheta\cos\varphi$, $A_{zy} = \sin\vartheta\sin\varphi$, $A_{zz} = \cos\vartheta$ relate the orientation of the magnetic field relative to the molecule-fixed coordinate system. A thermal and orientational average of any quantity is given by integration

$$\langle O_k\rangle = \frac{1}{4\pi}\int_{\vartheta=0}^{\pi}\int_{\varphi=0}^{2\pi}\sum_I \langle I|\hat{O}_k|I\rangle \times \frac{\exp(-E_I/kT)}{Q}A_{zk}\sin\vartheta\,\mathrm{d}\vartheta\mathrm{d}\varphi \quad (4.51)$$

with

$$Q = \sum_I \exp\left(\frac{-E_I}{kT}\right) \quad (4.52)$$

The theory of MCD intensities is an active research area as documented by many recent, important contributions [248–250]. One of the simplest approaches applied to the ZFS systems utilizes the equation

$$\Delta A = \frac{p_1 B + p_2 C}{kT} \quad (4.53)$$

with the fractional populations of the components

$$p_1 = \frac{d_1}{d_1 + d_2\exp(-\Delta/kT)} \quad (4.54)$$

$$p_2 = \frac{d_2}{d_1 + d_2\exp(-\Delta/kT)} \quad (4.55)$$

For the $S = 1$ system: $d_1 = 1$, $d_2 = 2$, $\Delta = D$; for the $S = 3/2$: $d_1 = 2$, $d_2 = 2$, and $\Delta = 2D$. Some data are collected in Table 38.

Table 38
ZFS parameters based upon MCD

System[a]	Experimental	Magnetic parameters (cm^{-1})[b]	Reference
$[Mn_4^{IV}Mn_8^{III}O_{12}(ac)_{16}]$, $S = 10$	$T = 4.2$ K, $B = 5$ T, $\lambda = 555$, 475 nm	$D = -0.42$	[253]
$[Fe^{II}(H_2O)_6]SiF_6$, $S = 2$	$T = 1.6$–40 K, $B = 7$ T, $\lambda = 550$ nm	$D = 11.9$, $E = 0.67$ (fixed)	[254]
$(NH_4)_2[Fe^{II}(H_2O)_6](SO_4)_2$, $S = 2$	$T = 1.6$–12 K, $B = 6$ T, $\lambda = 1000$ nm	$\delta = 8.3$, $g_z = 8.6$, $\Delta_a = -250$, $\lvert V\rvert = 150$	[255]
$[Fe^{II}(TMC)Br]Br$, $S = 2$	$T = 1.6$–12 K, $B = 6$ T, $\lambda = 900$ nm	$\delta = 1.33$, $g_z = 9.01$, $\Delta_a = -2000$, $\lvert V\rvert = 600$	[255]
Fe^{II} in superoxide-dismutase, cn = 5, $S = 2$	$T = 1.6$–12 K, $B = 6$ T, $\lambda = 950$ nm	$\delta = 2.9$, $g_z = 8.78$, $\Delta_a = -1200$, $\lvert V\rvert = 648$	[255]
Fe^{II} in soybean lipoxygenase, $S = 2$	$T = 1.6$–12 K, $B = 6$ T, $\lambda = 900$ nm	$\delta = 7.24$, $g_z = 8.20$, $\Delta_a = -450$, $\lvert V\rvert = 270$	[255]
Fe^{II} in SLO-1, cn = 5, $S = 2$	$T = 1.6$–35 K, $B = 6$ T, $\lambda = 1786$ nm	$\delta = 7$, $g_z = 9$, $\Delta_a = +700$, $\lvert V\rvert = 270$	[256]
Fe^{II} in SLO-1, cn = 6, $S = 2$	$T = 1.6$–35 K, $B = 6$ T, $\lambda = 1163$ nm	$\delta = 9.6$, $g_z = 10.5$, $\Delta_a = +450$, $\lvert V\rvert = 150$	[256]
Fe^{II} in 15-RLO, cn = 5, $S = 2$	$T = 1.6$–35 K, $B = 6$ T, $\lambda = 1163$ nm	$\delta = 4.4$, $g_z = 9.0$, $\Delta_a = -500$, $\lvert V\rvert = 270$	[256]
Fe^{II} in 15-HLO, cn = 5, $S = 2$	$T = 1.6$–35 K, $B = 6$ T, $\lambda = 1163$ nm	$\delta = 4$, $g_z = 9$, $\Delta_a = -500$, $\lvert V\rvert = 270$	[256]
$Fe^{II}{}_2$ in deoxy-N_3^--hemerythrin, $S_i = 2$	$T = 1.7$–49 K, $B = 6$ T, $\lambda = 940$ nm	$J > 1$, $D_1 = -3$, $D_2 = -3$ $J > 1$, $D_1 = -7$, $D_2 = +7$	[257]#
$Fe^{II}{}_2$ in deoxy-OCN^--hemerythrin, $S_i = 2$	$T = 1.7$–49 K, $B = 6$ T, $\lambda = 1040$ nm	$J > 1$, $D_1 = +5$, $D_2 = +5$ $J > 1$, $D_1 = -13$, $D_2 = +10$	[257]#
Co^{II} in Co(c)Zn(n)-HLADH,[a] cn = 4, $S = 3/2$	$T = 1.5$–300 K, $B = 5$ T, $\lambda = 662$ nm	$\Delta = 33$, $g_z = 6.6$, $g_x = 1.9$	[258]
Co^{II} in Co(c)Zn(n)-HLADH/NAD^+/pyrazole, cn = 4, $S = 3/2$	$T = 1.5$–300 K, $B = 5$ T, $\lambda = 674$ nm	$\Delta = -56$, $g_z = 7.1$, $g_x = 0.3$	[258]
Co^{II} in Zn(c)Co(n)-HLADH, cn = 4, $S = 3/2$	$T = 1.5$–300 K, $B = 5$ T, $\lambda = 733$ nm	$\Delta = 7$, $g_z = 2.2$, $g_x = 4.6$	[258]
$(Ph_4P)_2[Ni^{II}(SPh)_4]$, cn = 4, $S = 1$	$T = 4.2$–293 K, $B = 4.5$ T, $\lambda = 664$ nm	$D = 44.3$	[259]
Ni^{II} in rubredoxin, cn = 4, $S = 1$	$T = 4.2$–293 K, $B = 4.5$ T, $\lambda = 664$ nm	$D = 55.5$	[259]
Ni^{II} in Me-CoM-reductase, $S = 1$	$T = 1.6$–98 K, $B = 4.5$ T, $\lambda = 420$ nm	$D = 8.9$	[260]

[a] HLADH = horse liver alcohol dehydrogenase; LO-lipoxygenase; 15-RLO = rabbit reticulocyte; 15-HLO = mammalian 15-LO human recombinant.
[b] Axial crystal-field splitting for d^6 systems: $\Delta_a = E(^5B_{2g} \rightarrow {}^5E_g)$; $|V|$—rhombic CF splitting, δ—rhombic ZFS splitting; overall ZFS for d^7 systems: $\Delta = |2D(1 + 3E^2/D^2)^{1/2}|$.

A unique feature of the MCD experiment is that only a small concentration of the substance is required. This allows bioinorganic studies of enzymes which are difficult to obtain in larger amounts.

There are two extensive tabulations of D-parameters derived from MCD data but not reproduced here. First, Solomon et al. ([251], p. 3957) presented data for Fe^{II} distorted complexes spanning the cn = 4, 5, and 6.

Analogously, Larrabee et al. ([252], p. 4186) collected data for a number of Co^{II} distorted complexes, spanning the cn = 4 and 5. These cover metalloproteins as well as model compounds.

5. Conclusions

The ZFS originates in a fine structure of the lowest crystal-field multiplets: the electronic states in the given symmetry point group (the crystal-field terms) are further split owing to the spin–orbit interaction so that a small energy gap appears above the ground state.

The spin-Hamiltonian approach abstracts from the orbital part of the wave functions and utilizes only the spin kets $|S, M_S\rangle$. In the space spanned by the spin functions, the bilinear spin–spin interaction operator $\hat{H}^{s-s} = \hbar^{-2}[D(\hat{S}_z^2 - \hat{S}^2/3) + E(\hat{S}_x^2 + \hat{S}_y^2)]$ leads to the intreaction matrix which after diagonalization yields the zero-field energy levels. The energy gap D dictates regularity in evolution of the remaining energy levels of the same spin manifold (for $S > 3/2$). On including the spin-Zeeman term $\hat{H}_a^Z = \hbar^{-1}\mu_B g_a B_a \hat{S}_a$, the diagonalization of the spin-Hamiltonian matrix yields the magnetic energy levels for a given field: $\varepsilon_i(B)$. When the energy levels can be taken in an analytic form ($S = 1$ or 3/2), the partition function $Z(B)$ can be treated by means the apparatus of the statistical thermodynamics and then the magnetic functions (magnetization, magnetic susceptibility, heat capacity) can be obtained in the form of closed formulae. Otherwise the second-order perturbation theory in conjunction with the van Vleck equation brings a set of approximate, but closed formulae for the magnetic functions. Numerical diagonalization in the space spanned by the spin functions is no longer a problem so that the eigenvalues, partition function, and its derivatives leading to the magnetic functions is an easy task for computers. When desired, also the biquadratic spin–spin interaction can be involved.

The spin-Hamiltonian approach offers a powerful apparatus for analysis of experimental data as generated by different experimental techniques: the magnetic susceptibility and magnetization measurements, the EPR, calorimetry, far-infrared spectroscopy, circular magnetic dichroism, and some other experimental methods. The majority of experimental data published so far are interpreted in terms of the spin-Hamiltonian formalism: the magnetic parameters of interest (g_x, g_y, g_z, D, E, and χ_{TIP}) are taken as "constants" of the system under study. Nevertheless, such characteristics are model-dependent. Moreover, the spin-Hamiltonian formalism is of a little help when there is the first-order angular momentum present in the ground electronic state (like octahedral and tetrahedral T- terms).

The spin-Hamiltonian formalism involves the Λ-tensor, and evaluation of its components brings simple formulae in which the magnetic parameters are functions of the

Table 39
Range of D-values (cm^{-1}) as detected by susceptibility measurements for hexacoordinate mononuclear complexes

System	Compressed bipyramid	Octahedron	Elongated bipyramid	Minimum	Maximum	λ (cm^{-1})
V^{III}, $S = 1$	$^3A_{2g}$, ZFS case	$^3T_{1g}$	^3E_g	+3.7	+8.0	+105
Cr^{III}, $S = 3/2$	$^4B_{1g}$, ZFS case	$^4A_{2g}$, ZFS case	$^4B_{1g}$, ZFS case	+0.2	+1.0	+92
Mn^{III}, $S = 2$	$^5A_{1g}$, ZFS case	^5E_g	$^5B_{1g}$, ZFS case	−3.0	+3.1	+89
Fe^{III}, $S = 5/2$	$^6A_{1g}$, ZFS case	$^6A_{1g}$, ZFS case	$^6A_{1g}$, ZFS case	−2.1	+7.2	$\xi = 460$
Mn^{II}, $S = 5/2$	$^6A_{1g}$, ZFS case	$^6A_{1g}$, ZFS case	$^6A_{1g}$, ZFS case		+0.2	$\xi = 300$
Fe^{II}, $S = 2$	^5E_g	$^5T_{2g}$	$^5B_{2g}$, ZFS case	−5	+12	−100
Co^{II}, $S = 3/2$	$^4A_{2g}$, ZFS case	$^4T_{1g}$	^4E_g	+25	+83	−172
Ni^{II}, $S = 1$	$^3B_{1g}$, ZFS case	$^3A_{2g}$, ZFS case	$^3B_{1g}$, ZFS case	−22.3	+9.5	−315

spin–orbit splitting parameter $\lambda = \pm\xi/2S$ for a given term and the lowest excitation energies to terms bearing components of the angular momentum. This concept has been extended to involve different orbital reduction factors (κ_x, κ_y, κ_z). As seen from Table 39, the values of the D-parameter correlate with the magnitude of λ. In a regular octahedral geometry the D-parameter should vanish but the crystal structure counterparts usually bring some perturbation of the regular geometry.

No doubt that beyond the spin-Hamiltonian formalism is the calculation of the zero-field or magnetic energy levels in a complete d^n-space spanned, for example, by the basis set of atomic terms. (Equivalently, the basis set of the crystal-field terms, atomic multiplets, or the crystal-field multiplets can be applied when all the relevant operators, i.e. the interelectron repulsion, the crystal-field potential, and the spin–orbit coupling, are considered. These basis sets are interrelated through a unitary transformation that leaves the eigenvalues invariant.) Fig. 30 shows such a modeling of the D-parameter for Ni(II), Cr(III) and Re(IV) systems. The first case of Ni(II) shows sizable values of the D-parameter on the axial distortion of the octahedron. With strong axial and weak equatorial crystal field the spin-Hamiltonian predicts a value of about $D/hc = -37\,cm^{-1}$ (dark surface) but the exact multiplet splitting is only $-30\,cm^{-1}$ (white surface). This shows limits of the spin-Hamiltonian formalism. In the second case of Cr(III) the predicted D-values are much lowered in conformity with decrease of λ^2. In the last example of Re(IV), which is isoelectronic with Cr(III), the enhancement of λ^2 reflects into a tremendous increase of the D-parameter. Such type of calculations will be a subject of the different presentation.

With binuclear and polynuclear complexes the situation is less transparent. The experimental data are exclusively interpreted in terms of the spin-Hamiltonian that involves the isotropic exchange (J_{AB} constants) and the local anisotropy parameters (D_A). The pair-wise contribution D_{AB} to the D-tensor is, as a rule, omitted. Its effect, however, could be as substantial as the contribution of the local anisotropy parameters. No a reasonable correlation of the D-parameter values has been published so far. Moreover, the limits of the strong-exchange approach are often overlooked.

As pointed out at individual experimental techniques, each of them has certain limitations and no one can be declared as a best tool in determining the D-values. The susceptometry and calorimetry can determine larger values of D; otherwise very low temperatures are required. Commercial X-band EPR spectrometers are limited to small values of D; otherwise high-frequency/high-field experiments are necessary. Far-infrared spectroscopy, inelastic neutron scattering but also calorimetry require a massive sample and MCD is restricted to transparent (no black) samples. Therefore all these techniques could be viewed as complementary one to the other.

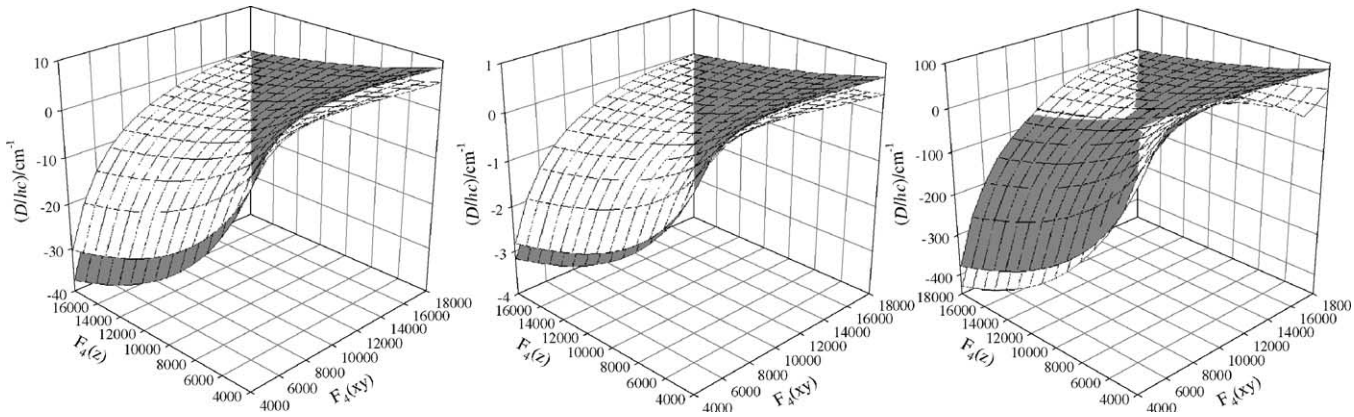

Fig. 30. Calculated D-parameters for Ni(II)—left, Cr(III)—centre, and Re(IV)—right systems at different tetragonal crystal fields. Two sets of D-values refer to the spin-Hamiltonian approach (dark) and the exact multiplet splitting (white).

Acknowledgements

Author is thankful to Slovak grant agencies (VEGA, 1/9252/02; APVT, 20-009902) for financial support.

References

[1] A. Caneschi, D. Gatteschi, R. Sessoli, A.-L. Barra, L.C. Brunel, M. Guillot, J. Am. Chem. Soc. 113 (1991) 5873.
[2] R. Sessoli, H.-L. Tsai, A.R. Schake, S. Wang, J.B. Vincent, K. Folting, D. Gatteschi, G. Christou, D. Hendrickson, J. Am. Chem. Soc. 115 (1993) 1804.
[3] R. Sessoli, D. Gatteschi, A. Caneschi, A.M. Novak, Nature 365 (1993) 141.
[4] D. Gatteschi, A. Caneschi, L. Pardi, R. Sessoli, Science 265 (1994) 1054.
[5] J.H. Eppley, H.-L. Tsai, N. de Vries, K. Folting, G. Christou, G. Hendrickson, J. Am. Chem. Soc. 117 (1995) 301.
[6] S.M.J. Aubin, M.W. Wemple, D.M. Adams, H.-L. Tsai, G. Christou, D. Hendrickson, J. Am. Chem. Soc. 118 (1996) 7746.
[7] S.M.J. Aubin, Z. Sun, H.J. Eppley, E.M. Rumberger, I.A. Guzei, K. Folting, P.K. Gantzel, A.L. Rheingold, G. Christou, D.N. Hendrickson, Inorg. Chem. 40 (2001) 2127.
[8] P. Atrus, C. Boskovic, J. Yoo, W.E. Streib, L.-C. Brunel, D.N. Hendrickson, G. Christou, Inorg. Chem. 40 (2001) 4199.
[9] C. Benelli, J. Cano, Y. Jornaux, R. Sessoli, G.A. Solan, R.E.P. Winpenny, Inorg. Chem. 40 (2001) 188.
[10] S.L. Castro, Z. Sun, C.M. Grant, J.C. Bollinger, D.N. Hendrickson, G. Christou, J. Am. Chem. Soc. 120 (1998) 2365.
[11] J.H. van Vleck, Theory of Electric and Magnetic Susceptibilities, Oxford University Press, Oxford, 1932.
[12] P.W. Selwood, Magnetochemistry, second ed., Interscience, New York, 1956.
[13] J.B. Goodenough, in Magnetism and Chemical Bond, Interscience, New York, 1963.
[14] A. Weiss, H. Witte, Magnetochemie, Verlag Chemie, Weinheim, 1973 (in German).
[15] F.E. Mabbs, D.J. Machin, Magnetism and Transition Metal Complexes, Chapman and Hall, London, 1973.
[16] R.L. Carlin, A.J. van Duyneveldt, Magnetic Properties of Transition Metal Compounds, Springer, New York, 1977.
[17] V.T. Kalinnikov, J.V. Rakitin, Vvedeniye v magnetochimiyu, Nauka, Moscow, 1980 (in Russian).
[18] A.S. Chakravarty, Introduction to the Magnetic Properties of Solids, Wiley, New York, 1980.
[19] D.C. Mattis, The Theory of Magnetism I. Statistics and Dynamics, in: Springer Series in Solid-State Sciences 17, Springer, Berlin, 1981.
[20] B.S. Tsukerblat, M.I. Belinskii, Magnetochemistry and Radiospectroscopy of Exchange Clusters, Schtiintsa, Kishinev, 1983 (in Russian).
[21] R.D. Wilett, D. Gatteschi, O. Kahn (Eds.), Magneto-Structural Correlations in Exchange Coupled Systems, NATO ASI Series, vol. 140, Reidel, Dordrecht, 1985.
[22] R.L. Carlin, Magnetochemistry, Springer, Berlin, 1986.
[23] D. Gignoux, in: K.H.J. Bushow (Ed.), Materials Science and Technology, vol. 3A, Part I, VCH, Weinheim, 1991, p. 367.
[24] D. Jiles, Introduction to Magnetism and Magnetic Material, Chapman and Hall, London, 1991.
[25] D. Gatteschi, O. Kahn, J.S. Miller, F. Palacio (Eds.), Magnetic Molecular Materials, NATO ASI Series, vol. 198, Kluwer Academic Publishers, Dordrecht, 1991.
[26] O. Kahn, Molecular Magnetism, VCH, New York, 1993.
[27] D. Craik, Magnetism, Wiley, Chichester, 1995.
[28] E. Coronado, P. Delhaes, D. Gatteschi, J.S. Miller (Eds.), Molecular Magnetism: From Molecular Assemblies to the Devices, NATO ASI Series, vol. 321, Kluwer Academic Publishers, Dordrecht, 1996.
[29] M.M. Turnbull, T. Sugimoto, L.K. Thompson (Eds.), Molecule-Based Magnetic Materials, Theory, Techniques, and Applications, ACS Symposium Series 644, Washington, 1996.
[30] J. Crangle, The Magnetic Properties of Solids (in The Structures and Properties of Solids, vol. 6), Arnold, London, 1977.
[31] S.G. Vulfson, Molecular Magnetochemistry, Gordon and Breach, 1998.
[32] H. Lueken, Magnetochemie, Teubner, Stuttgart, 1999 (in German).
[33] R. Boča, Theoretical Foundations of Molecular Magnetism, Elsevier, Amsterdam, 1999.
[34] K. Itoh, M. Kinoshita (Eds.), Molecular Magnetism, Gordon and Breach, Amsterdam, Kodanska, Tokyo, 2000.
[35] S.A. Altschuler, B.M. Kosyrew, Paramagnetische Elektronenresonanz, Harri Deutsch, Zürich, 1964.
[36] J.W. Orton, Electron Paramagnetic Resonance, Illiffe Books, London, 1968.
[37] A. Abragam, B. Bleaney, Electron Paramagnetic Resonance of Transition Ions, Clarendon Press, Oxford, 1970.
[38] C.P. Poole Jr., H.A. Farach, The Theory of Magnetic Resonance, Wiley, New York, 1972.
[39] J.E. Wetz, J.R. Bolton, Electron Spin Resonance, McGraw Hill, New York, 1972.
[40] W. Weltner Jr., Magnetic Atoms and Molecules, Dover, New York, 1983.
[41] J.R. Pilbrow, Transition Ion Electron Paramagnetic Resonance, Claredon Press, Oxford, 1990.
[42] A. Bencini, D. Gatteschi, EPR of Exchange Coupled Systems, Springer, Berlin, 1990.
[43] F.E. Mabbs, D. Collison, Electron Paramagnetic Resonance of d Transition Metal Compounds, Elsevier, Amsterdam, 1992.
[44] E.U. Condon, G.H. Shortley, The Theory of Atomic Spectra, Cambridge University Press, New York, 1935.
[45] G. Racah, Phys. Rev. 61 (1942) 186; 62 (1942) 438; 63 (1943) 367; 76 (1949) 1352.
[46] R. Rosenzweig, Phys. Rev. 88 (1952) 580.
[47] J.C. Slater, Quantum Theory of Atomic Structure, vol. I, II, McGraw-Hill, New York, 1960.
[48] A.P. Jucys, A.V. Savukynas, Mathematical Foundations of the Atomic Theory, Mintis, Vilnjus, 1972 (in Russian).
[49] I.I. Sobelman, Atomic Spectra and Radiative Transitions, Springer, Berlin, 1979.
[50] C.L. Ballhausen, Introduction to Ligand Field Theory, McGraw-Hill, New York, 1962.
[51] J.S. Griffith, The Theory of Transition Metal Ions, University Press, Cambridge, 1964.
[52] B.N. Figgis, Introduction to Ligand Fields, Wiley, New York, 1966.
[53] H.L. Schäfer, G. Gliemann, Ligand Field Theory, Wiley, London, 1969.
[54] S. Sugano, Y. Tanabe, H. Kanimura, Multiplets of Transition Metal Ions in Crystals, Academic Press, New York, 1970.
[55] A.B.P. Lever, Inorganic Electronic Spectroscopy, second ed., Elsevier, Amsterdam, 1984.
[56] B.S. Tsukerblat, Group Theory in Chemistry and Spectroscopy, Academic Press, London 1994.
[57] (a) A.B.P. Lever, E.I. Solomon, in: E.I. Solomon, A.B.P. Lever (Eds.), Inorganic Electronic Structure and Spectroscopy, vol. 1. Methodology, Wiley, New York, 1999. p. 83;
(b) E.I. Solomon, M.A. Hanson, in: E.I. Solomon, A.B.P. Lever (Eds.), Inorganic Electronic Structure and Spectroscopy, vol. 2. Applications and Case Studies, Wiley, New York, 1999, p. 43.
[58] B.N. Figgis, M.A. Hitchmann, Ligand Field Theory and Its Applications, Wiley, New York, 2000.

[59] M.E. Rose, Elementary Theory of Angular Momentum, Wiley, New York, 1957.
[60] D.M. Brink, G.R. Satchler, Angular Momentum, Claredon Press, Oxford, 1962.
[61] D.A. Varshalovich, A.N. Moskalev, V.K. Chersonskii, Kvantovaya teorija uglovovo momenta, Nauka, Leningrad, 1975 (in Russian).
[62] R.N. Zare, Angular Momentum, Wiley, New York, 1988.
[63] J.S. Griffith, The Irreducible Tensor Method for Molecular Symmetry Group, Prentice-Hall, London, 1962.
[64] B.R. Judd, Operator Techniques in Atomic Spectroscopy, McGraw-Hill, New York, 1963.
[65] B.G. Wybourne, Spectroscopic Properties of Rare Earths, Wiley, New York, 1965.
[66] M. Weissbluth, Struct. Bond. 2 (1967) 1.
[67] B.L. Silver, Irreducible Tensor Method, Academic Press, New York, 1976.
[68] E. König, S. Kremer, Ligand Field Energy Diagrams, Plenum Press, New York, 1977.
[69] E. König, S. Kremer, Magnetism Diagrams for Transition Metal Ions, Plenum Press, New York, 1979.
[70] W. Haberditzl, Quantenchemie, Band 4, Hüthig, Heidelberg, 1979 (in German).
[71] M. Gerloch, M.C. Slade, Ligand Field Parameters, Cambridge University Press, London, 1973.
[72] M. Gerloch, Magnetism and Ligand-Field Analysis, Cambridge University Press, London, 1983.
[73] S. Mitra, in: S.J. Lippard (Ed.), Progress in Inorganic Chemistry, vol. 22, Wiley, New York, 1977, p. 309.
[74] J.N. McElearney, R.W. Schwartz, S. Merchant, R.L. Carlin, J. Chem. Phys. 55 (1971) 466.
[75] J.J. Smit, L.J. de Jongh, D. de Klerk, R.L. Carlin, C.J. O'Connors, Physica B86–88 (1977) 1147.
[76] R.L. Carlin, C.J. O'Connor, S.N. Bhatia, Inorg. Chem. 15 (1976) 985.
[77] J. Baker, B.N. Figgis, Aust. J. Chem. 33 (1988) 2377.
[78] R.D. Chirico, R.L. Carlin, Inorg. Chem. 19 (1980) 3031.
[79] D.V. Behere, S. Mitra, Inorg. Chem. 19 (1980) 992.
[80] D.V. Behere, V.R. Maratha, S. Mitra, J. Am. Chem. Soc. 99 (1977) 4149.
[81] M. Gerloch, J. Lewis, R. Slade, J. Chem. Soc. A (1969) 1442.
[82] D. Nelson, L.W. ter Haar, Inorg. Chem. 32 (1993) 182.
[83] R.L. Carlin, C.J. O'Connor, S.N. Bhatia, J. Am. Chem. Soc. 98 (1976) 3523.
[84] R.L. Carlin, K.O. Joung, A. Paduan Filho, C.J. O'Connor, E. Sinn, J. Phys. C12 (1979) 293.
[85] R.A. Fisher, E.W. Hornung, J. Chem. Phys. 48 (1968) 4284.
[86] B.E. Myers, L.G. Polgar, S.A. Friedberg, Phys. Rev. B6 (1972) 3488.
[87] J.N. McElearney, D.B. Losee, S. Merchant, R.L. Carlin, Phys. Rev. 7 (1973) 3314.
[88] B.N. Figgis, P.A. Reynolds, A.H. White, B.A. Williams, S. Wright, J. Chem. Soc., Dalton Trans. (1981) 997.
[89] B.N. Figgis, B.J. Kennedy, K.S. Murray, P.A. Reynolds, S. Wright, Aust. J. Chem. 35 (1982) 1807.
[90] A.P. Ginsberg, R.L. Martin, R.W. Brookes, R.C. Sherwood, Inorg. Chem. 11 (1972) 2884.
[91] V.H. Press, S.A. Teukolsky, W.T. Vetteriling, B.P. Flannery, Numerical Recipes in Fortran, second ed., University Press, Cambridge, 1992.
[92] J.A. Nelder, R. Mead, Comput. J. 7 (1965) 308.
[93] N. Metropolis, A. Rosenbluth, M. Rosenbluth, A. Teller, E. Teller, J. Chem. Phys. 21 (1953) 1087.
[94] S. Kirkpatrick, C.D. Gelatt, M.P. Vecchi, Science 220 (1983) 671.
[95] S. Kirkpatrick, J. Stat. Phys. 34 (1984) 975.
[96] R.P. Brent, Algorithms for Minimization without Derivatives, Prentice-Hall, Englewood Cliffs, NJ, 1973.
[97] J. James, M. Roos, Program MINUIT Comput. Phys. Commun. 10 (1975) 345.
[98] D.E. Goldberg, Genetic Algorithms in Search, Optimization and Machine Learning, Addison-Wesley, 1989.
[99] Z. Michalewicz, Generic Algorithms + Data Structures = Evolution Programs, Springer, New York, 1994.
[100] L. Davis (Ed.), Handbook of Genetic Algorithms, Van Nostrand Reinhold, New York, 1991.
[101] R. Boča, L'. Dlháň, W. Haase, R. Herchel, A. Mašlejová, B. Papánková, Chem. Phys. Lett. 373 (2003) 402.
[102] A. Mašlejová, R. Boča, L. Dlháň, B. Papánková, I. Svoboda, H. Fuess, Chem. Phys. Lett. 347 (2001) 397.
[103] J. Paharová, J. Černák, R. Boča, Z. Žák, Inorg. Chim. Acta 346 (2003) 25.
[104] O. Waldman, J. Hassmann, P. Müller, D. Volkmer, U.S. Schubert, J.-M. Lehn, Phys. Rev. B58 (1998) 3277.
[105] C. Ruiz-Perez, P.A.L. Luiz, F. Lloret, M. Julve, Inorg. Chim. Acta 336 (2002) 131.
[106] R. Boča, M. Boča, M. Gembický, L. Jäger, C. Wagner, H. Fuess, Polyhedron, submitted for publication.
[107] B. Żurkowska, J. Mrozinski, M. Julve, F. Lloret, A. Mašlejová, W. Sawka-Dobrowolska, Inorg. Chem. 41 (2002) 1771.
[108] J. Černák, K.A. Abboud, J. Chomič, M.W. Meisel, M. Orendáč, A. Orendáčová, A. Feher, Inorg. Chim. Acta 311 (2000) 126.
[109] A. Herweijer, S.A. Friedberg, Phys. Rev. 4 (1971) 4009.
[110] T. Beissel, T. Glaser, F. Kesting, K. Weighardt, B. Nuber, Inorg. Chem. 35 (1996) 3936.
[111] M. Orendáč, A. Orendáčová, J. Černák, A. Feher, P.J.C. Signore, M.W. Meisel, M. Verdaguer, Phys. Rev. B52 (1995) 3435.
[112] F.W. Klaaijsen, J. Reedijk, H.T. Witteveen, Z. Naturforsch. A27 (1972) 1532.
[113] R. Boča, P. Baran, L. Dlháň, M. Hvastijová, G. Wltschek, Chem. Phys. Lett. 284 (1998) 254.
[114] A. Vermaas, W.A. Groeneveld, J. Reedijk, Z. Naturforsch. A32 (1977) 632.
[115] B.J. Kennedy, K.S. Murray, M.A. Hitchman, G.L. Rowbottom, J. Chem. Soc., Dalton Trans. (1987) 825.
[116] H.R. Jimenes, J. Salgado, J.M. Moratal, I. Morgenstern-Badarau, Inorg. Chem. 35 (1996) 2737.
[117] H. Frydendahl, H. Toflund, J. Becher, J.C. Dutton, K.S. Murray, L.F. Taylor, O.P. Anderson, E.R.T. Tiekink, Inorg. Chem. 34 (1995) 4467.
[118] P. Baltzer, A. Furrer, J. Hulliger, A. Stebler, Inorg. Chem. 27 (1988) 1543.
[119] A.K. Gregson, D.M. Doddrell, C.P. Healy, Inorg. Chem. 17 (1978) 1216.
[120] J. Mathe, S.J. Schinkel, W.A. van Amstel, Chem. Phys. Lett. 33 (1975) 528.
[121] B.N. Figgis, G.E. Toogood, J. Chem. Soc., Dalton Trans. (1972) 2177.
[122] B.J. Kennedy, S.K. Murray, Inorg. Chem. 24 (1985) 1552.
[123] L.B. Dugad, D.V. Behere, R.V. Marathe, S. Mitra, Chem. Phys. Lett. 104 (1984) 353.
[124] D.V. Behere, R.V. Marathe, S. Mitra, Chem. Phys. Lett. 81 (1981) 57.
[125] B.J. Kennedy, S.K. Murray, Inorg. Chem. 24 (1985) 1557.
[126] S.M. Saadek, K.L. Trojan, J.W. Kampf, W.E. Hatfield, V.L. Pecoraro, Inorg. Chem. 32 (1993) 3034.
[127] M.L. Kirk, M.S. Lah, C. Raptopoulou, D.P. Kessissoglou, W.E. Hatfield, V.L. Pecoraro, Inorg. Chem. 30 (1991) 3900.
[128] H.J. Gerritsen, E.S. Sabiski, Phys. Rev. 132 (1963) 1507.
[129] T. Glaser, T. Beissel, E. Bill, T. Weyhermüller, V. Schünemann, W. Mayer-Klaucke, A.X. Trautwein, K. Weighart, J. Am. Chem. Soc. 121 (1999) 2193.
[130] E.L. Laskowski, D.N. Hendrickson, Inorg. Chem. 17 (1978) 457.
[131] R. Boča, L. Dlháň, W. Linert, H. Ehrenberg, H. Fuess, W. Haase, Chem. Phys. Lett. 307 (1999) 359.

[132] V.R. Marathe, S. Mitra, Chem. Phys. Lett. 21 (1973) 62.
[133] C. Maricondi, W. Swist, D.K. Straub, J. Am. Chem. Soc. 91 (1969) 5205.
[134] V.R. Marathe, S. Mitra, Chem. Phys. Lett. 19 (1973) 140.
[135] D.V. Behere, S.K. Date, S. Mitra, Chem. Phys. Lett. 68 (1979) 544.
[136] H.-L. Shyu, H.-H. Wei, G.-H. Lee, Y. Wang, J. Chem. Soc., Dalton Trans. (2000) 915.
[137] B.W. Dale, R.J.P. Williams, C.E. Johnson, T.L. Thorp, J. Chem. Phys. 49 (1968) 3441.
[138] C.L. Klein, C. O'Connor, R.J. Majeste, L.M. Trefonas, J. Chem. Soc., Dalton Trans. (1982) 2419.
[139] P.J. van der Put, A.A. Schilperood, Inorg. Chem. 13 (1974) 2476.
[140] P.J.M.W.L. Birker, J.J. Bour, J.J. Steggerda, Inorg. Chem. 12 (1973) 1254.
[141] D.M. Eichhorn, J. Telser, C.L. Stern, B.M. Hoffman, Inorg. Chem. 33 (1994) 3533.
[142] N. Duran, W. Clegg, L. Curucull-Sanchez, R.A. Coxall, H.R. Jimenez, J.-M. Moratal, F. Lloret, P. Gonzalez-Duarte, Inorg. Chem. 39 (2000) 4821.
[143] R. Boča, H. Elias, W. Haase, M. Huber, R. Klement, L. Muller, H. Paulus, I. Svoboda, M. Valko, Inorg. Chim. Acta 278 (1998) 127.
[144] H. Jankovics, M. Daskalakis, C.P. Raptopoulou, A. Terzis, V. Tangoulis, J. Giapintzakis, T. Kiss, A. Saligoglou, Inorg. Chem. 41 (2002) 3366.
[145] L.L. Lohr, J.C. Miller, R.R. Sharp, J. Chem. Phys. 111 (1999) 10148.
[146] D.J. Mackey, S.V. Evans, R.F. McMeeking, J. Chem. Soc., Dalton Trans. (1978) 160.
[147] C. Hauser, T. Glaser, E. Bill, T. Weyhermüller, K. Weighardt, J. Am. Chem. Soc. 122 (2000) 4352.
[148] H.-L. Shyu, H.-H. Wei, Y. Wang, Inorg. Chim. Acta 290 (1999) 8.
[149] Z.Y. Zhang, C. Brouca-Cabarrecq, C. Hemmert, F. Dahan, J.-P. Tuchagues, J. Chem. Soc., Dalton Trans. (1995) 1453.
[150] J.-S. Sun, H. Zhao, X. Ouyang, R. Clerac, J.A. Smith, J.M. Clemente-Juan, C. Gomez-Garcia, E. Coronado, K.R. Dunbar, Inorg. Chem. 38 (1999) 5841.
[151] P. Garge, R. Chikate, S. Padhye, J.-M. Savariault, P. de Loth, J.-P. Tuchagues, Inorg. Chem. 29 (1990) 3315.
[152] C. Hemmert, M. Verelst, J.-P. Tuchagues, J. Chem. Soc., Chem. Commun. (1996) 617.
[153] L. Tommasi, L. Shechter-Barloy, D. Varech, J.-P. Battioni, B. Donnadieu, M. Verelst, A. Bousseksou, D. Mansuy, J.-P. Tuchagues, Inorg. Chem. 34 (1995) 1514.
[154] Md.J. Hossain, M. Yamasaki, M. Mikuriya, A. Kuribayashi, H. Sakiyama, Inorg. Chem. 41 (2002) 4058.
[155] H. Sakiyama, R. Ito, H. Kumagai, K. Inoue, M. Sakamoto, Y. Nishida, M. Yamasaki, Eur. J. Inorg. Chem. (2001) 2027, 2705.
[156] E.F. Hasty, L.J. Wilson, D.N. Hendrickson, Inorg. Chem. 17 (1978) 1834.
[157] R. Hernandez-Molina, A. Mederos, P. Gili, S. Dominguez, F. Lloret, J. Cano, M. Julve, C. Ruiz-Perez, X. Solans, J. Chem. Soc., Dalton Trans. (1997) 4327.
[158] J.C. Jansen, H. van Koningsveld, J.A.C. van Ooijen, J. Reedijk, Inorg. Chem. 19 (1980) 170.
[159] M.S. Hadad, D.N. Hendrickson, Inorg. Chem. 17 (1978) 2622.
[160] D.M. Duggan, D.N. Hendrickson, Inorg. Chem. 13 (1974) 2929.
[161] T. Rojo, R. Cortes, L. Lezama, M.I. Arriortua, K. Urtiaga, G. Willeneuve, J. Chem. Soc., Dalton Trans. (1991) 1779.
[162] M. Monfort, J. Ribas, X. Solans, Inorg. Chem. 33 (1994) 4271.
[163] E. Lambert, B. Chabut, S. Chardon-Noblat, A. Deronzier, G. Chottard, A. Bousseksou, J.-P. Tuchagues, J. Laugier, M. Bardet, J.-M. Latour, J. Am. Chem. Soc. 119 (1997) 9424.
[164] S.M. Ostrovski, R. Werner, K. Nag, W. Haase, Chem. Phys. Lett. 320 (2000) 295.
[165] V.K. Voronkova, J. Mrozinski, M.A. Yampolskaya, Yu.V. Yablokov, N.S. Evtushenko, M.S. Byrke, N.V. Gerbeleu, Inorg. Chim. Acta 238 (1995) 139.
[166] C.E. Schultz, H. Song, A. Mislankar, R.D. Orosz, C.A. Reed, P.G. Debrunner, W.R. Scheidt, Inorg. Chem. 36 (1997) 406.
[167] K. Shiren, S. Fujinami, M. Suzuki, A. Uehara, Inorg. Chem. 41 (2002) 1598.
[168] J.-P. Costes, J.M. Clemente-Juan, F. Dahan, F. Dumestre, J.-P. Tuchagues, Inorg. Chem. 41 (2002) 2886.
[169] R. Jimenez-Aparicio, F.A. Urbanos, J.M. Arrieta, Inorg. Chem. 40 (2001) 613.
[170] Y. Journaux, O. Kahn, J. Zarembowitch, J. Galy, J. Jaud, J. Am. Chem. Soc. 105 (1983) 7585.
[171] I. Morgenstern-Badarau, D. Cocco, A. Desideri, G. Rotilio, J. Jordanov, N. Dupre, J. Am. Chem. Soc. 108 (1986) 300.
[172] X.S. Tan, J. Sun, C.H. Hu, D.G. Fu, D.F. Xiang, P.J. Zheng, W.X. Tang, Inorg. Chim. Acta 257 (1997) 203.
[173] S.R. Marshall, A.L. Rheingold, L.N. Dawe, W.W. Shum, C. Kitamura, J.S. Miller, Inorg. Chem. 41 (2002) 3599.
[174] A. Scuiler, V. Marvaud, M. Verdaguer, R. Boča, unpublished.
[175] O. Atakol, R. Boča, F. Ercan, I. Ercan, W. Haase, unpublished.
[176] J.M. Dominguez-Vera, F. Camara, J.M. Moreno, E. Colacio, H. Stoeckli-Evans, Inorg. Chem. 37 (1998) 3046.
[177] R. Vicente, A. Escuer, J. Ribas, Polyhedron 11 (1992) 857.
[178] Y. Pei, Y. Journaux, O. Kahn, Inorg. Chem. 27 (1988) 399.
[179] E.Q. Gao, J.-K. Tang, D.-Z. Liao, Z.-H. Jiang, S.-P. Yan, G.-L. Wang, Inorg. Chem. 40 (2001) 3140.
[180] I. Morgenstern-Badarau, H.H. Wickman, Inorg. Chem. 24 (1985) 1889.
[181] Z. Tomkowicz, P. Fleischhauser, W. Haase, M. Baran, R. Szymczak, A.J. Zaleski, R. Jablonski, J. Magn. Magn. Mat. 172 (1997) 128.
[182] F. Varrett, Y. Allain, A. Miedan–Gros, Solid State Commun. 14 (1974) 17.
[183] F. Varrett, J. Phys. Chem. Solids 37 (1976) 257.
[184] J.J. Smit, H.J. van Wijk, L.J. de Jongh, R.L. Carlin, Chem. Phys. Lett. 62 (1979) 158.
[185] J.T. Vallin, G.D. Watkins, Phys. Rev. B9 (1974) 2051.
[186] G.H. McCabe, Y. Shapira, V. Bindilatti, N.F. Oliveira Jr., A. Twardowski, W. Mac, E.J. McNiff Jr., M. Demianiuk, Solid State Commun. 95 (1995) 841.
[187] V. Bindilatti, A.N. Anisimov, N.F. Oliveira Jr., Y. Shapira, M. Goiran, F. Yang, S. Iber, M. Averous, M. Demianiuk, Phys. Rev. B50 (1994) 16464.
[188] S. Isber, M. Averous, Y. Shapira, V. Bindilatti, A.N. Anisimov, N.F. Oliveira Jr., V.M. Orera, M. Demianiuk, Phys. Rev. B51 (1995) 15211.
[189] P. Bergerat, O. Kahn, M. Guillot, Inorg. Chem. 30 (1991) 1965.
[190] G.L. Abbati, A. Cornia, A.C. Fabretti, A. Caneschi, D. Gatteschi, Inorg. Chem. 37 (1998) 1430.
[191] S.M.J. Asubin, Z. Sun, H.J. Eppley, E.M. Rumberger, I.A. Guzei, K. Folting, P.K. Gantzel, A.L. Rheingold, G. Christou, D.N. Hendrickson, Inorg. Chem. 40 (2001) 2127.
[192] T. Kuroda-Sowa, S. Fukuda, S. Miyoshi, M. Maekawa, M. Munakata, H. Miyasaka, M. Yamashita, Chem. Lett. (2002) 682.
[193] J.M. Clemente-Juan, C. Mackiewicz, M. Verelst, F. Dahan, A. Bousseksou, Y. Sanakis, J.-P. Tuchagues, Inorg. Chem. 41 (2002) 1478.
[194] A. Caneschi, A. Cornia, A.C. Fabretti, S. Foner, D. Gatteschi, R. Grandi, L. Schenetti, Chem. Eur. J. 2 (1996) 1379.
[195] A. Cornia, A.G.M. Jansen, M. Affronte, Phys. Rev. B60 (1999) 12177.
[196] K.L. Taft, C.D. Delfs, G.C. Papaefthymiou, S. Foner, D. Gatteschi, S.J. Lippard, J. Am. Chem. Soc. 116 (1994) 823.
[197] J.M. Clemente-Juan, B. Chansou, B. Donnadieu, J.-P. Tuchagues, Inorg. Chem. 39 (2000) 5515.
[198] S.T. Ochsenbein, M. Murrie, E. Rusanov, H. Stoeckli-Evans, C. Sekine, H.U. Güdel, Inorg. Chem. 41 (2002) 5133.
[199] C.G. Pierpont, D.N. Hendrickson, D.M. Duggan, F. Wagner, E.K. Barefield, Inorg. Chem. 14 (1975) 604.

[200] M.I. Arriortua, R. Cortes, J.L. Mesa, L. Lezama, T. Rojo, G. Villeneuve, Transit. Met. Chem. 13 (1988) 371.
[201] M.I. Arriortua, R. Cortes, J.L. Mesa, L. Lezama, T. Rojo, X. Solans, M. Font-Bardia, Inorg. Chim. Acta 174 (1990) 263.
[202] R. Vicente, A. Escuer, J. Ribas, X. Solans, M. Font-Bardia, Inorg. Chem. 32 (1993) 6117.
[203] T. Othsuka, J. Phys. Soc. Jpn. 14 (1959) 1245.
[204] L.C. Jackson, Phil. Mag. 4 (1959) 269.
[205] J.S. Haynes, S.J. Retting, J.R. Sams, R.C. Thompson, J. Trotter, Can. J. Chem. 64 (1986) 429.
[206] F.F. Charron Jr., W.M. Reiff, Inorg. Chem. 25 (1986) 2786.
[207] K.D. Hodges, R.G. Wollmann, E.K. Barefield, D.N. Hendrickson, Inorg. Chem. 16 (1977) 2746.
[208] D.J. Mackey, R.F. McMeeking, M.A. Hitchman, J. Chem. Soc., Dalton Trans. (1979) 299.
[209] B.W. Dockum, W.M. Reiff, Inorg. Chim. Acta 120 (1986) 61.
[210] P.R. Edwards, C.E. Johnson, R.J.P. Williams, J. Chem. Phys. 47 (1967) 2074.
[211] P.L.W. Tregenna-Piggott, H. Weihe, J. Bendix, A.-L. Barra, H.-U. Güdel, Inorg. Chem. 38 (1999) 5928.
[212] J. Krzystek, L.A. Pardi, L.-C. Brunel, D.P. Goldberg, B.M. Hoffman, S. Licoccia, J. Telser, Spectrochim. Acta A58 (2002) 1113.
[213] J. Bendix, H.B. Gray, G. Golubkov, Z. Gross, J. Chem. Soc., Chem. Commun. (2000) 1957.
[214] A.-L. Barra, D. Gatteschi, R. Sessoli, G.L. Abbati, A. Cornia, A.C. Fabretti, M.G. Uytterhoeven, Angew. Chem. Intl. Ed. Engl. 36 (1997) 2329.
[215] J. Limburg, J.S. Vrettos, R.H. Crabtree, G.W. Brudvig, J.C. dePaula, A. Hassan, A.-L. Barra, C. Duboc-Toia, M.-N. Collomb, Inorg. Chem. 40 (2001) 1698.
[216] J. Telser, L.A. Pardi, J. Krzystek, L.-C. Brunel, Inorg. Chem. 37 (1998) 5769.
[217] C.J. O'Connor, R.L. Carlin, Inorg. Chem. 14 (1975) 291.
[218] R.S. Rubins, J. Chem. Phys. 60 (1974) 4189.
[219] R.S. Rubins, S.K. Jani, J. Chem. Phys. 66 (1977) 3297.
[220] Y. Ajiro, S.A. Friedberg, N.S. van der Ven, Phys. Rev. B12 (1975) 39.
[221] W.M. Pontuschka, A. Piccini, C.J.A. Quadros, S. Isotani, Phys. Lett. A44 (1973) 57.
[222] J.F. Suassuna, C. Rettori, H. Vargas, G.E. Barberis, C.E. Hennies, N.F. Oliviera Jr., J. Phys. Chem. Solids 38 (1977) 1075.
[223] L.A. Pardi, A.K. Hassan, F.B. Hulsbergen, J. Reedijk, A.L. Spek, L.-C. Brunel, Inorg. Chem. 39 (2000) 159.
[224] T.M. Brill, J.P. Boucher, L.C. Brunel, J.P. Renard, M. Verdaguer, Physica B204 (1995) 303.
[225] P.B. Sczaniecki, J. Lesiak, J. Magn. Reson. 46 (1982) 185.
[226] J. Reedijk, B. Nieuwenhuijse, Rec. Trav. Chim. 91 (1972) 533.
[227] C. Krebs, T. Glaser, E. Bill, T. Wezhermüller, W. Meyer-Klaucke, K. Weighardt, Angew. Chem., Int. Ed. 38 (1999) 359.
[228] M.W. Makinen, B.M. Yim, Proc. Natl. Acad. Sci. U.S.A. 78 (1981) 6221.
[229] M.V. Makinen, L.C. Kuo, M.B. Yim, G.B. Wells, J.M. Fukuyama, J.E. Kim, J. Am. Chem. Soc. 107 (1985) 5245.
[230] R.R. Joyce, P.L. Richards, Phys. Rev. 179 (1969) 375.
[231] P.M. Champion, A.J. Sievers, J. Chem. Phys. 66 (1977) 1819.
[232] H. Spering, R. Zimmermann, G. Ritter, Phys. Stat. Solidi 662 (1974) 123.
[233] V. Petrouleas, A. Simipoulos, A. Kostikas, D. Coucouvanis, J. Phys. (Paris) 6 (1976) 159.
[234] P.L. Richards, W.S. Caughey, H. Eberspaecher, G. Feher, M. Malley, J. Chem. Phys. 47 (1967) 1187.
[235] G.C. Brackett, P.L. Richards, W.S. Caughey, J. Chem. Phys. 54 (1971) 4383.
[236] N. McElearney, R.W. Schwartz, A.E. Siegel, R.L. Carlin, J. Am. Chem. Soc. 93 (1971) 4337.
[237] J.J. Fritz, H.L. Pinch, J. Am. Chem. Soc. 78 (1956) 6223.
[238] A. Lewicki, A.I. Schindler, I. Miotkowski, B.C. Crooker, J.K. Furdyna, Phys. Rev. B43 (1991) 5713.
[239] J.W. Stout, W.B. Hadley, J. Chem. Phys. 40 (1964) 55.
[240] S. Murakawa, T. Wakamatsu, M. Nakano, M. Sorai, H. Suga, J. Chem. Thermodyn. 19 (1987) 1275.
[241] T. Nilsson, J. Svoboda, P.-O. Westlund, J. Kowalewski, J. Chem. Phys. 109 (1998) 6364.
[242] T. Nilsson, G. Parigi, J. Kowalewski, J. Phys. Chem. A106 (2002) 4476.
[243] P.J. Stephens, J. Chem. Phys. 52 (1970) 3489.
[244] A.B. Buckingham, P.J. Stephens, Ann. Rev. Phys. Chem. 17 (1966) 399.
[245] S.B. Piepho, P.N. Schatz, Group Theory in Spectroscopy with Applications to Magnetic Circular Dichroism, Wiley, New York, 1983.
[246] E.I. Solomon, E.G. Pavel, K.E. Loeb, C. Campochiaro, Coord. Chem. Rev. 144 (1995) 369.
[247] M.K. Johnson, in: L. Que (Ed.), Physical Methods in Inorganic and Bioinorganic Chemistry, University Science, Mill Valley, 2000, p. 233.
[248] F. Neese, E.I. Solomon, Inorg. Chem. 38 (1999) 1847.
[249] V.S. Oganesyan, S.J. George, M.R. Cheesman, A.J. Thomson, J. Chem. Phys. 110 (1999) 762.
[250] V.S. Oganesyan, A.J. Thomson, J. Chem. Phys. 113 (2000) 5003.
[251] E.C. Pavel, N. Kitajima, E.I. Solomon, J. Am. Chem. Soc. 120 (1998) 3949.
[252] J.A. Larrabee, C.M. Alessi, E.T. Asiedu, J.O. Cook, K.R. Hoerning, L.J. Klingler, G.S. Okin, S.G. Santee, T.L. Volkert, J. Am. Chem. Soc. 119 (1997) 4182.
[253] E.J.L. McInnes, E. Pidcock, V.S. Oganesyan, M.R. Cheesman, A.K. Powell, A.J. Thomson, J. Am. Chem. Soc. 124 (2002) 9219.
[254] C. Campochiaro, E.G. Pavel, E.I. Solomon, Inorg. Chem. 34 (1995) 4669.
[255] J.W. Whittaker, E.I. Solomon, J. Am. Chem. Soc. 110 (1988) 5329.
[256] M.A. Pavlovski, Y. Zhang, T.E. Westre, Q.-F. Gan, E.G. Pavel, C. Campochiaro, B. Hedman, K.O. Hodgson, E.I. Solomon, J. Am. Chem. Soc. 117 (1995) 4316.
[257] R.C. Reem, E.I. Solomon, J. Am. Chem. Soc. 109 (1987) 1216.
[258] M.T. Werth, S.-F. Tang, G. Formicka, M. Zeppezauer, M.K. Johnson, Inorg. Chem. 34 (1995) 218.
[259] A.T. Kowal, I.C. Zambrano, I. Moura, J.J.G. Moura, J. leGall, M.K. Johnson, Inorg. Chem. 27 (1988) 1162.
[260] C.L. Hamilton, R.A. Scott, M.K. Johnson, J. Biol. Chem. 264 (1989) 11605.
[261] R. Sharp, S.M. Abernathy, L.L. Lohr, J. Chem. Phys. 107 (1997) 7620.
[262] S.M. Abernathy, J.C. Miller, L.L. Lohr, R.R. Sharp, J. Chem. Phys. 109 (1998) 4035.
[263] S. Vongtragool, B. Gorshunov, M. Dressel, J. Krzystek, D.M. Eichhorn, J. Telser, Inorg. Chem. 42 (2003) 1788.
[264] A. Mukhin, B. Gorshunov, M. Dressel, C. Sangregorio, D. Gatteschi, Phys. Rev. B 63 (2001) 214411.
[265] M. Dressel, B. Gorshunov, K. Rajagopal, S. Vongtragool, A.A. Mukhin, Phys. Rev. B 67 (2003) 060405.
[266] S. Vongtragool, B. Gorshunov, A.A. Mukhin, J. vam Slaregen, M. Dressel, A. Müller, Phys. Chem. Chem. Phys. 5 (2003) 2778.